THE THERMAL DECOMPOSITION

of

INORGANIC SOLIDS

Thesis presented for the degree of Doctor of Philosophy

by

BRIAN R. PHILLIPS, B.Sc.

University of Edinburgh

September 1961

ABSTRACT OF THESIS.

Name of Candidate BRIAN ROSS PHILLIPS, B.Sc.

Address c/o Arnold, 4 Kings Road, Cheadle Hulme, Cheshire

Degree Doctor of Philosophy *Date* October 1961

Title of Thesis The Thermal Decomposition of Inorganic Solids

A brief outline has been given of the present knowledge of the kinetics of the thermal decomposition of inorganic solids. The isothermal decomposition of potassium metaperiodate crystals, which were 300 u and 40 u in linear dimensions, has been studied, together with the effects on the subsequent decomposition, of storage and pre-irradiation with ultraviolet light.

The stoichiometric equation $2KIO_4 \longrightarrow 2KIO_3 + O_2$ accurately represented the decomposition with no detectable intermediates. The kinetics of the decomposition involved three mechanisms. Initially, there was the decomposition of external and internal crystal surfaces. This accounted for not more than 3% of the decomposition and for one half of the total reaction time. Storage for two years did not affect the rate of the initial decomposition but pre-irradiation more than doubled the rate. This was followed by the acceleration or autocatalytic stage, which was expressed in terms of a branching plane mechanism in which the planes interfere, viz.

$$\ln \frac{\alpha}{1-\alpha} = kt + C.$$

It is considered that the branching occurred along dislocations, dividing the crystal into particles which were approximately of mozaic block size. These particles then decomposed by means of a contracting sphere mechanism, giving rise to the decay stage. The maximum rate generally occurred at 50% decomposition. The effect of storage probably facilitated the branching at imperfections, while pre-irradiation appeared to increase the number of imperfections.

The activation energy for the decomposition of 46 ± 4 kcal mole^{-1} is similar to the heat of reaction $KIO_4 \longrightarrow KIO_3 + O$ $\Delta H = 50$ kcal mole^{-1}. This suggested that the activation energy is connected with the probable primary chemical step, the rupture of the iodine-oxygen bond.

The isothermal decomposition of potassium permanganate-perchlorate solid solutions has been investigated with respect to the effect of the potassium perchlorate on the potassium permanganate decomposition. The rate of the decomposition was reduced due to the change in environment of the permanganate ion. The kinetics for pure potassium permanganate appeared to be those of the branching plane mechanism, but increasing perchlorate content resulted in the kinetics for solid solutions of 75% potassium perchlorate being expressed by a power law with $n = 2$, which represented two dimensional bulk growth of the reaction interface. The main effect of the addition of perchlorate to the permanganate lattice was a reduction in the 'A factor' for the decomposition of the permanganate ion.

Use other side if necessary.

THE UNIVERSITY *of* EDINBURGH

Preface

The thesis is concerned firstly with an investigation of the isothermal decomposition of potassium metaperiodate and secondly with that of potassium permanganate - potassium perchlorate solid solutions.

Abstract

A brief outline has been given of the present knowledge of the kinetics of the thermal decomposition of inorganic solids. The isothermal decomposition of potassium metaperiodate crystals, which were 300 μ and 40 μ in linear dimensions, has been studied, together with the effects on the subsequent decomposition, of storage and pre-irradiation with ultraviolet light.

The stoichiometric equation $2KIO_4 \longrightarrow 2KIO_3 + O_2$ accurately represented the decomposition with no detectable intermediates. The kinetics of the decomposition involved three mechanisms. Initially, there was the decomposition of external and internal crystal surfaces. This accounted for not more than 3% of the decomposition and for one half of the total reaction time. Storage for two years did not affect the rate of the initial decomposition but pre-irradiation more than doubled the rate. This was followed by the acceleration or autocatalytic stage, which was expressed in terms of a branching plane mechanism in which the planes interfere, viz.

$$\ln \frac{\alpha}{1 - \alpha} = kt + C.$$

It is considered that the branching occurred along dislocations, dividing the crystal into particles which were approximately of mozaic block size. These particles then decomposed by means of a contracting sphere mechanism, giving rise to the decay stage. The maximum rate generally occurred at 50% decomposition. The effect of storage probably facilitated the branching at

imperfections, while pre-irradiation appeared to increase the number of imperfections.

The activation energy for the decomposition of 46 ± 4 kcal $mole^{-1}$ is similar to the heat of reaction $KIO_4 \longrightarrow KIO_3 + O$ $\Delta H = 50$ kcal $mole^{-1}$. This suggested that the activation energy is connected with the probable primary chemical step, the rupture of the iodine-oxygen bond.

The isothermal decomposition of potassium permanganate-perchlorate solid solutions has been investigated with respect to the effect of the potassium perchlorate on the potassium permanganate decomposition. The rate of the decomposition was reduced due to the change in environment of the permanganate ion. The kinetics for pure potassium permanganate appeared to be those of the branching plane mechanism, but increasing perchlorate content resulted in the kinetics for solid solutions of 75% potassium perchlorate being expressed by a power law with $n = 2$, which represented two dimensional bulk growth of the reaction interface. The main effect of the addition of perchlorate to the permanganate lattice was a reduction in the 'A factor' for the decomposition of the permanganate ion.

Acknowledgments

I thank my supervisor, Dr. Duncan Taylor, for his unceasing guidance and advice.

I thank Professor T.L. Cottrell for the interest he has shown in this work.

I thank G.R. Inglis for performing some of the preliminary experiments reported in the second section of the thesis.

I thank Professors J.P. Kendall, E.L. Hirst and T.L. Cottrell for the provision of laboratory facilities.

I thank the Department of Scientific and Industrial Research for the award of a Research Studentship (1958-61).

C O N T E N T S

page

SECTION II

THE ISOTHERMAL DECOMPOSITION OF POTASSIUM PERMANGANATE-POTASSIUM PERCHLORATE SOLID SOLUTIONS

General Introduction

In reactions in the solid state new solid phases are produced which entail a spacial propagation of the reaction. It is this spacial aspect which characterises solid state reactions, and is an important factor in the mechanism and kinetics.

A simple solid reaction is a polymorphic transformation of the type

$$\text{Solid}_1 \rightleftharpoons \text{Solid}_2,$$

which is reversible in the case of tin[1] an enantiotropic change, or irreversible as in azoxybenzene[2] a monotropic change.

The more general class of inorganic reactions studied are of the type

$$\text{A solid} \rightleftharpoons \text{B solid} + \text{C gas}.$$

Endothermic reactions of this type may be complicated by the occurrence of both dissociation and recombination processes, but the information gained about nucleation and the interface reaction is worth the experimental and theoretical complications involved. Work in this field has been restricted to the dehydration of salt hydrates and the dissociation of metal carbonates. A comprehensive review has been given by Garner[3].

Irreversible exothermic decompositions,

$$\text{A solid} \longrightarrow \text{B solid} + \text{C gas},$$

to which category potassium metaperiodate and potassium permanganate belong, have been fairly systematically studied, especially the decomposition of azides and oxalates. The kinetics are easily followed by measuring the pressure of the

evolved gases or the loss in weight of solid A.

Langmuir[4] pointed out that when A → B to form another phase, it is necessary that the reaction occurs only at the boundary between the two phases. The formation of a stable fragment of phase B, called a growth nucleus, involves the free energy of nucleation, and can only occur when the local fluctuations in the lattice energy of the solid are sufficient to supply the necessary activation energy. The energy required is least at imperfections in the crystal lattice such as dislocations[5], grain boundaries and Smekal cracks, and at the surfaces of very small crystals. Growth of nuclei is preferred at these sites since large lattice stresses can not be supported in their vicinity. This has been experimentally shown by Hedges and Mitchell[6] for the photolysis of silver bromide.

When the free energy of activation of nucleus formation is substantially higher than that for growth of the nuclei, a few compact nuclei are formed; this has been observed with barium azide[8] and for the decomposition of hydrates[9,10]. On the other hand if these free energies are of the same order a large number of diffuse nuclei are formed which may not grow to visible size.

The subsequent decomposition is mainly governed by the continued production and/or growth of these nuclei. A review of the different mechanisms has been given by Jacobs and Tompkins[11] and by Garner[12].

The pressure time curves for isothermal decompositions are generally divided into portions, (1) an acceleration stage AB and

(2) a decay stage BC.

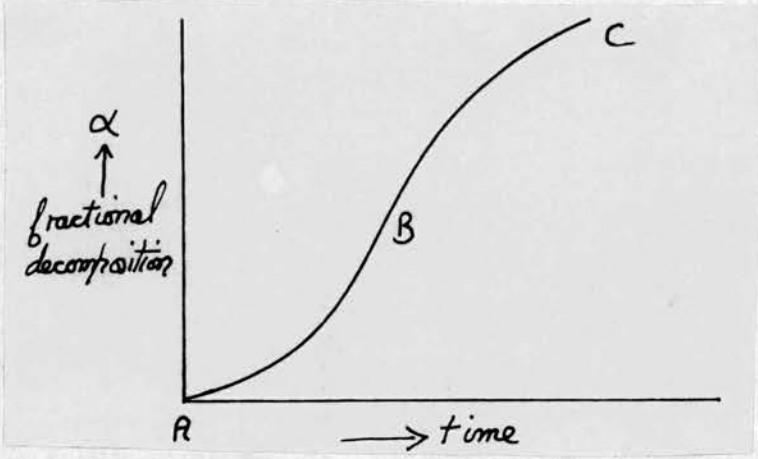

In addition and preceding AB, an initial evolution of a small amount of gas may occur, as for example with mercury fulminate[13,14,15,16] and lithium aluminium hydride[17]. The acceleration of the reaction is due to an increase in the area of the decomposition interface with time, explained by the growth of individual nuclei and an increase in the number of these nuclei.

When nucleation is very efficient and there is a rapid coverage of the surface of the crystals with small nuclei only the decay stage is observed. This occurs in lead azide[18].

Theoretical relationships between 'α' and 't', ('α' = fraction decomposed at time 't'), are derived in terms of production and growth of nuclei.

Crystal imperfections can be considered as 'germ' nuclei. Their conversion into 'growth' nuclei is governed by one of two laws. (1) The rate of formation of growth nuclei decreases exponentially with time, as the number of germ nuclei are used up. (2) The rate of formation varies as a power of the time. In both cases the rate of nucleation is constant when either the

probability of a germ nucleus becoming a growth nucleus is small or when the power of the time is zero. These growth nuclei grow in either one, two or three dimensions and give rise to transformation-time equations of the form $\alpha = At^n + B$. This power law represents the 'normal' growth of nuclei, where 'n' is a constant composed of the dimensions of growth and rate of nucleation. The power law holds well for barium azide[8,19], calcium azide[20], silver oxide[21,22] and aged mercury fulminate[16].

However this law takes no account of the ingestion of germ nuclei by growth nuclei and the effect of overlapping of the nuclei which will occur at about $\alpha = 0.5$. These factors were considered by Arami[23], who developed an equation

$$\alpha = 1 - e^{kt^n}$$

which should apply for both the acceleration and decay periods, although if the interface, between product and reactant collapses and each molecule has an equal chance of decomposing a unimolecular decay law will result. Erofeyev[24] and Mampel[25] have arrived at the same formula by different approaches. The Avrami equation has been successfully applied by Burgers and Groen[1] to the kinetics of the allotropic transformation of tin.

There is a further type of reaction where the acceleration period shows an exponential increase of 'α' with time. This exponential relationship has too physical interpretations. The first involves a 'branching plate' mechanism, where the increase in the area of the interface reaction is not caused by the production and growth of nuclei, but the creation of fresh surfaces by cracking. It is considered that the product molecules

on the surfaces of the crystal produce lateral stresses, which are relieved by cracks along which nucleus formation is favoured. The reaction therefore spreads into the crystal down these crevices and covers the inner surfaces with product molecules. The cracking process is repeated on the fresh surfaces and the reaction proceeds through the solid by a system of branching planes of decomposed material. When the rate of decomposition is governed by the rate of branching an exponential law results

$$\alpha = De^{kt},$$

where k is the probability of branching. When these chains interfere it is necessary to include a further term - the probability of termination - which alters the exponential law to

$$\ln_e \frac{\alpha}{1-\alpha} = kt + C.$$

Prout and Tompkins[27] were the first to apply this equation to the decomposition of potassium permanganate. It has subsequently been applied to the other alkali and alkaline earth permanganates. The Prout-Tompkins equation also holds for fresh mercury fulminate[16], lead oxalate[28], ammonium dichromate[29] and lanthanum oxalate[30].

The second mechanism by which an exponential law can be explained is where nuclei are produced by diffusion of the product into the reactant, thus creating a rapid increase in the number of growth nuclei. This was first proposed by Garner[31] and recently developed by Hill[32] in his studies involving potassium permanganate.

For the decay period, a decrease in the rate with time can best be explained by a decrease in the interface area of the reaction as the decomposition progresses. A contracting-sphere is the simplest three dimensional case where the decomposition progresses from the outside of a spherical particle to the centre. This has adequately explained the results in the case of mercury oxalate[33] and silver oxalate[34]. If this interface collapses the rate will depend on the number of unreacted molecules a unimolecular decay law resulting. The latter law is modified if the unreacted molecule, before it can decompose, has to be contiguous with a product molecule. Under these conditions the pressure time relationship is the same as the Prout-Tompkins equation for the acceleration.

In many decompositions studied the age of the crystal has been found to have a marked effect. For mercury fulminate[16], a chemical explanation is possible due to slow decomposition on storage at room temperature. But in general physical ageing has been observed[35], the mechanism for which is not clearly defined.

Irradiation with electro-magnetic waves or high energy particles, prior to decomposition, can also produce changes in the subsequent decomposition as in silver oxalate[34,36,37]. This appears to be primarily due to the production of growth nuclei or points from which the Prout-Tompkins branching may take place. Herley and Prout[38,39,40] have made an extensive study of the effect of irradiation on the permanganates.

Measurements of electrical conductivity of solids are of qualitative value in giving an activation energy for the conduction

process, which may be compared with that for the rate determining stage of the reaction[29]. Its use in showing the coalescence of metallic nuclei at the maximum rate stage, when the nuclei are three dimensional has been shown for the alkaline earth azides[20] by Garner and Reeves. Garner and Haycock have used the conducting properties of lithium aluminium hydride[17] to show the initial production of F^1 centres and their diffusion from the surface into the lattice where they increase the conductivity. The association of these F^1 centres causes a sharp drop in conductivity when they form nuclei, and the conductivity then remains constant until the metallic nuclei coalesce.

Infra-red absorption measurements on the solid and the partially decomposed solid can give further evidence regarding the mechanism of the decomposition. For ammonium dichromate[29] the presence of an intermediate was indicated but the identity was not established.

Section I

The isothermal decomposition of potassium metaperiodate

1. Introduction

Related salts known as the periodates are best understood as being salts of acids derived from the hypothetical iodine heptoxide by the addition of water step by step. With one molecule of water, metaperiodic acid is formed, of empirical formula HIO_4. This gives rise to potassium metaperiodate, a colourless transparent solid crystallising in tetragonal bipyramids. Mellor[41] in a survey of early work reports that the salt decomposes at 570° - 670°K to give potassium iodate and oxygen. It will be shown later that the stoichiometric equation,

$$KIO_4 = KIO_3 + \tfrac{1}{2}O_2$$

accurately represents the reaction with no detectable intermediates. This is an exothermic reaction with $\Delta H = -9$ kcal mole^{-1} at 298°K, as calculated from the heats of formation of potassium metaperiodate[42,43] and potassium iodate[42].

Potassium metaperiodate thus appears to be suitable for the study of solid state kinetics as it decomposes to give a single solid phase and one of the permanent gases.

2. Experimental

2. 1. Chemistry of the reaction

The white solid produced by the decomposition of potassium metaperiodate at 550°K was soluble in water. The addition of silver nitrate solution gave a white precipitate which was insoluble in dilute nitric acid, but soluble in dilute ammonium hydroxide solution, leaving no residue. The solid product was thus potassium iodate and as no iodide ions were observed, there is no further decomposition to potassium iodide. It was concluded that the uncondensable gas released was oxygen.

In subsection 2. 6. known amounts of the salt were decomposed and the quantity of oxygen liberated was measured. In all cases the quantity of oxygen evolved was 0.5 ± 0.01 mole per mole of potassium metaperiodate. The quantity of the solid product potassium iodate corresponded to 1 mole of potassium metaperiodate. For example in run A1, 21.34 mg of KIO_4 produced 20.83 mg of KIO_3 giving a loss in weight of 1.51 mg. The final pressure of oxygen evolved corrected to 273°K in 6.673 l. was 119.3 μ which is equivalent to 1.50 mg of oxygen.

Therefore the moles of oxygen produced per mole of KIO_4 was 0.505 calculated from the final pressure and 0.51 calculated from the loss in weight. This agrees with $2KIO_4 \longrightarrow 2KIO_3 + O_2$.

X-ray powder photographs of the product were identical to those of recrystallised analar potassium iodate.

In a search for intermediate products infra-red absorption measurements (Nujol mull technique, Hilger H800 spectrophotometer)

were carried out on analar potassium metaperiodate and on samples that had been separately 0.3, 25, 50, 75 and 100% decomposed at 550°K. The relative intensities of the very strong metaperiodate ion peak[44] 848 cm^{-1} decreased linearly with the percentage decomposition as the very strong iodate ion peak[44] 738 cm^{-1} increased. No peaks were observed other than those of metaperiodate and iodate.

Thus the reaction is

$$2KIO_4 \longrightarrow 2KIO_3 + O_2,$$

with no detectable intermediates.

2. 2. Apparatus and procedure

The apparatus (Fig. Ia) and experimental procedures were similar to those described by Simpson and Taylor[29]. Decompositions were carried out in a closed system, in which the pressure increase in a known volume, was measured by a McLeod gauge. The Pyrex reaction vessel carrying the thermal couple pocket was centrally situated in an electrically heated furnace. The sample contained in a small bucket constructed from 2 cm^2 of 0.0025 cm thick platinum foil, could be lowered into the furnace by means of the winch, to which the bucket was attached by a fine platinum wire. The furnace was stabilised to better than 0.1° by a Sunvic Resistance Thermometer Controller type RT2, with the A.C. mains basic power supply stabilised by a voltage stabiliser. The thermocouple with one junction at the bottom of the reaction vessel and the other held at 0° in ice, was calibrated in steps of 5° from 470° - 570°K against a standard Pt/Pt Rh thermocouple; the voltage was read to

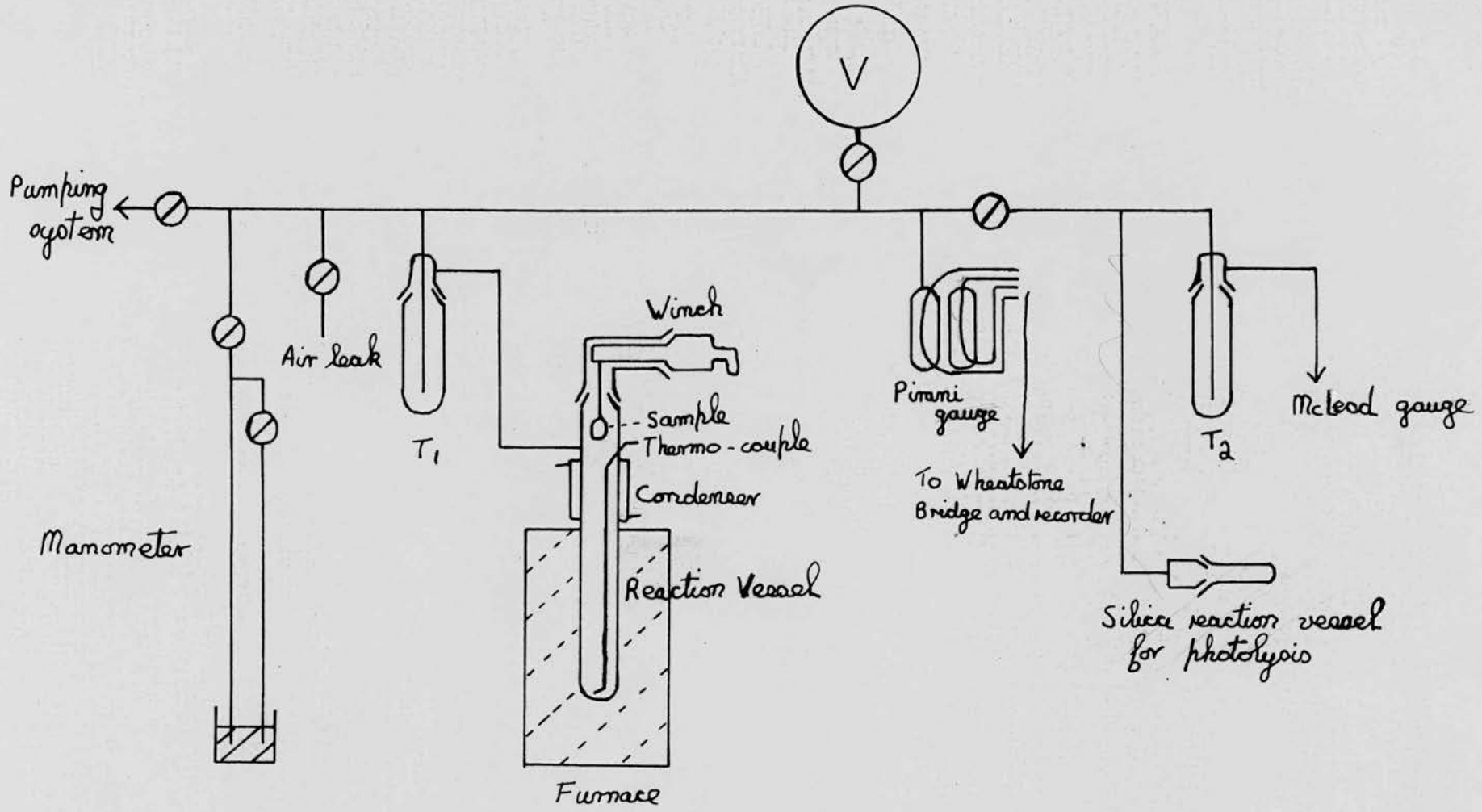

Apparatus for pressure measurements

Fig. Ia.

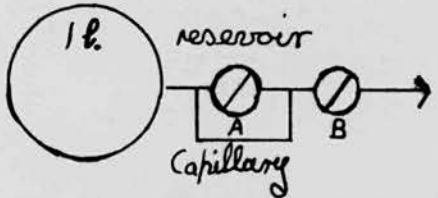

Apparatus for diffusion measurements

Fig I b.

0.001 mv on a Tinsley potentiometer type 3184D.

The gases from the reaction vessel passed through trap T_1 into the vacuum line. V consisted of three bulbs any of which could be connected to the vacuum line to give pressures in the desired range. The pressures were measured by a McLeod gauge measuring from 10^{-3} μ to 1.6×10^2 μ.

In section II experiments on potassium permanganate were carried out in an identical apparatus, but using a pressure gauge of the compensating Pirani type. It was operated at constant voltage by a Wheatstone bridge method, the out of balance voltage being fed, through a shunt into a Sunvic recorder. A linear response was obtained up to 10^2 μ, the gauge being calibrated against a standard McLeod gauge.

The volume of each section of the system was found by expanding a known pressure of dry air from a known volume, through the air leak into each section, and measuring the resultant pressure on the manometer. From Boyle's law the volume of each section was calculated, small volumes, where necessary, being calculated from their dimensions. The volumes given in Table I are the mean of three determinations and were obtained with the reaction vessel and both traps at room temperature. The pressures read on the McLeod or Pirani gauges were converted to pressures at 273°K by a correction factor calculated from the respective volumes and temperatures, of the reaction vessel, of the cold traps and of the remaining volume of the system.

Table I

Section of Thesis	Section of system	Mean volume c.c.	$\frac{p\ 273^{\circ}K}{p\ \text{measured}}$ = correction factor
I	Reaction line + T_1 + T_2	608	1.00
	McLeod gauge	376	
	Bulb 1	1100	-
	Bulb 2	2303	-
	Bulb 3	2335	-
	Total volume (added)	6722	0.94
II	Reaction line + T_1 + T_2	369	1.38
	McLeod gauge	230	-
	Total volume (added)	599	1.23

The pumping system consisted of a glass two stage mercury diffusion pump, backed by a Speedivac rotary oil pump, the unit giving a vacuum of 10^{-3} μ. Apieson 'L' grease was used for all joints and taps.

Rate of diffusion of air through the apparatus.

An attempt was made to find the maximum rates of gas evolution from the reaction vessel that could be measured on the McLeod gauge, without correction having to be applied for diffusion effects. The apparatus shown in Fig. Ia was adapted with that shown in Fig. Ib substituted for the winch. The rate of flow through the

capillary into the apparatus was controlled by the pressure in the reservoir, and the pressure in the apparatus adjusted to what was required. With tap A closed and tap B open gas (air) was allowed to flow for 3 min., tap B then closed and the pressure P_I in the McLeod gauge read. After 5 min. the pressure P_F was again measured, $P_I - P_F$ is the error due to diffusion. The rates and pressures were varied and the following conclusions were drawn.

With bulb V closed and with the maximum rates encountered experimentally, there was no measurable difference between P_I and P_F. With the bulb V open and a rate of 3 μ min^{-1}, when the initial pressure in the apparatus was 50 μ, $P_I - P_F$ was 1 μ. This represented the extreme experimental conditions and resulted in an error of 2%. For the fast runs no correction was made for this error.

As $P_I > P_F$, the gases entered the McLeod gauge before the volume bulbs and generally for a given rate the lowering of the initial pressure increased the error. These results were obtained with the furnace on and the cold trap 1 surrounded by liquid nitrogen; when the cold trap was removed the error was doubled due to temperature effects.

Experimental procedure.

With the weighed crystals (10 - 20 mg) in the platinum bucket the total volume was pumped out overnight, a vacuum of 10^{-3} μ being obtained. The system was isolated from the pumps and the taps to the volume bulbs closed. If after an hour the pressure remained below 10^{-2} μ, the sample was lowered into the furnace so that it

made good contact with the bottom of the pocket containing the thermocouple. The thermocouple indicated a maximum heating up time of 5 min and gave no evidence of self heating of the crystals during decomposition.

With liquid nitrogen surrounding T_1, the McLeod gauge measured the pressure of oxygen evolved during the decomposition, readings being taken every five minutes. When the pressure reached ca 10^2 μ the total volume of the system was used. The final pressure was recorded at least one hour after the apparent end point had been attained.

2. 3. Growth of Crystals

Analar potassium metaperiodate was used as the initial material. Due to its low solubility (ca 6 g. $l.^{-1}$ at 20°C), difficulties were encountered in producing crystals of suitable size. The effect on a saturated solution of stirring during cooling, of the rate of cooling and evaporation, and of the time of growth, were investigated. The following procedure was finally adopted.

A saturated solution of the salt was prepared at 60°C from ca 6 g. and 600 ml. of dust-free distilled water, allowed to come to equilibrium at room temperatures, and then decanted into a 9 inch crystallising dish. This solution was evaporated slowly at room temperature in a draught of air, over a period of a month, fresh mother liquor being added occasionally to keep the volume ca 500 ml. The resulting crystals were dried and sieved. The largest crystals that were reasonably free from visible imperfections, such as steps on the crystal faces and occlusions, were used in the

experiments. They passed through the British Standard sieve of mesh number 52 and were held by number 60, therefore they had linear dimensions of ca 250 - 300 μ. 1 g. of crystals of these dimensions were obtained from six sets of evaporations as described above and are referred to as 'large' crystals.

'Small' crystals, that appeared under the microscope to be free from obvious imperfections, were made by the rapid cooling of a saturated solution from 90°C to room temperature. The crystals, that passed through a 300 mesh sieve, and thus had linear dimensions < 50 μ, were used in the experiments. As the crystals did not readily pass through the sieve, and were visible under the microscope their linear dimensions were taken as ca 40 μ.

The following batches of material were prepared by the above procedures.

Large crystals

Material A made in diffuse light.

B material A after storage for 18 months.

C repeat of material A but made in the dark.

D material C after pre-irradiation with u.v. light as subsequently described (2. 4.).

E similar to material A but stored for 12 months.

Small crystals

F made as described.

G material F after storage for 24 months.

H repeat of material F.

K material H after pre-irradiation with u.v. light.

The above material was stored, until required, in the dark, in a vacuum desiccator over calcium chloride. It was experimentally determined that 300 mg. of crystals dried at 110°C for a week lost <0.03 mg. in weight. Thus the water content was less than 0.01%.

The kinetic experiments performed on material A and F were started immediately after the preparation of the crystals, and extended over a period of four months, but for material C and H the experiments were concluded within three weeks.

2. 4. Effect of ultraviolet irradiation and electron bombardment

The small photolytic decomposition of potassium metaperiodate, was measured using the apparatus shown in Fig. Ia. The tap between the thermal reaction vessel and the McLeod gauge was closed making the volume of the system used 500 ml. The source of the ultraviolet light was a 300 w Hanovia mercury lamp, placed 8 cm. from the vitreous silica tube. To avoid thermal effects a copper sulphate solution contained in a silica vessel was interposed between the lamp and the silica tube; this ensured that the temperature of the tube did not rise above 35°C.

Crystals were spread in a layer in the silica tube and this was attached to the apparatus. With liquid nitrogen surrounding T_2, and when a vacuum of 0.1 μ was held for 10 h., the irradiation was begun. The increase in pressure was measured over a period of 20 h. using the McLeod gauge. This procedure was repeated with crystals of varying sizes. It was concluded that the rate of evolution of gas varied with the surface area exposed to

irradiation and that the rate, corrected for a slight blank rate, was ca 0.004 μ h^{-1} cm^{-2} in the 500 ml. This represents ca 1 x 10^{-10} mole of oxygen h^{-1} cm^{-2}.

After 10 h. irradiation the crystals were noticeably yellow. The colour could be destroyed by heating for 30 sec. at 550°K, or 2 h. at 370°K, or by the effect of daylight for 3 months at room temperature.

Material C, fresh large crystals, and H fresh small crystals were pre-irradiated for 18.5 h. under conditions similar to those used in the photolytic experiments. In this case the silica tube was shaken every ½ h. to expose fresh surfaces. The pre-irradiated material is designated D and K respectively.

It was not possible to estimate directly the volume of oxygen liberated in the above experiments due to the necessity to shake the tube, but this was found from the known rate of photolytic decomposition, and the size of the crystals. The fractional decomposition 'α' after 18.5 h. irradiation for material D was ca 5 x 10^{-5} and for material K was ca 35 x 10^{-5}.

Microscopic examination of the crystals before and after irradiation failed to show any observable differences, apart from the slight yellow coloration, although the subsequent thermal decomposition (2.6) was radically altered.

Sawkhill[45] in a detailed study of the effects of an electron beam on silver azide showed that after decomposition only silver remained and it was in two forms, randomly orientated as shown by the rings on the diffraction photograph, and highly orientated as shown by the intense arcs on the rings.

The effect of an electron beam on potassium metaperiodate was observed employing a Metropolitan Vickers Electron microscope 6. Using 50 kvolt potential and a tube current of 100 μ amp., the electrons were focused on a single crystal of ca 1 μ linear dimensions and a diffraction photograph taken.

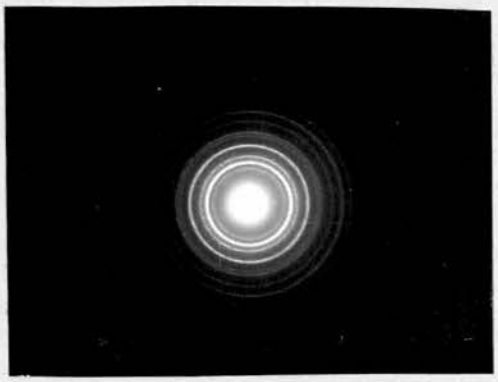

It can be seen from the photograph that sets of rings were obtained. The two strong reflections (rings two and four as counted from the centre), are due to the (100) and (110) crystal planes in KIO_3 as deduced from the structure given by Smith[46], while the first and third rings are probably due to the (111) and (110) planes of KIO_4[47]. Diffraction photographs during the decomposition of crystals ca 0.1 μ showed rings of ca 100 spots. This is to be expected because a crystal of 0.1 μ will give rise to fewer particles than one of 1 μ. These photographs clearly show that potassium metaperiodate decomposes in an electron beam and breaks up into randomly oriented parts.

2. 5. Visual observations of the decomposition

When crystals of material A were heated (2° - 3°/min) in air on a hot-stage microscope, white diffuse opaque centres developed, (510° - 520° K) at visible imperfections in the crystals, and by 550° K these had spread throughout the crystals. At 570° K the crystal broke into two or three fragments, and with the rising temperature there was rapid decrepitation. The direction of the cracking and splintering was random and bore no relationship to the crystal axes. Above 580° K no further changes were noted, the small fragments being white and opaque.

Small crystals became gradually white in colour, but there was no sign of decrepitation. They retained their original crystal form at the end of the decomposition.

By the use of a vapour bath in place of the furnace (Fig. Ia) and a glass bucket substituted for the platinum one, a continuous observation was made on the decomposition as it progressed at a fixed temperature. For the unirradiated crystals dimethyl phthalate boiling at 553° K was used as the liquid in the vapour bath and for the irradiated crystals ethyl cinimate boiling at 543° K.

For the large crystals A, with reference to graph I, over the stage O - A (α = 0.0 - 0.003), there was a steady but infrequent fragmentation. For A - B (α = 0.003 - 0.006) occasional fragmentation occurred but at a quarter of the rate for OA. At the end of this stage the crystals appeared to be mainly opaque, and 90% of them were structurally intact.

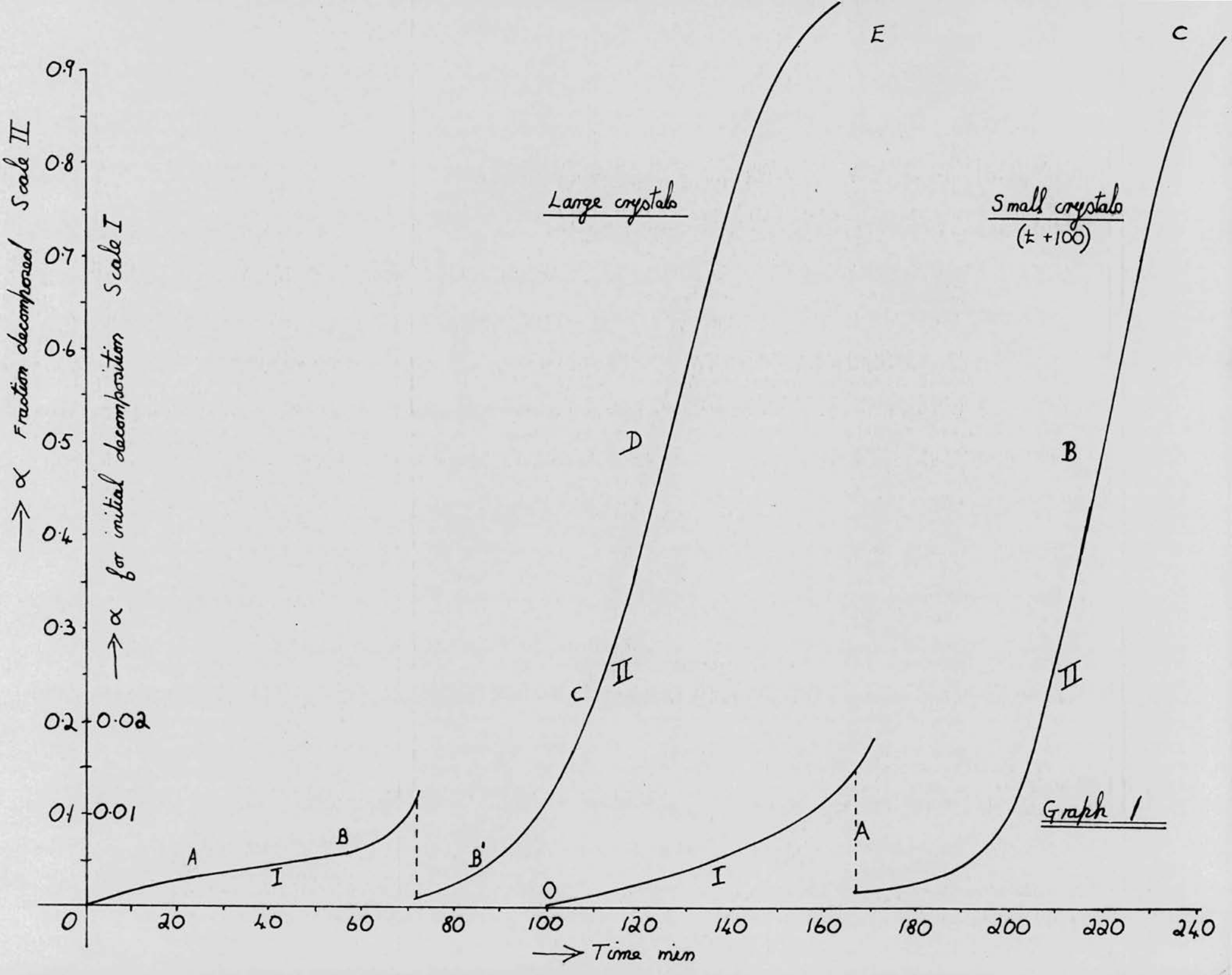
E
C
Large crystals
Small crystals
(± +100)
D
B
C
II
II
A
B
B'
O
A
I
I
Graph 1
0.9
0.8
0.7
0.6
0.5
0.4
0.3
0.2
0.1
0
0.02
0.01
→ α Fraction decomposed Scale II
→ α for initial decomposition Scale I
0
20
40
60
80
100
120
140
160
180
200
220
240
→ Time min

Vigorous decrepitation was observed for the acceleration stage B - C (α = 0.01 - 0.30), but following this there were no further signs of fragmentation.

For the large pre-irradiated crystals D, the vigorous decrepitation did not begin until α = ca 0.03, and for the intermediate stage B - B^1 the rate of fragmentation was the same as for OA; at B^1 some crystals were still intact.

The size distribution of the fragments at the end of the decomposition showed that 30% were less than 50 μ, 60% between 50 and 150 μ and 10% greater than 150 μ. It will be noted that the average dimension of these particles is greater than that of the small crystals.

It is apparent that the clouding of the crystals as decomposition progresses is due to the formation of potassium iodate.

2. 6. Kinetics of the decomposition

Kinetic measurements were carried out on material A - K (2.3.) as described in the experimental procedure (2.2). The α-time curves were of the general form shown in graph 1 and were analysed in terms of the following relationships between α and t, where α is the ratio of the pressure at time t, to the final pressure. Thus α represents the fraction of the material decomposed at time t.

Large crystals; material A B C D and E:

The linear relationship between α and t, section AB, was represented by $\frac{d\alpha}{dt} = k_1 = R_L$, with α_L the fraction decomposed at B the end of the linear stage, which occurred at ca $\alpha = 0.005$.

For the large pre-irradiated material D the section BB^1 of the curve fitted a power law with $n = 4$, $(\alpha - \alpha_L) = k_4(t - t_o)^4$, where t_o is the time at the start of the mechanism. From a plot of $(\alpha - \alpha_L)^{\frac{1}{4}}/t$ the constants $k_4^{\frac{1}{4}}$ and t_o are obtained.

The acceleration stage, BD in the case of unirradiated material and B^1D for irradiated material, is adequately fitted by the Prout-Tompkins equation corrected for the initial decomposition α_L,

$$\log_{10} \frac{\alpha - \alpha_L}{1 - \alpha} = \frac{k}{2.3}t + C_1.$$

The decay stage of the reaction DE is described in terms of a contracting sphere mechanism,

$$\alpha = 1 - \left[C_2 - k_3(t - t_o)\right]^3$$

where t_o is the time at the start of the mechanism and C_2 and k_3 are constants. A plot of $(1 - \alpha)^{\frac{1}{3}}/t$ gives the constant k_3. This equation is discussed later.

Small crystals; material F G H and K:

The first 2 - 3% of the reaction, stage OA, is fitted by a power law with n = 2, $\alpha = k_2(t - t_o)^2$. The factor $\alpha^{\frac{1}{2}}$ is plotted against 't' to give the constant $k_2^{\frac{1}{2}}$.

The acceleration stage AB and decay stage BC are fitted by Prout-Tompkins equation and the contracting sphere equation respectively, as for the large crystals. Generally the decay stage began at α = 0.5.

The following tables and graphs show a cross section of the runs performed at various temperatures in the range 529° - 561° K. The tables give the respective functions of α as required by the above analysis and the graphs show the plots of the different functions.

An alternative analysis for the acceleration stage is that of a power law with n = 3, and so included in the tables is the function $\alpha^{\frac{1}{3}}$. The merits, graphical and kinetic, of this equation compared with the Prout-Tompkins equation, are discussed in section 3.

The following abbreviations have been used in the subsequent tables:

$$\underline{PT} = \log_{10} \frac{\alpha}{1-\alpha} \; ; \quad \underline{PT_L} = \log_{10} \frac{\alpha - \alpha_L}{1-\alpha} \; ; \quad \underline{PT_P} = \log_{10} \frac{\alpha - \alpha_P}{1-\alpha} \; ;$$

$$\underline{\alpha_L^{\frac{1}{3}}} = (\alpha - \alpha_L)^{\frac{1}{3}} \; ; \quad \underline{\alpha_P^{\frac{1}{3}}} = (\alpha - \alpha_P)^{\frac{1}{3}} \; ; \quad \underline{\alpha_L^{\frac{1}{4}}} = (\alpha - \alpha_L)^{\frac{1}{4}} \; ,$$

where α_L is as previously given and α_P is the fractional decomposition at the end of the initial power law growth.

In 2.6.6. the constants k_x are tabulated for the various runs together with the respective Arrhemies activation energy plots.

2. 6. 1. Kinetic results for large crystals A and B

Tables 2, 3, 4 and 5 and graphs 2, 3, 4, 5 and 6 illustrate the effect of 18 months ageing on large crystals. Material A is fresh crystals, and B is the same material after storage for 18 months. The most notable features are, the much increased rate for the acceleration stage, and the onset of the decay stage at $\alpha = 0.2$ for the aged material compared with $\alpha = 0.5$ for the unaged. The pre-acceleration, linear stage AB, starts at ca $\alpha = 0.002$ and continues to $\alpha = 0.005$; this is little affected by ageing.

Tables 2 and 3, analysis of material A.

Tables 4 and 5, analysis of material B.

Graphs 2 and 3, the α - t curves for material A and B respectively.

Graph 4a and b, linear stage, the α - t curves showing the pre-acceleration stage of the decomposition for material A and B.

Graph 5, acceleration stage, plot of Prout-Tompkins factor for material A and B.

Graph 6, decay stage, plot of the contracting sphere factor for A and B.

Table 2. Material A. Large crystals.

Run		A2				A12		
Temp		555.2°K				551.2°K		
α_L		0.0055				0.006		
Time min	$\alpha \times 10^2$	PT_L	$\alpha_L^{\frac{1}{3}}$	$(1-\alpha)^{\frac{1}{3}}$	$\alpha \times 10^2$	PT_L	$\alpha_L^{\frac{1}{3}}$	$(1-\alpha)^{\frac{1}{3}}$
10	0.08				0.15			
15	0.12				0.22			
20	0.24				0.27			
25	0.32				0.32			
30	0.37				0.36			
35	0.42				0.41			
40	0.48				0.45			
45	0.55				0.49			
50	0.74	0.95			0.53			
55	0.90	1.66	0.16		0.59			
60	1.77	2.09	0.23		0.66	0.81	0.087	
65	3.41	2.47	0.31		0.78	1.20	0.117	
70	6.33	2.79	0.39		0.93	1.44	0.140	
75	10.5	3.04	0.46		1.42	1.88	0.203	
80	17.7	3.32	0.55	0.94	2.21	2.21	0.252	
85	26.5	3.54	0.64	0.90	3.44	2.47	0.305	
90	37.0	3.76	0.71	0.86	5.01	2.66	0.353	
95	52.1	4.03	0.80	0.79	7.76	2.88	0.415	
100	65.1	4.26	0.86	0.71	11.4	3.08	0.476	
105	79.9	4.57	0.93	0.59	15.5	3.24	0.530	0.95
110	88.3	4.85	0.96	0.50	21.9	3.43	0.597	0.93
115	94.4	5.23	0.98	0.40	29.3	3.62	0.664	0.89
120					38.1	3.78	0.721	0.86
125					47.2	3.94	0.775	0.81
130					58.0	4.13	0.831	0.75
135					68.0	4.32	0.877	0.69
140					77.6	4.52	0.916	0.61
145					87.8	4.83	0.955	0.50
150					94.6	5.24	0.982	0.38

Table 3.

Run		A21			A26	A34	A46
Temp		545.5°K			540.9	535.7	530.4°K
α_L		0.006			0.005	0.004	0.004
Time min	$\alpha \times 10^2$	PT_L	$\alpha_L^{\frac{1}{3}}$	$(1-\alpha)^{\frac{1}{3}}$	$\alpha \times 10^2$	$\alpha \times 10^2$	$\alpha \times 10^2$
10	0.15				0.07	0.05	0.02
20	0.24				0.15	0.10	0.06
30	0.32				0.18	0.11	0.09
40	0.37				0.23	0.14	0.12
50	0.42				0.26	0.18	0.15
55	0.44				0.28	0.21	0.15
60	0.47				0.30	0.21	0.16
65	0.49				0.32	0.22	0.17

Table 3 continued

Time min	$\alpha \times 10^2$	A21 PT_L	A21 $\alpha_L^{\frac{1}{3}}$	$(1-\alpha)^{\frac{1}{3}}$	A26 $\alpha \times 10^2$	A34 $\alpha \times 10^2$	A46 $\alpha \times 10^2$
70	0.52				0.33	0.23	0.18
80	0.59				0.37	0.25	0.20
90	0.68				0.40	0.27	0.21
100	0.86				0.43	0.30	0.22
110	1.53	1.96	0.209		0.47	0.32	0.23
120	3.46	2.47	0.305		0.51	0.34	0.25
125	4.70	2.63	0.344		0.55	0.36	
130	5.89	2.75	0.375		0.59	0.37	0.26
135	8.0	2.88	0.423		0.64	0.38	
140	10.4	3.04	0.461		0.72	0.40	0.27
145	13.1	3.16	0.500		0.85	0.42	
150	16.5	3.26	0.542		0.97	0.43	0.28
155	20.3	3.38	0.580		1.29	0.45	
160	24.2	3.49	0.618		1.73	0.48	0.30
165	30.4	3.61	0.662		2.26	0.51	
170	36.0	3.72	0.703	0.87	2.94	0.53	0.31
175	41.3	3.84	0.741	0.84	3.57	0.55	
180	47.9	3.95	0.779	0.81	4.73	0.59	0.33
185	52.9	4.04	0.806	0.79	5.85	0.62	
190	59.8	4.17	0.840	0.74	7.30	0.64	0.34
195	65.8	4.28	0.870	0.70	9.2	0.69	
200	71.8	4.41		0.66	11.5	0.75	0.35
205	76.9	4.52		0.62	14.2	0.81	
210	82.0	4.66		0.56	17.4	0.93	0.36
215	85.7	4.78		0.52	19.8	1.08	
220	89.2	4.90		0.48	23.5	1.26	0.38
225	91.2	5.02		0.43	27.0	1.66	
230	95.0	5.28		0.37	30.9	2.10	0.40
235					34.5	2.6	0.41
240					38.0	3.1	0.42
245					43.2	3.7	0.43
250					47.8	4.6	0.46
255					52.0	5.6	0.47
260					57.5	6.1	0.48
265					61.0	7.7	0.50
270					65.9	8.8	0.52
275					68.9	10.2	0.55
280					73.0	12.0	0.56
285					77.2	13.6	0.58
290					80.2	15.8	0.63
295					82.6	18.2	0.67
300					85.6	20.9	0.70
310					92.2	25.0	0.83
320						30.4	1.00
330						37.0	1.20
340						43.2	1.70

Table 4. Material B, aged material A.

Run	B1			B6			
Temp	542.5°K			539.6°K			
α_L	0.0055			0.0042			
Time min	$\alpha \times 10^2$	PT_L	$(1-\alpha)^{\frac{1}{3}}$	$\alpha \times 10^2$	PT_L	$\alpha_L^{\frac{1}{3}} \times 10$	$(1-\alpha)^{\frac{1}{3}}$
5	0.04			0.01			
10	0.06			0.04			
15	0.10			0.07			
20	0.11			0.11			
25	0.14			0.13			
30	0.17			0.15			
35	0.19			0.17			
40	0.23			0.18			
45	0.26			0.20			
50	0.29			0.23			
55	0.32			0.25			
60	0.34			0.26			
65	0.37			0.29			
70	0.40			0.31			
75	0.43			0.33			
80	0.45			0.35			
85	0.47			0.36			
90	0.52			0.38			
95	0.59			0.40			
100	0.67			0.42			
105	0.77	1.35		0.44			
110	0.98	1.63		0.47			
115	1.61	2.02		0.52			
120	3.47	2.46		0.58			
125	9.1	2.97	0.97	0.72			
130	17.5	3.31	0.94	0.91	1.69	1.7	
135	26.5	3.54	0.90	1.64	2.09	2.30	
140	36.3	3.75	0.86	3.07	2.42	2.98	
145	46.7	3.93	0.81	6.14	2.78	3.85	
150	55.0	4.09	0.76	11.2	3.08	4.76	0.96
155	64.8	4.26	0.71	19.0	3.36	5.71	0.93
160	70.8	4.37	0.66	26.7	3.55	6.41	0.90
165	75.9	4.49	0.62	34.8	3.72	7.01	0.87
170	81.0	4.61	0.575	43.0	3.87	7.53	0.83
175	84.3	4.71	0.54	50.4	4.00		0.79
180	85.2	4.74	0.53	59.7	4.17		0.74
185	88.0	4.85	0.49	67.1	4.30		0.69
190	89.8	4.94	0.47	70.8	4.38		0.66
195	91.7	5.04	0.44	76.6	4.51		0.62
200				80.4	4.61		0.58
205				84.5	4.73		0.54
210				85.7	4.77		0.52
215				88.0	4.83		0.49
220				89.2			0.48
225				91.5			0.44

Table 5. Material B, aged material A.

Run	B3				B2	B5		
Temp	538.0°K				537.5°K	545.5°K		
α_L	0.004					0.0045		
Time min	α x10^2	PT_L	$\alpha_L^{\frac{1}{3}}$ x10	$(1-\alpha)^{\frac{1}{3}}$	α x10^2	α x10^2	PT_L	$(1-\alpha)^{\frac{1}{3}}$
10	0.06				0.03	0.07		
20	0.10				0.07	0.18		
30	0.14				0.10	0.26		
40	0.18				0.13	0.33		
50	0.21				0.16	0.40		
60	0.25				0.18	0.46		
70	0.27				0.20	0.57		
80	0.30				0.23	0.73	1.45	
85	0.32				0.24	1.03	1.76	
90	0.34				0.26	2.80	2.37	
95	0.35				0.27	7.8	2.88	
100	0.36				0.29	17.5	3.31	0.94
105	0.37				0.29	30.2	3.63	0.89
110	0.39				0.31	42.0	3.85	0.83
115	0.41				0.32	53.7		0.78
120	0.43				0.34	63.0		0.72
125	0.46				0.36	71.9		0.66
130	0.50				0.39	78.6		0.60
135	0.55	1.17			0.41	82.7		0.56
140	0.66	1.41	1.37		0.46	85.9		0.52
150	1.17	1.92	2.00		0.62			
155	2.30	2.20	2.58		0.84			
160	4.10	2.48	3.30		1.3			
165	6.9	2.84	4.02		2.4			
170	11.6	3.10	4.82		5.34			
175	17.2	3.30	5.52	0.94	8.9			
180	23.7	3.51	6.16	0.915	14.0			
185	32.2	3.67	6.83	0.88	20.0			
190	37.4			0.86	26.9			
195	45.2			0.82	34.3			
200	52.5			0.785	41.9			
205	60.3			0.74	48.5			
210	65.0			0.705	55.0			
220	73.1			0.65	65.6			
225	76.8			0.615	70.8			
230	80.0			0.585	75.0			
235	81.8			0.57	78.0			
240	85.8			0.52	81.5			
245	86.8			0.51	83.5			
250	87.3							
255	89.7							
260	91.2							

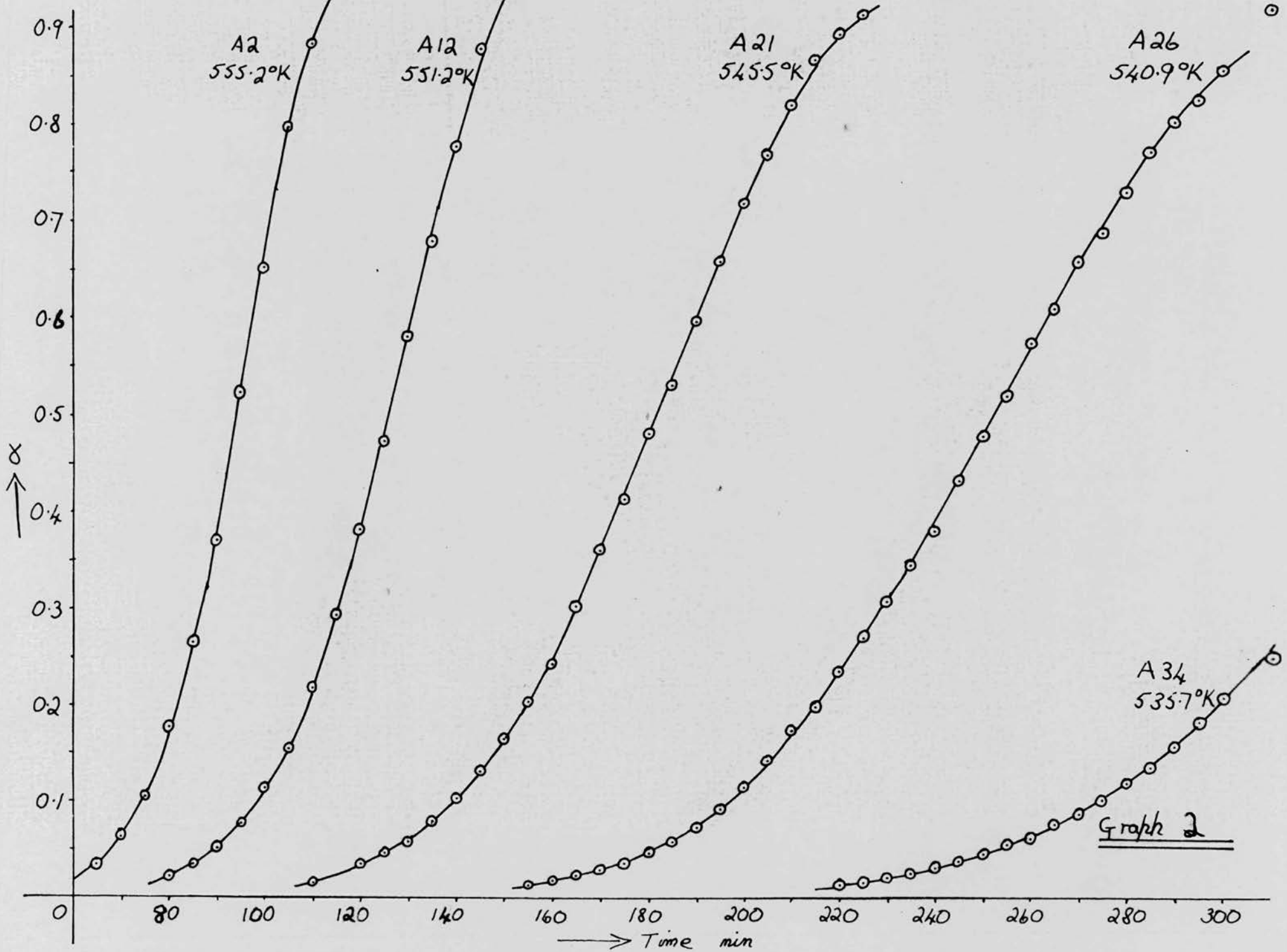
A2
555·2°K
A12
551·2°K
A21
545·5°K
A26
540·9°K
A34
535·7°K
0·9
0·8
0·7
0·6
0·5
0·4
0·3
0·2
0·1
0
x
80
100
120
140
160
180
200
220
240
260
280
300
Time min

Graph 2

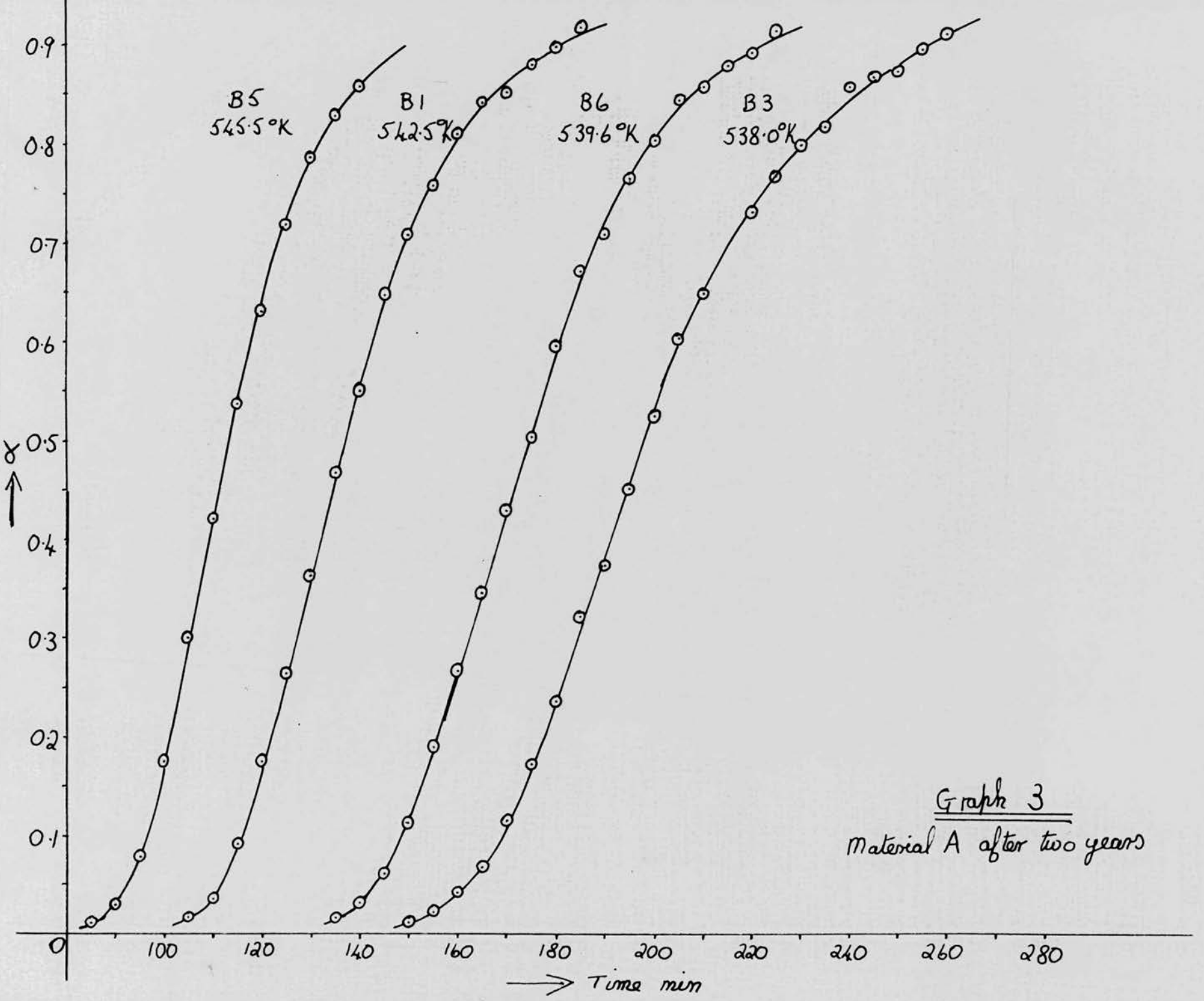

Graph 3

Material A after two years

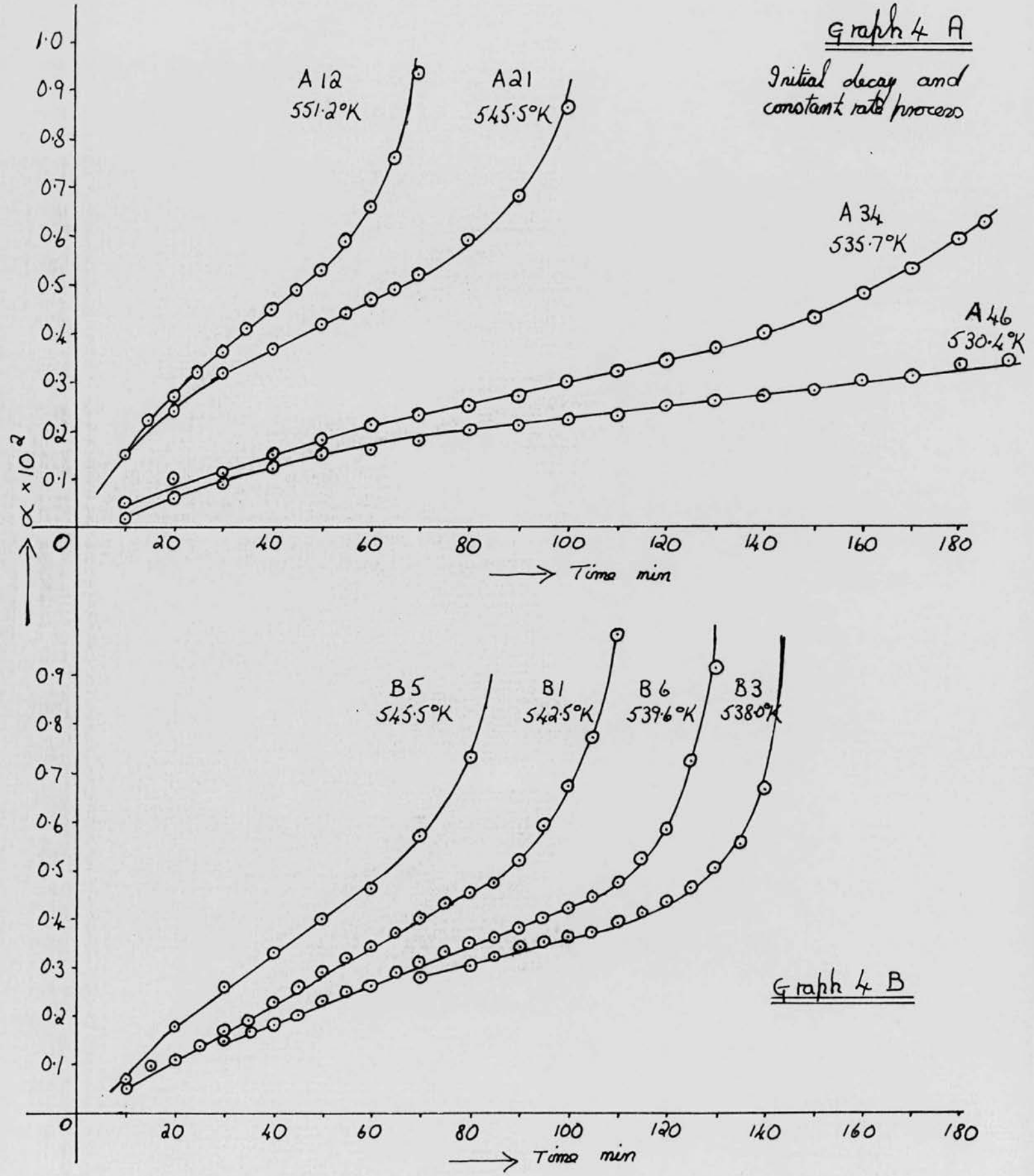
Graph 4 A
Initial decay and constant rate process
A 12
551·2°K
A21
545·5°K
A 34
535·7°K
A46
530·4°K
α × 10²
1·0
0·9
0·8
0·7
0·6
0·5
0·4
0·3
0·2
0·1
0
20
40
60
80
100
120
140
160
180
Time min
B5
545·5°K
B1
542·5°K
B6
539·6°K
B3
538·0°K
Graph 4 B

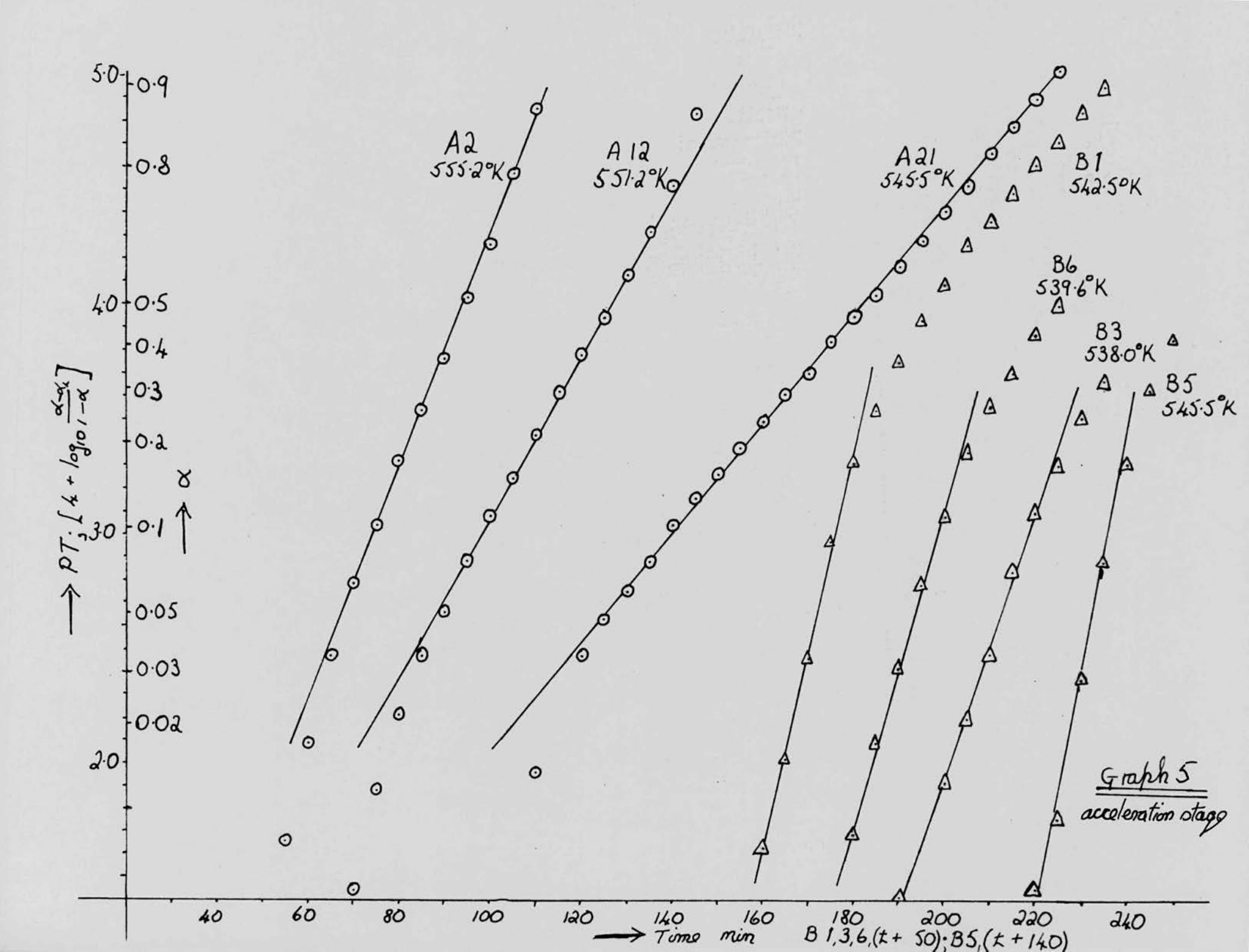
A2
555·2°K
A12
551·2°K
A21
545·5°K
B1
542·5°K
B6
539·6°K
B3
538·0°K
B5
545·5°K
5·0
4·0
3·0
2·0
0·9
0·8
0·5
0·4
0·3
0·2
0·1
0·05
0·03
0·02
α
40
60
80
100
120
140
160
180
200
220
240
Time min
B 1,3,6,(t + 50); B5,(t + 140)
Graph 5
acceleration stage

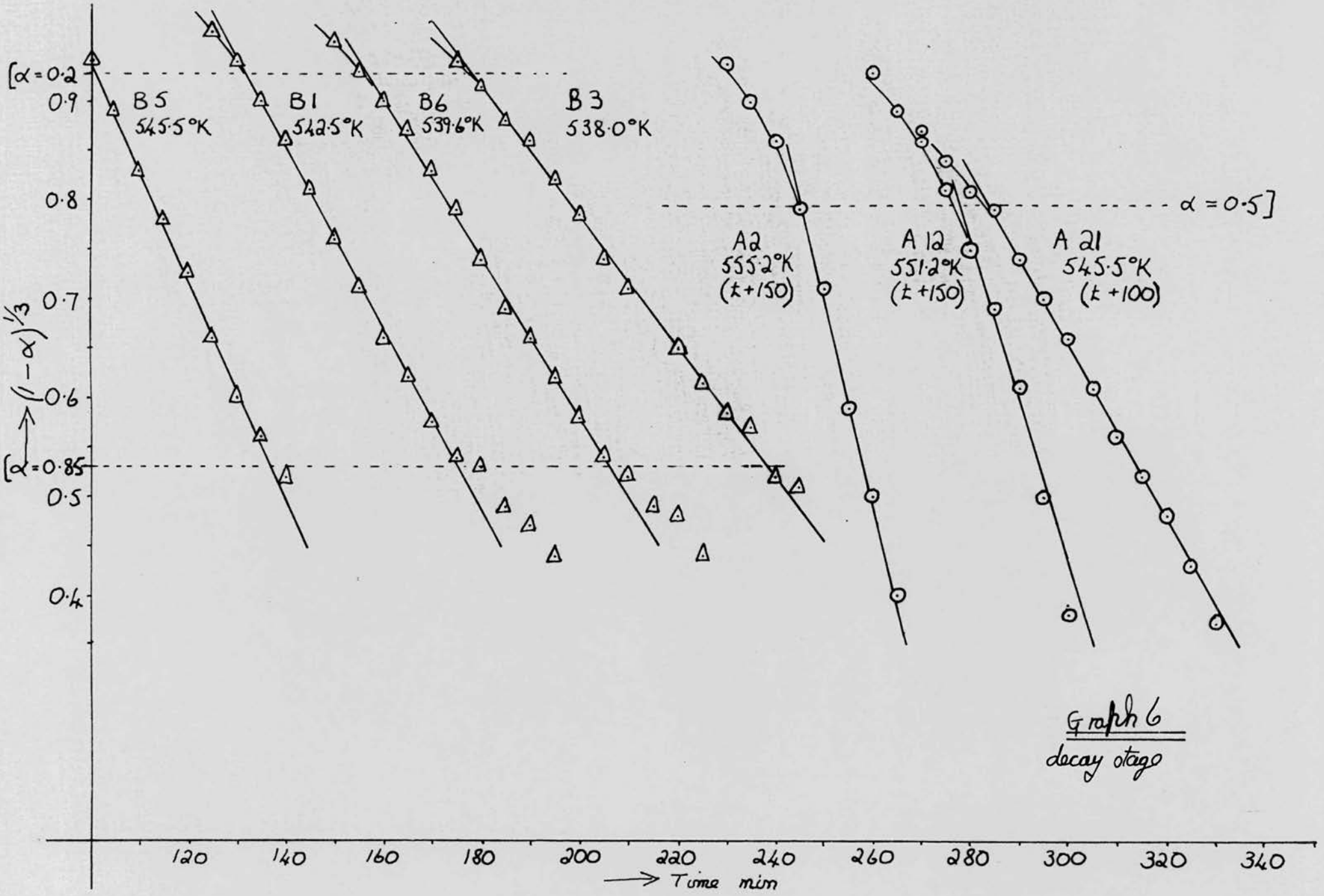

Graph 6

decay otago

2. 6. 2. Kinetic results for large crystals C and D

Tables 6, 7, 8, 9 and 10 and graphs 7, 8, 9, 10, 11 and 12 illustrate the effect of 18.5 h. pre-irradiation with u.v. on the large crystals. Material C is fresh crystals, a preparation similar to A and material D is C after 18.5 h. pre-irradiation. The most notable feature is the overall increase in rate for all the stages. The decay stage began at $\alpha = 0.4$ compared with $\alpha = 0.5$ for fresh material; and a power law growth has been introduced from $\alpha = 0.005$ to $\alpha = 0.04$, which precedes the acceleration stage. Material C is similar to A, but with a much superior fit for the Prout-Tompkins equation at low α's.

Tables 6, 7 and 8, analysis of material C.

Tables 9 and 10, analysis of material D.

Graph 7, 'α' - 't' curves for C and D.

Graph 8, linear stage, the 'α' - 't' curves for material C and D showing the pre-acceleration stage of the decomposition.

Graph 9, $\alpha^{\frac{1}{4}}/t$ for material D, showing the fit for the power law with n = 4.

Graph 10, acceleration stage, plot of Prout-Tompkins factor for material C.

Graph 11, acceleration stage, plot of Prout-Tompkins factor for material D. Note the positive deviation at low percentage decomposition due to the power law growth, which is not the case in the unirradiated material C.

Graph 12, decay stage, plot of contracting sphere factor for C and D.

Table 6. Material C. Large fresh crystals.

Run	C2				C4	
Temp	553.8°K				549.8°K	
α_L	0.0051				0.007	
Time min	$\alpha \times 10^2$	PT_L	$\alpha_L^{\frac{1}{3}}$	$(1-\alpha)^{\frac{1}{3}}$	$\alpha \times 10^2$	$(1-\alpha)^{\frac{1}{3}}$
5	0.04				0.10	
10	0.14				0.20	
15	0.24				0.26	
20	0.30				0.31	
25	0.35				0.36	
30	0.38				0.44	
35	0.42				0.48	
40	0.45				0.53	
45	0.48				0.59	
50	0.51				0.66	
55	0.56				0.73	
60	0.66	1.18	0.114		0.77	
65	0.87	1.56	0.153		0.86	
70	1.14	1.80	0.185		0.97	
75	1.72	2.08	0.230		1.06	
80	2.73	2.36	0.281		1.24	
85	5.64	2.73	0.372		1.44	
90	10.6	3.05	0.466		1.87	
95	20.1	3.39	0.581	0.923	2.25	
100	32.7	3.68	0.686	0.88	2.61	
105	50.6	4.00	0.797	0.79	3.51	
110	62.4	4.21	0.851	0.73	4.88	
115	77.1	4.51		0.62	6.83	
120	86.7	4.80		0.51	10.3	
125	93.0	5.12		0.41	15.4	
130					22.9	0.92
135					32.1	0.88
140					42.6	0.83
145					52.9	0.78
150					65.0	0.71
155					73.5	0.65
160					81.0	0.57
165					88.9	0.48
170					94.5	0.39

Table 7. Material C. Large fresh crystals.

Run				C5			
Temp				545.5			
α_L				0.006			
Time min	$\alpha \times 10^2$	PT_L	$\alpha_L^{\frac{1}{3}} \times 10$	$(1-\alpha)^{\frac{1}{2}}$	$(1-\alpha)^{\frac{1}{3}}$	$R \times 10^3$	A
10	0.04						
20	0.21						
25	0.26						
30	0.29						
35	0.32						
40	0.36						
45	0.39						
50	0.42						
55	0.44						
60	0.47						
65	0.50						
70	0.53						
75	0.57						
80	0.60						
90	0.69	1.00	1.00				
95	0.74	1.16	1.13				
100	0.82	1.31	1.28				
105	0.92	1.51	1.48				
110	1.04	1.64	1.64				
115	1.19	1.77	1.81				
120	1.42	1.91	2.02			0.54	6.7
125	1.69	2.04	2.22			0.74	6.4
130	2.15	2.24	2.60			0.88	6.3
135	2.59	2.35	2.80			1.16	6.7
140	3.32	2.45	3.01			1.66	7.0
145	4.25	2.58	3.32			2.46	6.3
150	5.91	2.75	3.75			3.52	6.4
155	8.06	2.91	4.21			4.82	6.3
160	10.8	3.06	4.67			6.5	6.5
165	14.9	3.22	5.23			8.8	6.8
170	19.9	3.38	5.78			11.2	7.2
175	25.9	3.53	6.31			12.7	7.5
180	31.8	3.66	6.78			14.3	7.8
185	40.3	3.82	7.35	0.77	0.84	15.2	8.8
190	48.6	3.96	7.83	0.72	0.80	15.8	9.3
195	55.3	4.08	8.18	0.67	0.77	16.0	9.9
200	63.0	4.22	8.54	0.61	0.72	16.0	10.1
205	70.2	4.36		0.55	0.67	15.0	10.4
210	78.0	4.53		0.47	0.61	13.5	10.8
217	86.2	4.77		0.37	0.52	10.0	11.9
220	89.0	4.89		0.33	0.50	9.0	11.7
225	92.3	5.07		0.28	0.42		
230	95.5	5.33			0.36		

Table 8. Material C. Large fresh crystals.

Run	C1	C9		C10		
Temp	544.2°K	540.5°K		542.1°K		
α_L	0.006	0.0056		0.005		
Time min	$\alpha \times 10^2$	$\alpha \times 10^2$	PT_L	$\alpha \times 10^2$	PT_L	$(1-\alpha)^{\frac{1}{3}}$
10	0.05	0.04		0.06		
20	0.19	0.15		0.13		
30	0.27	0.25		0.19		
40	0.34	0.30		0.24		
50	0.39	0.33		0.30		
60	0.42	0.36		0.33		
70	0.47	0.40		0.36		
80	0.51	0.43		0.40		
90	0.56	0.46		0.42		
100	0.62	0.50		0.47		
105	0.67	0.51		0.49		
110	0.71	0.54		0.50		
115	0.80	0.55		0.54		
120	0.91	0.57		0.57		
125	1.03	0.58		0.60		
130	1.23	0.61		0.64		
135	1.50	0.64		0.70		
140	1.75	0.68		0.77	1.43	
145	2.09	0.74		0.88	1.58	
150	2.37	0.80	1.35	1.01	1.71	
155	3.59	0.90	1.54	1.16	1.82	
160	4.44	1.00	1.64	1.36	1.93	
165	5.86	1.08	1.72	1.60	2.04	
170	7.9	1.20	1.81	1.90	2.15	
175	10.5	1.37	1.91	2.28	2.25	
180	14.1	1.53	1.99	2.60	2.32	
185	18.3	1.68	2.05	3.47	2.47	
190	23.2	2.44	2.27	4.30	2.60	
195	28.3	2.63	2.32	5.60	2.74	
200	35.9	3.08	2.40	7.74	2.89	
205	42.9	3.63	2.49	10.4	3.04	
210	48.5	4.52	2.60	12.4	3.14	
215	55.6	5.56	2.71	16.6	3.28	
220	63.2	6.95	2.83	20.3	3.40	
225	69.2	8.6	2.93	24.9	3.51	
230	74.3	10.9	3.06	29.6	3.61	
235	80.8	13.6	3.17	35.1	3.72	0.868
240	87.0	16.5	3.28	40.3	3.82	0.848
245	88.9	19.9	3.38	47.4	3.95	0.810
250	93.5	23.7	3.48	53.7	4.06	0.776
260		33.0	3.68	63.5	4.23	0.718
270		42.6	3.86	74.2	4.45	0.641
280		52.3	4.03	82.8	4.67	0.561
290		62.0	4.21	89.5	4.92	0.472
300				93.3	5.14	0.406

Table 9. Material D. Fresh large pre-irradiated crystals.

Run	D3				D2				D1			
Temp	538.5°K				535.4°K				541.8°K			
α_L	0.006				0.0045				0.0052			
Time min	$\alpha \times 10^2$	$\alpha \times 10^2$	PT_L	$\alpha_L^{\frac{1}{4}} \times 10$	$\alpha \times 10^2$	PT_L	$\alpha_L^{\frac{1}{4}} \times 10$	$\alpha_p^{\frac{1}{3}} \times 10$
5	0.03	0.03			0.04			
10	0.08	0.08			0.11			
15	0.17	0.16			0.19			
20	0.20	0.17			0.26			
25	0.25	0.20			0.30			
30	0.29	0.23			0.36			
35	0.33	0.26			0.40			
40	0.37	0.30			0.47			
45	0.40	0.34			0.52			
50	0.44	0.36			0.59			
55	0.49	0.39			0.63			
60	0.54	0.42			0.75		2.2	
65	0.58	0.44			0.92			
70	0.62	0.48			1.14	1.79	2.8	
75	0.70	0.54			1.37	1.93	3.0	
80	0.81	0.61		2.0	1.68	2.06	3.3	
85	0.94	0.66			2.15	2.21	3.6	
90	1.09	0.76		2.4	2.77	2.35	3.9	
95	1.24	0.85			3.65	2.49	4.2	
100	1.51	0.92		2.6	5.87	2.75	4.8	2.9
105	1.77	1.07			10.0	3.03	5.6	4.0
110	2.17	1.24		3.0	18.6	3.34	$(1-\ )^{\frac{1}{3}}$	5.3
115	2.60	1.43			31.1	3.64	0.88	6.5
120	3.26	1.66		3.3	43.2	3.87	0.83	7.35
125	4.61	1.98	2.18		56.0	4.10	0.76	8.1
130	7.9	2.30	2.27	3.7	69.5	4.35	0.67	
135	10.5	2.72	2.36		77.7	4.53	0.61	
140	17.2	3.23	2.44	4.1	83.5	4.69	0.55	
145	25.8	4.52	2.63		87.5	4.82	0.50	
150	36.9	5.46	2.73	4.7				
155	46.7	6.83	2.83	5.0				
160	55.6	9.45	2.99					
165	65.1	14.2	3.20					
170	73.0	19.7	3.38	$(1-\ )^{\frac{1}{3}}$				
175	78.0	26.9	3.56	0.90				
180	82.3	35.0	3.74	0.87				
185	85.1	44.1	3.89	0.82				
190	86.5	52.0	4.04	0.77				
195	89.4	59.9	4.17	0.74				
200	91.5	67.2	4.30	0.69				
205		73.6	4.43	0.64				
210		77.2	4.54	0.61				
215		81.4	4.63	0.57				

Table 10. Material D. Fresh large pre-irradiated crystals.

Run	D6					D4			D5		
Temp	531.0°K					529.0°K			532.6		
α_L	0.0055					0.0045			0.005		
Time min	α x10^2	α x10^2	PT_L	$\alpha_L^{\frac{1}{4}}$ x10	$\alpha_P^{\frac{1}{3}}$ x10	α x10^2	PT_L	$(1-\alpha)^{\frac{1}{3}}$			
10	0.06	0.09				0.08					
20	0.13	0.15				0.18					
30	0.16	0.18				0.20					
40	0.20	0.23				0.25					
50	0.24	0.27				0.29					
60	0.28	0.32				0.33					
70	0.33	0.34				0.38					
80	0.37	0.38				0.43					
90	0.42	0.41				0.47					
100	0.45	0.45				0.53					
110	0.50	0.50				0.62					
120	0.55	0.56		1.83		0.74					
130	0.63	0.63		2.05		0.86					
140	0.74	0.70		2.25		1.08					
150	0.86	0.79		2.41		1.30					
160	1.02	0.90		2.61		1.68					
170	1.26	1.06		2.79		2.20					
180	1.53	1.24		2.98		3.07					
190	1.96	1.47		3.18		4.00	2.58				
200	2.80	1.74		3.38		5.85	2.73				
205	3.04	1.93				7.16	2.85				
210	3.48	2.12		3.59		8.65	2.95				
215	3.78	2.36				13.5	3.17				
220	4.32	2.57		3.82		18.0	3.33				
225	5.13	2.94				23.6	3.48				
230	6.28	3.22		4.07		30.3	3.63	0.89			
235	8.0	3.66				36.0	3.75	0.86			
240	10.4	4.22	2.59	4.40		43.0	3.87	0.83			
245	14.0	4.83	2.65		2.40	49.7	3.99	0.795			
250	17.7	5.51	2.73	4.74	2.71	55.4	4.09	0.76			
255	23.0	6.67	2.82		3.18	62.0	4.21	0.724			
260	28.4	8.4	2.94		3.67	66.2	4.29	0.70			
265	34.1	9.9	3.01		4.02	71.5	4.39	0.66			
270	39.7	12.6	3.14		4.51	75.5	4.49	0.63			
275	45.0	15.6	3.25	$(1-\ )^{\frac{1}{3}}$	4.96	78.6	4.56	0.60			
280	51.1	18.8	3.35		5.36	81.4	4.64	0.57			
285	55.8	23.6	3.48	0.914	5.88	84.1	4.72	0.54			
290	62.1	27.5	3.56	0.90	6.28						
300	71.0	37.0	3.76	0.855	6.94						
310	77.7	47.3	3.95	0.81	7.60						
320	84.0	58.1	4.13	0.75							
330	88.0	65.9	4.28	0.70							
340	91.0	74.3	4.44	0.64							
350		79.1	4.58	0.59							
360		84.5	4.66	0.54							

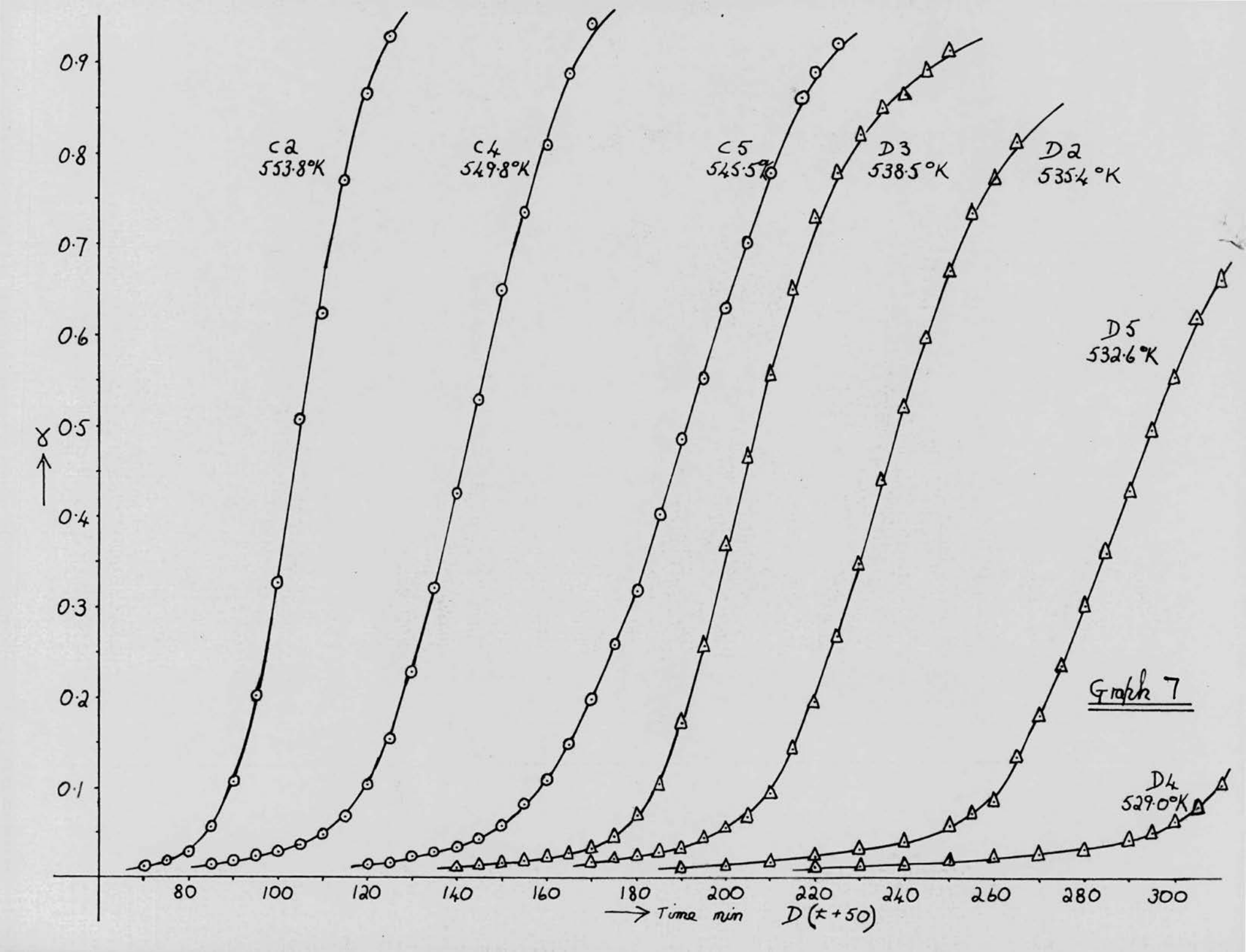
C2
553·8°K
C4
549·8°K
C5
545·5°K
D3
538·5°K
D2
535·4°K
D5
532·6°K
D4
529·0°K
Graph 7
y
0·9
0·8
0·7
0·6
0·5
0·4
0·3
0·2
0·1
80
100
120
140
160
180
200
220
240
260
280
300
Time min
D (t + 50)

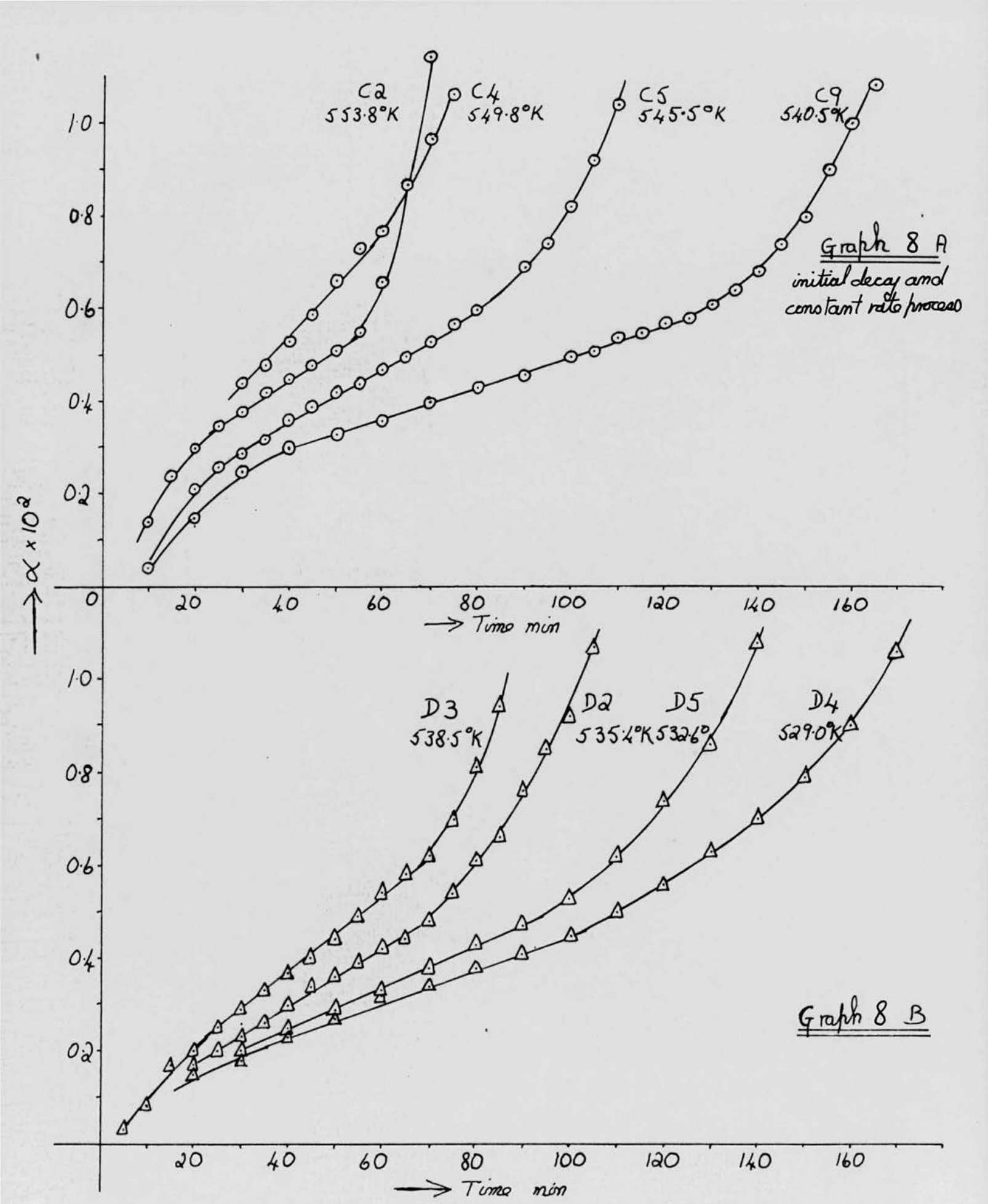
C2
553·8°K
C4
549·8°K
C5
545·5°K
C9
540·5°K
1·0
0·8
0·6
0·4
0·2
0
20
40
60
80
100
120
140
160
→ Time min
α x 10²
Graph 8 A
initial decay and
constant rate process
D3
538·5°K
D2
535·4°K
D5
532·6°
D4
529·0°K
1·0
0·8
0·6
0·4
0·2
20
40
60
80
100
120
140
160
→ Time min
Graph 8 B

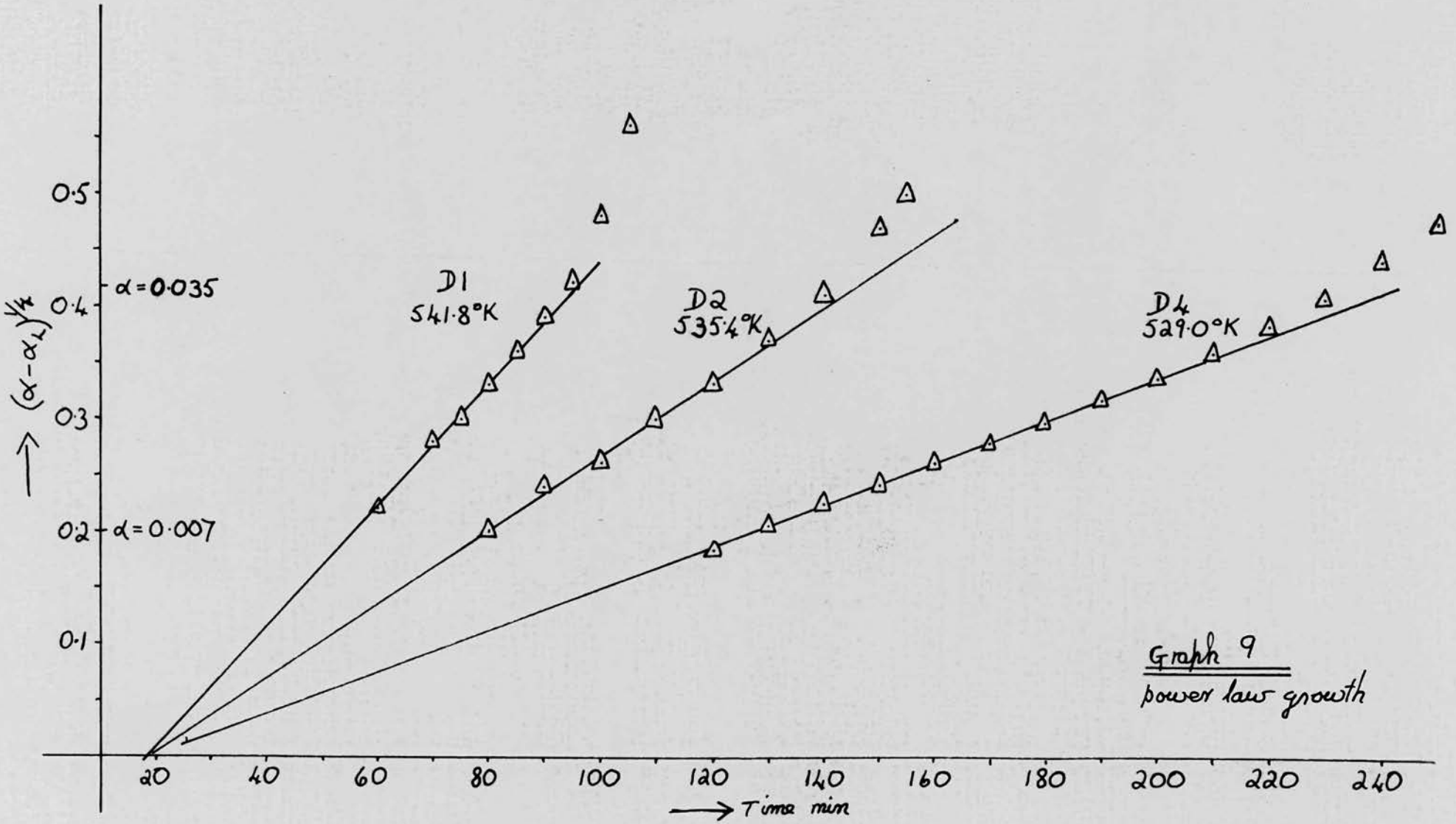

Graph 9
power law growth

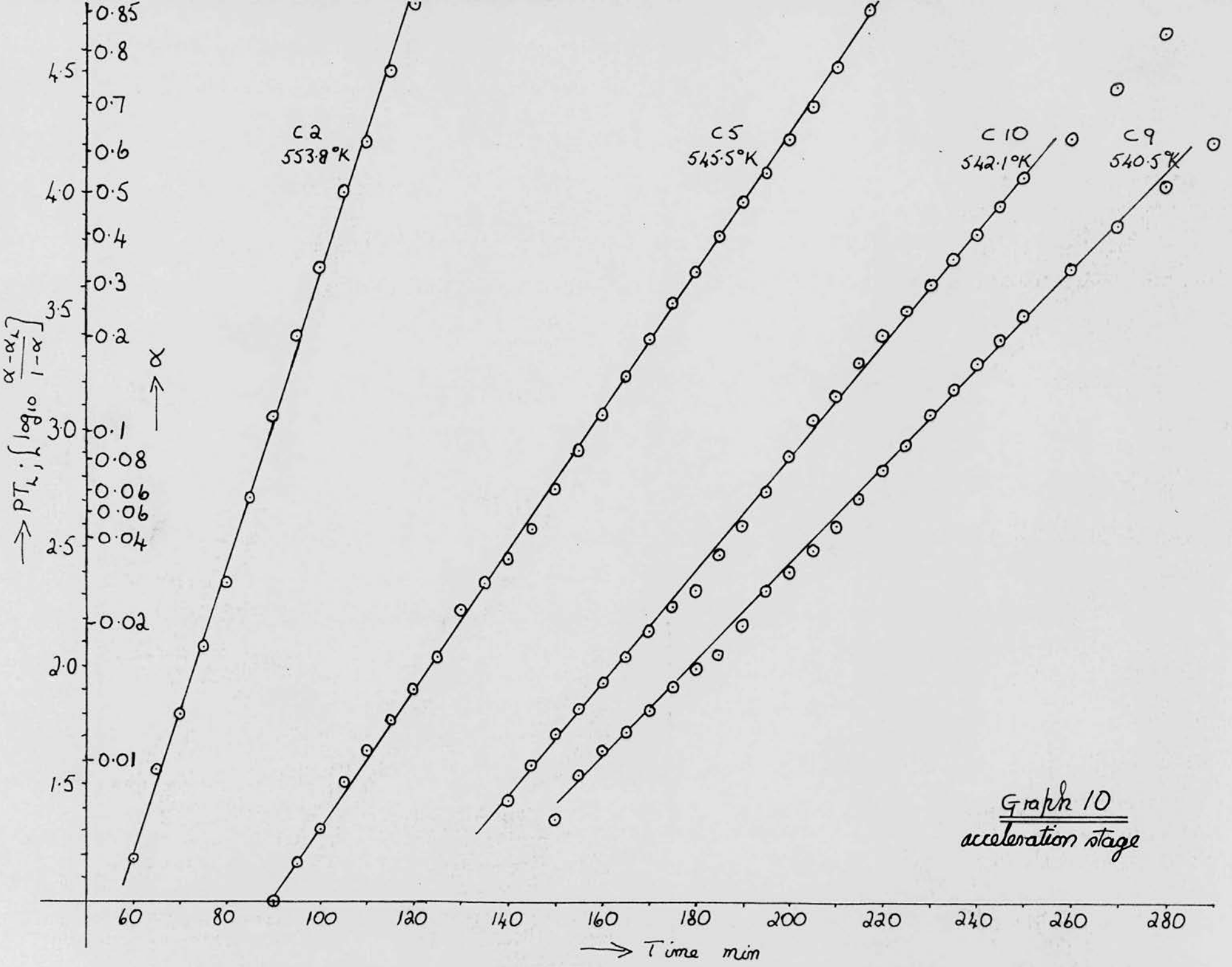

Graph 10
acceleration stage

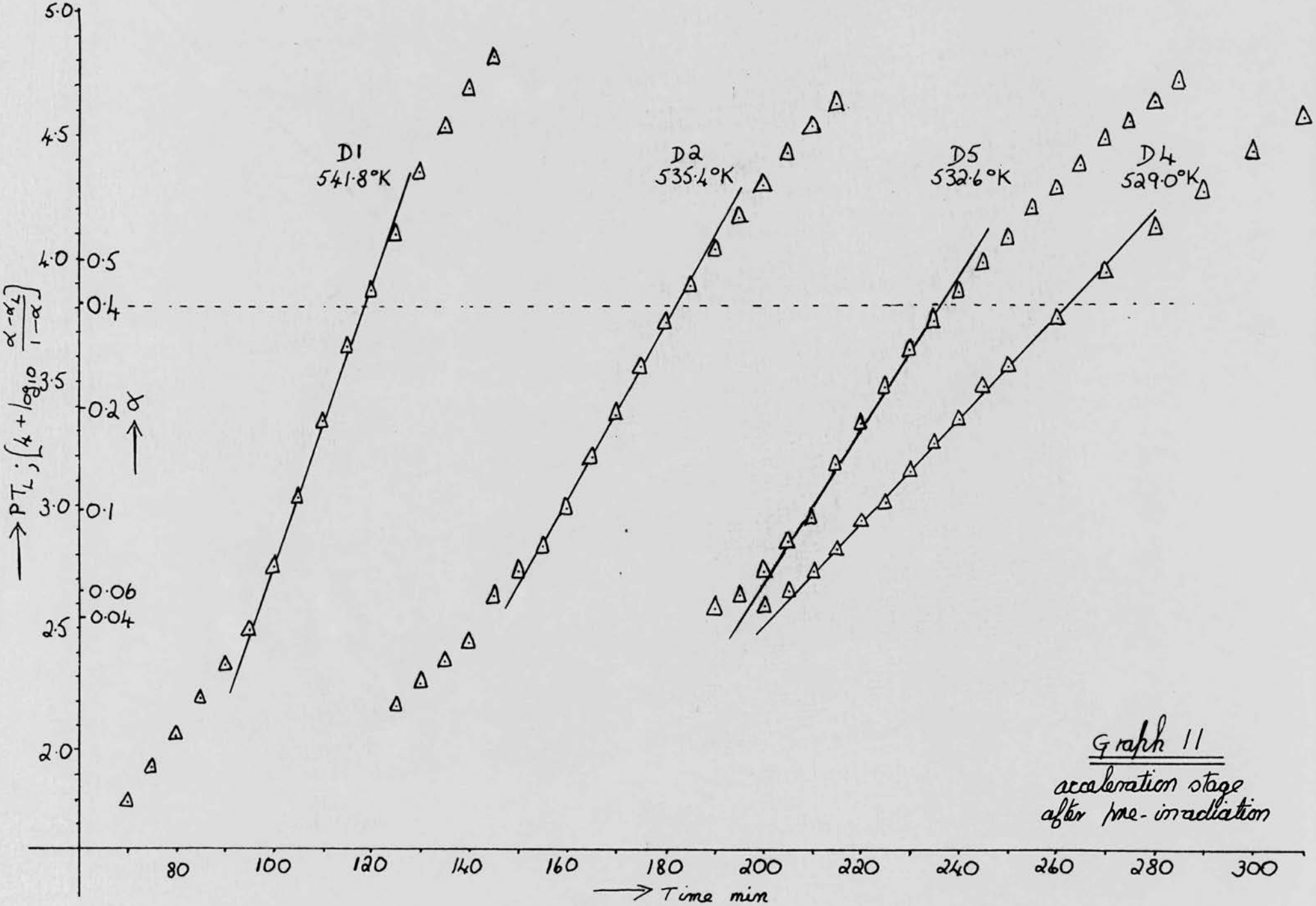

Graph 11

acceleration stage
after pre-irradiation

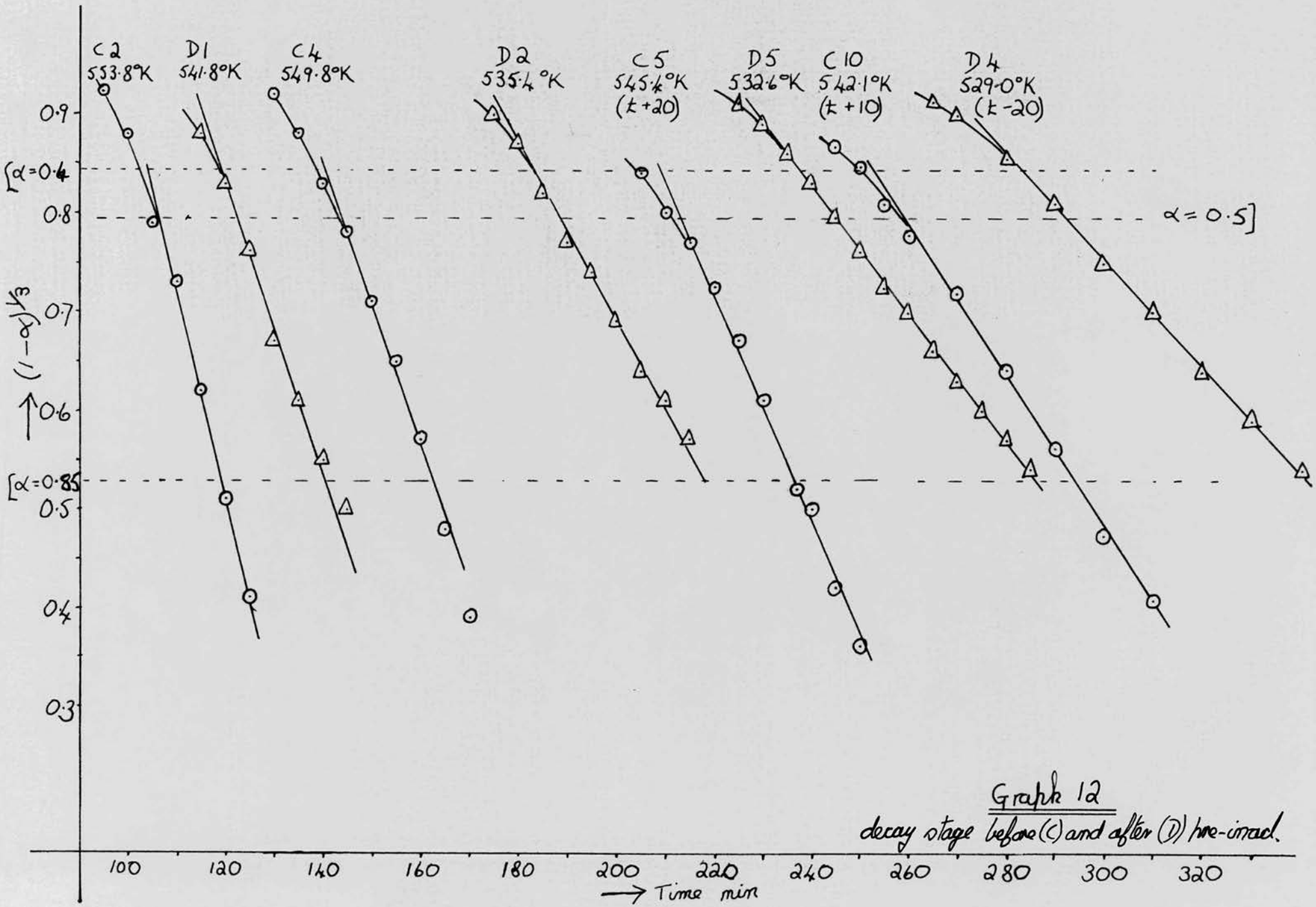

Graph 12

decay stage before (C) and after (D) hre-irrad.

2. 6. 3. Kinetic results for large crystals E with varying times of pre-irradiation.

Material E is similar to A but has been stored for a year. Run E8 is for the unirradiated material and E16 shows the effect of a further 2 months storage. Runs E9 - 15 illustrate the effect of varying times of pre-irradiation with u.v. under similar conditions to those described in 2.4. The most notable feature is the extension of the acceleration stage from $\alpha = 0.2$ to $\alpha = 0.4$, together with a much increased rate of decay and the introduction of the initial power law.

Table 11, analysis of material E.

Graph 13, 'α' - 't' curves for material E.

Graph 14, graphical analysis of runs E8, 9, 15.

Table 11. Material E.

Material E was made similar to A but stored for a year. The runs were performed at 545.3°K on crystals that had been pre-irradiated with u.v. from 0 - 18.5 hours. Run E16 was performed 2 months after run E8.

Run	E8			E16			E9			E10	E12	E14	E15			
Time of irradiation h.	0			0			2			3.25	7.25	14.9	18.5			
Time min at $\alpha = 0.006$	87			90			75			65	60	40	30			
Time min	$\alpha \times 10^2$	PT_L	$(1-\alpha)^{\frac{1}{3}}$	$\alpha \times 10^2$	$\alpha \times 10^2$	PT_L	$(1-\alpha)^{\frac{1}{3}}$	$\alpha \times 10^2$	$\alpha \times 10^2$	$\alpha \times 10^2$	Time min	$\alpha \times 10^2$	$\alpha_L^{\frac{1}{4}} \times 10$	PT		
25											32	0.67				
30											36	0.75	2.0			
35											40	0.82	2.2			
40											45	1.08	2.6			
45										0.60	48	1.27	2.9			
50										0.75	52	1.51	3.1			
55										0.98	56	2.00	3.4			
60										1.35	60	2.75	3.8			
65										2.31	64	3.84	4.2			
70										3.59	69	6.6	5.0			
75								0.60		6.74	72	10.2	$(1-\alpha)^{\frac{1}{3}}$			
80								0.74			76	23.6	0.91			
85								1.07	1.67		80	42.8	0.83			
90		0.65					0.60	1.77	2.07		85	64.4	0.71			
95		1.10	1.70				1.02	4.24	2.58		88	75.2	0.63			
100		2.56	2.32				3.58	13.0	3.15	0.96	92	85.5	0.53			
105		7.47	2.87				8.50	26.1	3.54	0.91	96	92.8	0.42			
110		14.0	3.20		0.95		16.7	40.7	3.83	0.84	101	96.8	0.32			
115		22.1	3.44		0.92		27.2	54.3	4.05	0.78						
120		30.9	3.64		0.88		37.5	67.1	4.30	0.69						
125		39.6			0.85		48.0	76.5		0.62						
130		48.3			0.80		57.4	84.0		0.54						
135		55.2			0.77		65.6	88.8		0.49						
140		63.5			0.71		73.2	92.0		0.43						
145		70.3			0.67		79.0	94.5		0.37						
150		74.4			0.64		85.0									
155		79.0			0.60		88.2									
160		82.2			0.565		92.3									
165		87.2			0.51		95.0									
170		89.0			0.48		96.7									

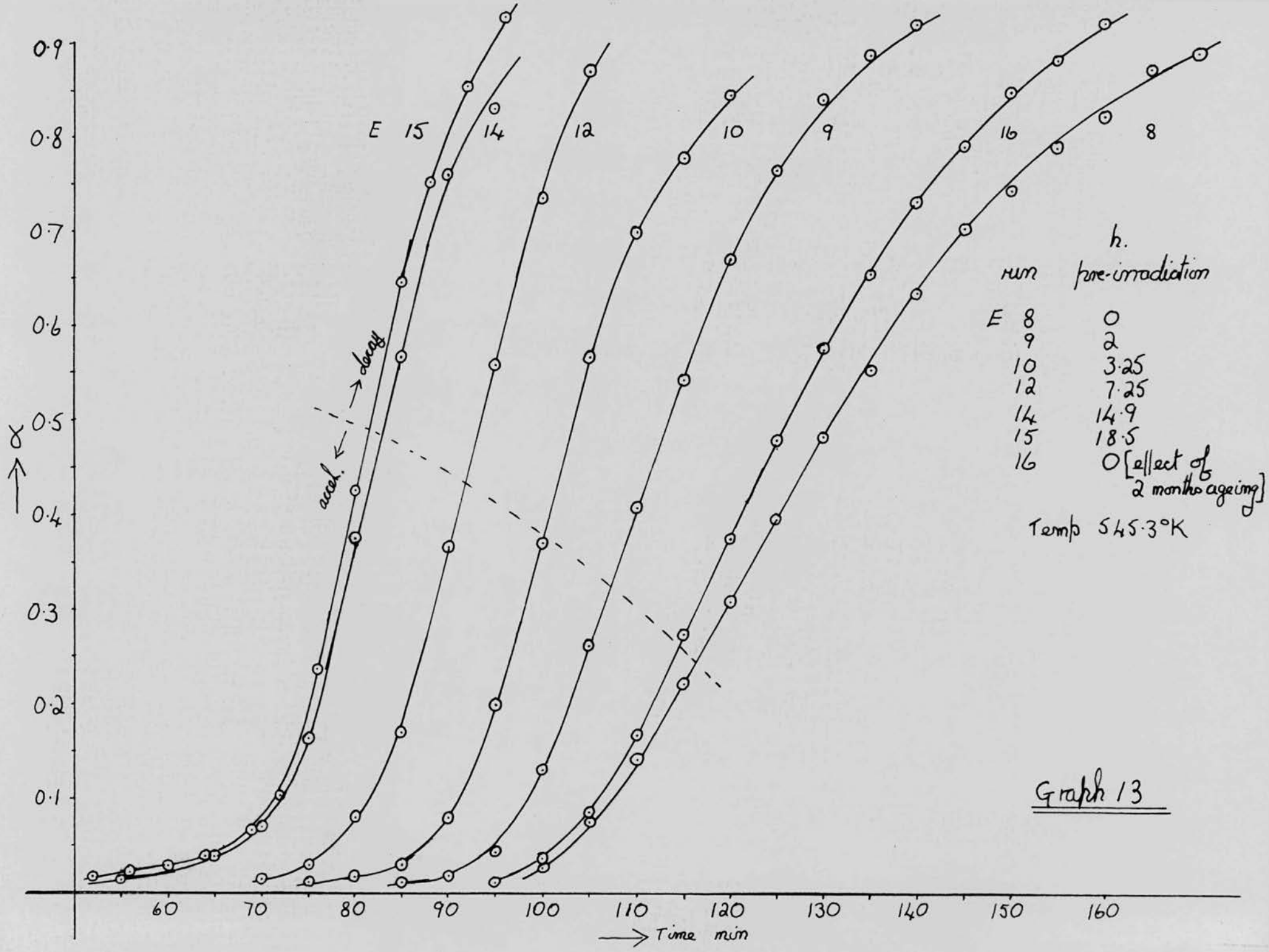
0·9
0·8
0·7
0·6
0·5
0·4
0·3
0·2
0·1
α
E 15
14
12
10
9
16
8
accel.
decay
60
70
80
90
100
110
120
130
140
150
160
Time min
h.
run
pre-irradiation
E 8 0
9 2
10 3·25
12 7·25
14 14·9
15 18·5
16 0 [effect of 2 months ageing]
Temp 545·3°K

Graph 13

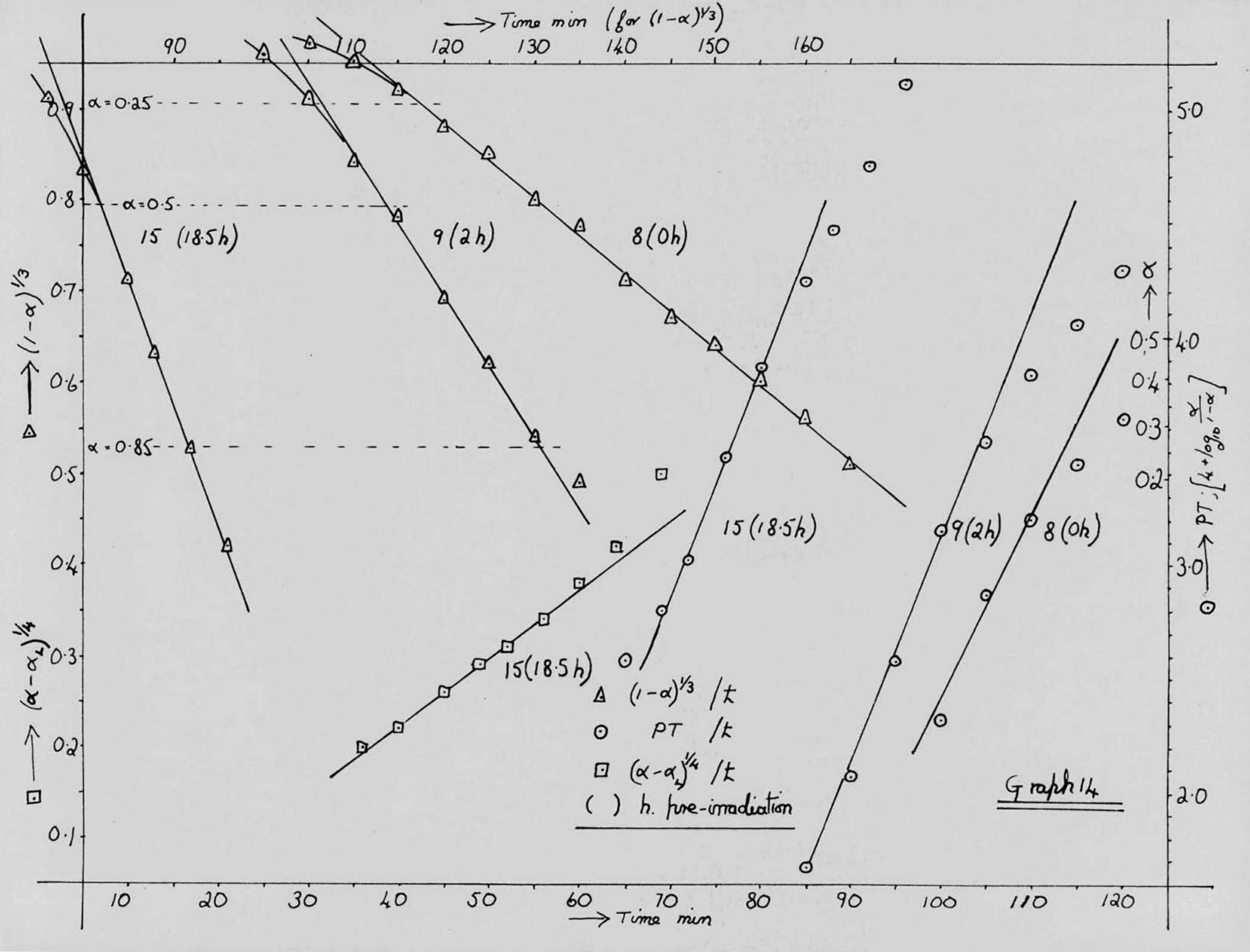
Time min (for $(1-\alpha)^{1/3}$)
90
110
120
130
140
150
160
$\alpha = 0.25$
$\alpha = 0.5$
$\alpha = 0.85$
15 (18.5h)
9 (2h)
8 (0h)
$(1-\alpha)^{1/3}$
$(\alpha-\alpha_4)^{1/4}$
0.9
0.8
0.7
0.6
0.5
0.4
0.3
0.2
0.1
15(18.5h)
15 (18.5h)
9(2h)
8 (0h)
α
PT; $[4 + \log_{10}\frac{\alpha}{1-\alpha}]$
5.0
4.0
3.0
2.0
0.5
0.4
0.3
0.2
$(1-\alpha)^{1/3}/t$
PT /t
$(\alpha-\alpha_4)^{1/4}/t$
( ) h. pre-irradiation
Graph 14
10
20
30
40
50
60
70
80
90
100
110
120
Time min

2. 6. 4. Kinetic results for small crystals F and G

Tables 12, 13, 14 and 15 and graphs 15, 16, 17 and 18, illustrate the effect of two years ageing on the small crystals. Material F is fresh crystals and G is the same material after storage for two years. The most notable feature is an increase in the rate of the acceleration stage. For both F and G the initial power law growth continues to ca α = 0.03 and the large negative values of 't_o' are to be noted. The acceleration stage in both cases ceases at α = 0.5.

Tables 12, 13 and 14, analysis of material F.

Tables 14 and 15, analysis of material G.

Graph 15, the 'α' - 't' curves for F and G.

Graph 16a and b, plot of $\alpha^{\frac{1}{2}}/t$ showing the fit for the power law with n = 2, for F and G.

Graph 17, acceleration stage, the plot of the Prout-Tompkins factor for F and G. In F23 and 28 a correction has been made for the initial power law growth; this has improved the fit for the lower values of 'α'.

Graph 18, decay stage, the plot of the contracting sphere factor for F and G.

Table 12. Material F. Fresh small crystals.

Run		F14				F3			F9
Temp		551.2°K				555.2°K			560.6°K
α_ρ		0.035							
Time min	$\alpha \times 10^2$	$\alpha^{\frac{1}{2}} \times 10$	PT	$\alpha_\rho^{\frac{1}{3}} \times 10$	$\alpha \times 10^2$	$\alpha^{\frac{1}{2}} \times 10$	PT	$\alpha \times 10^2$
5	0.08	0.30			0.06	0.25		0.08
10	0.21	0.46			0.22	0.47		0.28
15	0.30	0.56			0.38	0.62		0.42
20	0.41	0.64			0.56	0.75		0.70
25	0.56	0.74			0.79	0.89		1.03
30	0.70	0.84			0.99	0.99		1.46
35	0.90	0.92			1.33	1.15		2.00
40	1.07	1.03			1.64	1.28		2.69
45	1.3	1.14			1.98	1.41		3.60
50	1.59	1.26			2.39	1.55		5.70
55	1.89	1.37			2.88	1.70		12.2
60	2.22	1.49			3.58	1.89		31.6
65	2.58	1.61			4.46	2.12	2.84	61.2
70	2.96	1.72			6.45	———		85.5
75	3.41	1.85			10.0	$(1-\alpha)^{\frac{1}{3}}$	3.00	97.0
80	3.97	1.99	2.62		19.4		3.38	
85	4.87	2.21	2.71		37.8	0.85	3.78	
90	5.98	———	2.80		58.4	0.75	4.14	
95	8.1		2.95	2.76	73.0	0.65	4.40	
100	12.7	$(1-\alpha)^{\frac{1}{3}}$	3.16	4.06	87.5	0.50	4.84	
105	20.5	0.93	3.41	5.25	96.3	0.33	5.42	
110	30.9	0.88	3.65	6.29				
115	43.7	0.83	3.89	7.22				
120	57.5	0.75	4.13	8.01				
125	71.2	0.66	4.39	8.67				
130	82.2	0.56	4.66					
135	90.0	0.46	4.95					
140	97.2	0.30	5.54					

Table 13. Material F. Fresh small crystals.

Run		F28			F35		F43	
Temp		540.9°K			535.7°K		530.4°K	
α_P		0.033						
Time min	$\alpha \times 10^{-2}$	$\alpha^{\frac{1}{2}} \times 10$	PT_ρ	$\alpha_\rho^{\frac{1}{3}}$	$\alpha \times 10^2$	$\alpha^{\frac{1}{2}} \times 10$	$\alpha \times 10^2$	$\alpha^{\frac{1}{2}} \times 10$
10	0.15	0.39			0.12	0.34	0.08	
20	0.20	0.45			0.25	0.5	0.14	0.37
30	0.31	0.56			0.33	0.57	0.19	0.43
40	0.44	0.66			0.40	0.63	0.24	0.49
50	0.57	0.76			0.49	0.70	0.28	0.53
60	0.74	0.86			0.59	0.77	0.34	0.58
70	0.94	0.97			0.67	0.82	0.42	0.65
80	1.15	1.07			0.71	0.88	0.47	0.69
90	1.37	1.17			0.92	0.96	0.53	0.73
100	1.59	1.26			1.03	1.01	0.61	0.78
110	1.92	1.38			1.23	1.11	0.68	0.82
120	2.18	1.48					0.79	0.89
130	2.52	1.59			1.55	1.24	0.85	0.92
140	2.88	1.70			1.74	1.32	0.96	0.98
150	3.33	1.82			1.93	1.39	1.01	1.02
160	4.05	2.01	1.87	1.96	2.14	1.46	1.16	1.08
165	4.33		2.01	2.17				
170	4.80		2.18	2.47	2.38	1.54	1.32	1.15
175	5.32		2.33	2.71				
180	6.00		2.46	3.08	2.54	1.59	1.38	1.17
185	7.28		2.63	3.42				
190	8.7		2.78	3.78	2.82	1.68	1.50	1.22
195	11.0		2.94	4.25				
200	14.5		3.11	4.82	3.07	1.75	1.64	1.28
205	17.4		3.24	5.20				
210	22.6	$(1-\alpha)^{\frac{1}{3}}$	3.38	5.78	3.40	1.84	1.84	1.35
215	27.6		3.53	6.24				
220	33.3	0.87	3.65	6.69	3.70	1.92	1.86	1.36
225	38.9	0.85	3.76	7.09				
230	44.4	0.82	3.87	7.43	3.90	1.97	2.08	1.44
235	51.2	0.79	4.00	8.00				
240	57.8	0.75	4.11	8.17	4.62	2.14	2.24	1.50
245	63.5	0.71	4.22					
250	69.4	0.67	4.33		5.14	2.27	2.40	1.55
255	75.1	0.63	4.46			PT		
260	80.5	0.58	4.58		6.48	2.84	2.59	1.61
265	84.4	0.54	4.72					
270	88.5	0.49	4.87		8.92	2.99	2.78	1.67
275	92.5	0.42	5.08					
280	94.8	0.37	5.25		12.6	3.18	2.94	1.71
290					18.0	3.34	3.18	1.78
300					24.0	3.50	3.40	1.84
310					31.6	3.67	3.70	1.92
320					40.5	3.82	4.11	2.03
330					48.5	3.98	4.69	2.16

Table 14. Material F and G.

Run		F23			G1		
Temp		545.5°K			539.6°K		
α_P		0.035					
Time min	$\alpha \times 10^2$	$\alpha^{\frac{1}{2}} \times 10$	PT_P	$\alpha_P^{\frac{1}{3}} \times 10$	$\alpha \times 10^2$	$\alpha^{\frac{1}{2}} \times 10$	PT
5	0.09				0.11	0.34	
10	0.17	0.41			0.20		
15	0.21	0.46			0.21	0.46	
20	0.28	0.53			0.26	0.50	
25	0.33	0.57			0.31	0.55	
30	0.47	0.68			0.36		
35	0.54	0.73			0.43	0.66	
40	0.68	0.82					
45	0.79	0.89			0.55	0.74	
50	0.96	0.98					
55	1.07	1.03					
60	1.28	1.13			0.74	0.81	
65	1.42	1.19			0.83	0.91	
70	1.54	1.24			0.91	0.95	
75	1.68	1.29			1.01	1.00	
80	1.90	1.38			1.1	1.05	
85	2.13	1.46			1.2	1.09	
90	2.34	1.53			1.31	1.14	2.12
95	2.56	1.60			1.45	1.20	2.16
100	2.83	1.68			1.83	1.35	2.26
105	3.08	1.75			2.30	1.52	2.37
110	3.32	1.82			3.40		2.55
115	3.70	1.92			5.11		2.73
120	4.04	2.01	1.70		8.0		2.93
125	4.66	2.16	2.06	2.23	12.5		3.15
130	5.41		2.31	2.67	18.8		3.36
135	6.44		2.50	3.09	25.6	$(1-\alpha)^{\frac{1}{3}}$	3.54
140	8.22		2.71	3.61	34.2	0.87	3.72
145	10.9		2.92	4.20	42.9	0.83	3.87
150	15.3		3.14	4.90	51.3	0.79	4.02
		$(1-\alpha)^{\frac{1}{3}}$					
155	21.3		3.35	5.62	61.3	0.73	
160	27.6		3.52	6.17	70.0	0.67	
165	34.9		3.69	6.80	77.4	0.61	
170	44.3	0.82	3.84	7.42	82.5	0.56	
175	52.3	0.78	4.00	7.93	87.5	0.50	
180	61.3	0.73	4.14	8.33	90.5	0.46	
185	69.5	0.67	4.29		92.0	0.43	
190	78.1	0.60					
195	87.0	0.51					
200	92.5	0.42					

Table 15. Material G. Aged small crystals.

Run	G2				G3		
Temp	529.2°K				535.0°K		
α_P	0.024						
Time min	$\alpha \times 10^2$	$\alpha^{\frac{1}{2}} \times 10$	PT	$\alpha_P^{\frac{1}{3}} \times 10$	$\alpha \times 10^2$	$\alpha^{\frac{1}{2}} \times 10$	PT
10	0.09	0.30			0.12	0.34	
20	0.14	0.37			0.18	0.43	
40	0.24	0.49			0.37	0.61	
60	0.35	0.59			0.58	0.76	
80	0.46	0.68			0.82	0.90	
100	0.61	0.78			1.12	1.06	
110	0.70	0.84			1.28	1.13	
120	0.77	0.88					
130	0.86	0.93			1.81	1.35	
140	0.97	0.98			2.25	1.50	2.35
150	1.09	1.04			3.12	1.77	2.49
155	1.15	1.07			3.86		2.59
160	1.21	1.10			4.98		2.70
165	1.27	1.13			6.61		2.82
170	1.38	1.17			8.65		2.95
175	1.45	1.20			11.3		3.10
180	1.45	1.20			15.1		3.25
185	1.50	1.22			18.6		3.36
190	1.57	1.25			22.3		3.46
195	1.64	1.28			27.4		3.58
						$(1-\alpha)^{\frac{1}{3}}$	
200	1.72	1.31			32.7	0.88	3.71
210	1.90	1.38			45.6	0.82	3.92
220	2.09	1.45	2.32		55.4	0.76	4.10
230	2.38	1.54	2.38		66.6	0.69	4.30
240	2.81	1.67	2.46	1.58	75.0	0.63	4.48
250	3.54	1.88	2.55	2.29	82.4	0.56	4.67
260	4.80		2.71	2.88	85.1	0.53	4.76
270	6.69		2.85	3.50	91.3	0.44	5.02
280	9.7		3.03	4.18			
290	13.3		3.18	4.79			
		$(1-\alpha)^{\frac{1}{3}}$					
300	18.0		3.33	5.38			
310	23.5	0.91	3.49	5.95			
320	29.7	0.89	3.63	6.49			
330	37.0	0.86	3.78	7.02			
340	45.1	0.82	3.91	7.53			
350	52.3	0.78	4.04	7.94			
360	59.4	0.74	4.17				
370	67.0	0.69	4.29				
380	72.5	0.65	4.42				
390	76.8	0.61	4.52				
400	83.1	0.55	4.70				
415	86.7	0.51	4.81				
420	90.1	0.46	4.96				

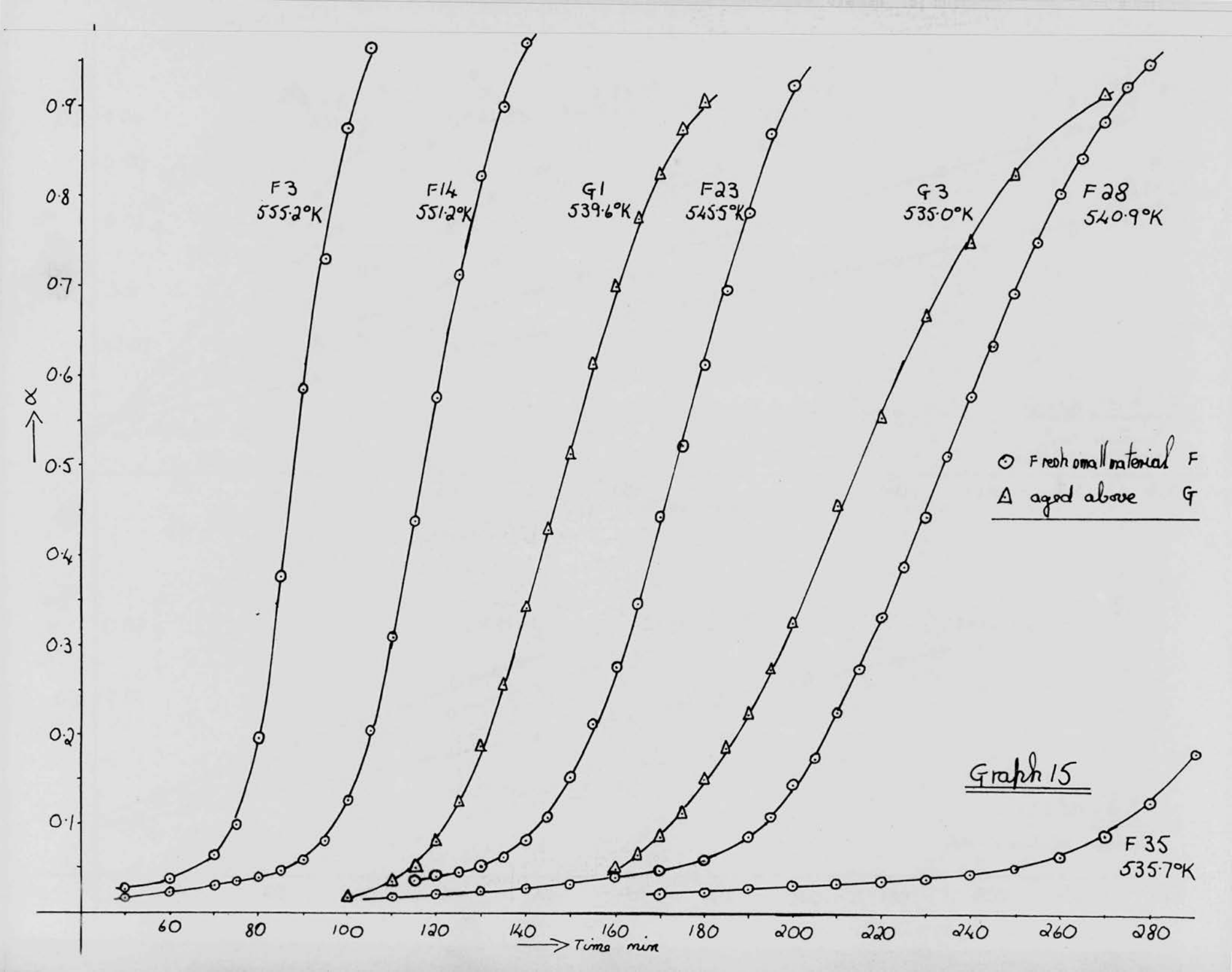
F3
555·2°K
F14
551·2°K
G1
539·6°K
F23
545·5°K
G3
535·0°K
F28
540·9°K
F35
535·7°K
Fresh small material F
aged above G
Graph 15
α
Time min
0·9
0·8
0·7
0·6
0·5
0·4
0·3
0·2
0·1
60
80
100
120
140
160
180
200
220
240
260
280

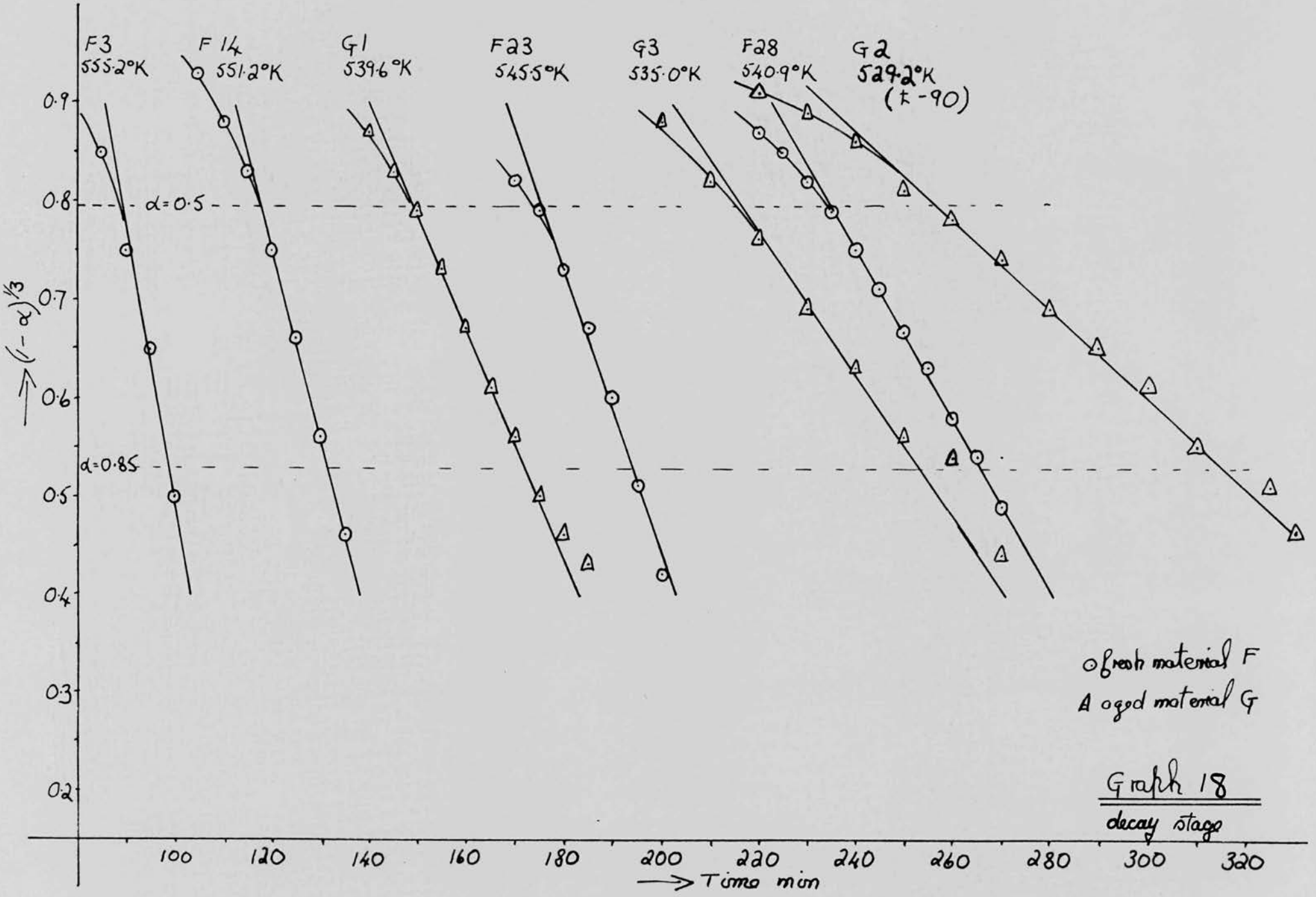

Graph 18

decay stage

2. 6. 5. Kinetic results for small crystals H and K

Tables 16, 17 and 18 and graphs 19, 20, 21 and 22 illustrate the effect of 18.5 h. pre-irradiation with u.v. on the small crystals. Material H is fresh crystals similar in preparation to material F, and K is H after pre-irradiation. The most notable feature is the overall increase in the rate of decomposition. For both H and K, the initial power law growth extends to ca α = 0.02 and the acceleration stage ceases at α = 0.5. Material H is similar to F for both the acceleration and decay stages, but the rate for the initial power law growth is less.

Tables16, 17 and 18, analyses for materials H and K.

Graph 19, the 'α' - 't' curves for H and K.

Graph 20a and b, plot of $\alpha^{\frac{1}{2}}/t$ showing the fit for the power law with n = 2, for H and K.

Graph 21, acceleration stage, plot of the Prout-Tompkins factor for H and K.

Graph 22, decay stage, plot of the contracting sphere factor for H and K.

Table 16. Material H and K.

Run	H2			H3			K1	K9
Temp	546.8°K			552.7°K			541.3°K	539.8°K
Time min	$\alpha \times 10^2$	$\alpha^{\frac{1}{2}} \times 10$	PT	$\alpha \times 10^2$	$\alpha^{\frac{1}{2}} \times 10$	PT	$\alpha \times 10^2$	$\alpha \times 10^2$
5	0.05	0.22		0.04	0.20		0.05	0.05
10	0.09	0.30		0.12	0.35		0.11	0.11
15	0.13	0.36		0.18	0.43		0.15	0.15
20	0.18	0.43		0.25	0.50		0.20	0.20
25	0.23	0.48		0.32			0.27	0.26
30	0.29	0.54		0.42			0.34	0.34
35	0.36	0.60		0.49			0.42	0.41
40	0.42	0.65		0.59	0.77		0.50	0.48
45	0.50	0.72		0.70	0.84		0.61	0.57
50	0.59	0.77		0.85	0.92		0.71	0.68
55	0.71	0.84		1.0	1.0		0.83	0.79
60	0.85	0.92			1.08		1.04	0.91
65	0.94	0.97		1.33	1.15		1.26	1.03
70	1.08	1.04		1.67	1.29		1.56	1.22
75	1.22	1.10		1.97	1.40	2.30	2.07	1.43
80	1.38	1.17		2.25		2.36	2.97	1.77
85	1.51	1.23		2.78		2.46	4.72	2.17
90	1.70	1.30		3.50		2.56	9.8	3.07
95	1.96	1.40		5.11		2.83	17.6	4.36
100	2.25		2.35	8.90		3.09	32.4	6.48
					$(1-\alpha)^{\frac{1}{3}}$			
105	2.53		2.41	17.2		3.32	45.0	10.2
110	2.72		2.45	27.5		3.58	54.1	17.0
115	3.17		2.51	40.0	0.84	3.82	65.4	26.5
120	3.62		2.57	57.2	0.75	4.13	74.8	36.7
125	4.22		2.64	68.9	0.68	4.34	82.5	45.7
130	5.26		2.74	81.1	0.57	4.62	87.1	57.9
135	7.24		2.89	89.4	0.47	4.93	93.8	68.2
140	10.0		3.05	94.3	0.38			76.5
145	14.6		3.23					82.7
150	21.0		3.42					88.3
		$(1-\alpha)^{\frac{1}{3}}$						
155	28.6		3.60					
160	37.2	0.86	3.77					
165	46.1	0.81	3.93					
170	57.0	0.75	4.14					
175	66.5	0.69	4.30					
180	75.5	0.63	4.49					
185	83.4	0.55	4.70					
190	89.3	0.47	4.92					
195	95.7	0.35	5.35					
200								

Table 17. Material H and K.

Run	H1			K3				K5			
Temp	541.8°K			533.4°K				530.2			
Time min	$\alpha \times 10^2$	$\alpha^{\frac{1}{2}} \times 10$	PT	$\alpha \times 10^2$	$\alpha^{\frac{1}{2}} \times 10$	PT	$\alpha_p^{\frac{1}{3}} \times 10$	$\alpha \times 10^2$	$\alpha^{\frac{1}{2}} \times 10$	PT	$\alpha^{\frac{1}{3}} \times 10$
10	0.05	0.23		0.09	0.30			0.09	0.30		
20	0.12	0.35		0.14	0.37			0.14	0.37		
30	0.19	0.43		0.19	0.44			0.19	0.43		
40	0.26	0.51		0.24	0.49			0.26	0.51		
50	0.36	0.60		0.32	0.57			0.33	0.57		
60	0.46	0.68		0.41	0.64			0.42	0.65		
70	0.60	0.77		0.49	0.70			0.51	0.71		
80	0.77	0.89		0.61	0.78			0.66	0.81		
90	0.94	0.97		0.71	0.84			0.74	0.86		
100	1.06	1.03		0.87	0.93			0.87	0.93		
110	1.25	1.12		1.12	1.06			0.98	0.99		
120	1.49	1.22		1.44	1.20			1.09	1.04		
125	1.64	1.28		1.92	1.39	2.28		1.19			
130	1.74	1.32		2.18		2.34	2.28	1.27	1.13		
135	1.98	1.40		2.65		2.42	2.55	1.39			
140	2.13	1.46		3.54		2.55	2.94	1.46	1.21		
145	2.50			4.44		2.68	3.25	1.61			
150	2.90			5.47		2.76	3.55	1.59	1.26		
155	3.14			7.94		2.94	4.11	1.69			
160	3.38			10.4		3.06	4.55	2.04	1.43		
165	3.69			15.0		3.25	5.19	2.38			
170	3.75			19.4	$(1-\alpha)^{\frac{1}{3}}$	3.38	5.69	2.57	1.60		
175	4.20			24.8		3.52	6.20	2.92		2.46	
180	4.92		2.71	31.2		3.66	6.71	3.30		2.52	2.62
185	6.11		2.81	37.5	0.85	3.78	7.15	4.06		2.62	2.96
190	7.0		2.88	44.8	0.82	3.91	7.59	4.65		2.69	3.14
195	8.8		2.98	51.3	0.79	4.02	7.95	5.56		2.77	3.45
200	10.3		3.06	58.5	0.75	4.15		7.5		2.90	3.91
205	13.1		3.18	64.5	0.71	4.26		9.0		3.01	4.31
210	16.8		3.30	71.0	0.66	4.41		11.0		3.10	4.61
		$(1-\alpha)^{\frac{1}{3}}$									
215	21.5		3.44	76.5	0.62	4.51		13.3		3.19	4.90
220	26.6		3.56	81.2	0.57	4.64		16.7		3.30	5.34
225	32.6	0.88	3.68	84.2	0.54	4.73		19.9		3.39	5.69
230	38.6	0.85	3.80	87.8	0.50	4.86		24.9		3.52	6.16
235	43.9	0.825	3.89	90.2	0.46	4.96		29.0		3.61	6.54
240	51.5	0.79	4.03					33.3	$(1-\alpha)^{\frac{1}{3}}$	3.70	6.82
245	57.4	0.75	4.13					38.2	0.85	3.79	7.15
250	66.6	0.694	4.30					43.5	0.82	3.89	7.49
255	72.3	0.65	4.42					47.7	0.806	3.96	7.73
260	80.9	0.57	4.63					54.0	0.77	4.07	8.07
265	84.0	0.54	4.72					58.9	0.74	4.16	
270	89.6	0.47	4.93					63.2	0.72	4.23	
275	96.4	0.33						67.0	0.69	4.31	
280								70.8	0.66	4.38	
285								73.5	0.64	4.44	

Table 18. Material K. Fresh small crystals pre-irradiated.

Run	K2				K7		
Temp	536.8°K				540.5°K		
α_P	0.013						
Time min	$\alpha \times 10^2$	$\alpha^{\frac{1}{3}} \times 10$	PT	$\alpha_P^{\frac{1}{3}} \times 10$	$\alpha \times 10^2$	$\alpha^{\frac{1}{3}} \times 10$	PT
5	0.08	0.28			0.13	0.36	
10	0.11	0.33			0.22	0.47	
15	0.16	0.40			0.33	0.57	
20	0.21	0.46			0.42	0.65	
25	0.24	0.49			0.50	0.71	
30	0.31	0.56			0.59	0.77	
35	0.36	0.60			0.74	0.86	
40	0.42	0.66			0.88	0.94	
45	0.48	0.69			1.08	1.04	
50	0.55	0.74			1.21	1.10	
55	0.61	0.78			1.43	1.20	
60	0.71	0.84			1.67	1.29	
65	0.80	0.89			1.94	1.39	
70	0.91	0.96			2.28	1.51	
75	1.04	1.02			2.67	1.63	
80	1.19	1.09			3.06	1.74	
85	1.39	1.18			4.10		
90	1.53	1.24			5.54		2.77
95	1.91	1.38	2.28		8.2		3.00
100	2.18	1.48	2.34		14.6		3.23
						$(1-\alpha)^{\frac{1}{3}}$	
105	2.80		2.46	2.35	22.0		3.45
110	3.64		2.58	2.98	32.6	0.88	3.68
115	6.00		2.81	3.68	43.3	0.83	3.88
120	8.09		2.94	4.14	54.6	0.77	4.08
125	12.0		3.13	4.79	65.0	0.70	4.27
130	18.2	$(1-\alpha)^{\frac{1}{3}}$	3.35	5.56	75.0	0.63	4.48
135	25.6		3.52	6.27	82.5	0.56	4.67
140	33.7	0.87	3.71	6.89	88.0	0.49	4.86
145	43.7	0.82	3.89	7.53	91.2	0.46	5.02
150	52.4	0.78	4.10	8.01	94.5	0.38	5.23
155	62.1	0.72	4.21	8.48			
160	69.4	0.67	4.35				
165	75.5	0.63	4.49				
170	81.0	0.575	4.63				
175	87.1	0.505	4.88				
180	91.4	0.44	5.03				

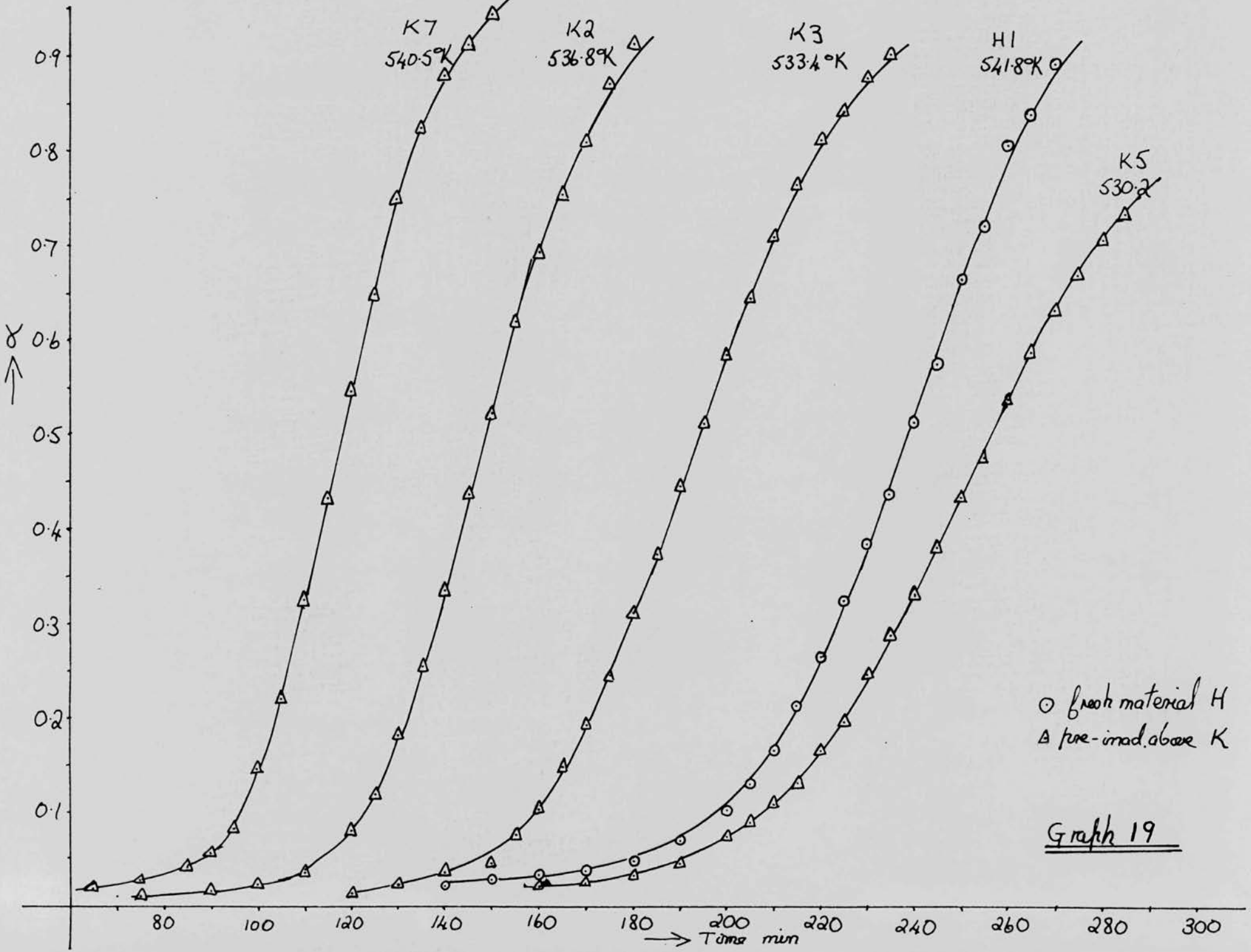
K7
540·5°K
K2
536·8°K
K3
533·4°K
H1
541·8°K
K5
530·2°K
0·9
0·8
0·7
0·6
0·5
0·4
0·3
0·2
0·1
γ
80
100
120
140
160
180
200
220
240
260
280
300
Time min
○ fresh material H
△ pre-irrad. above K

Graph 19

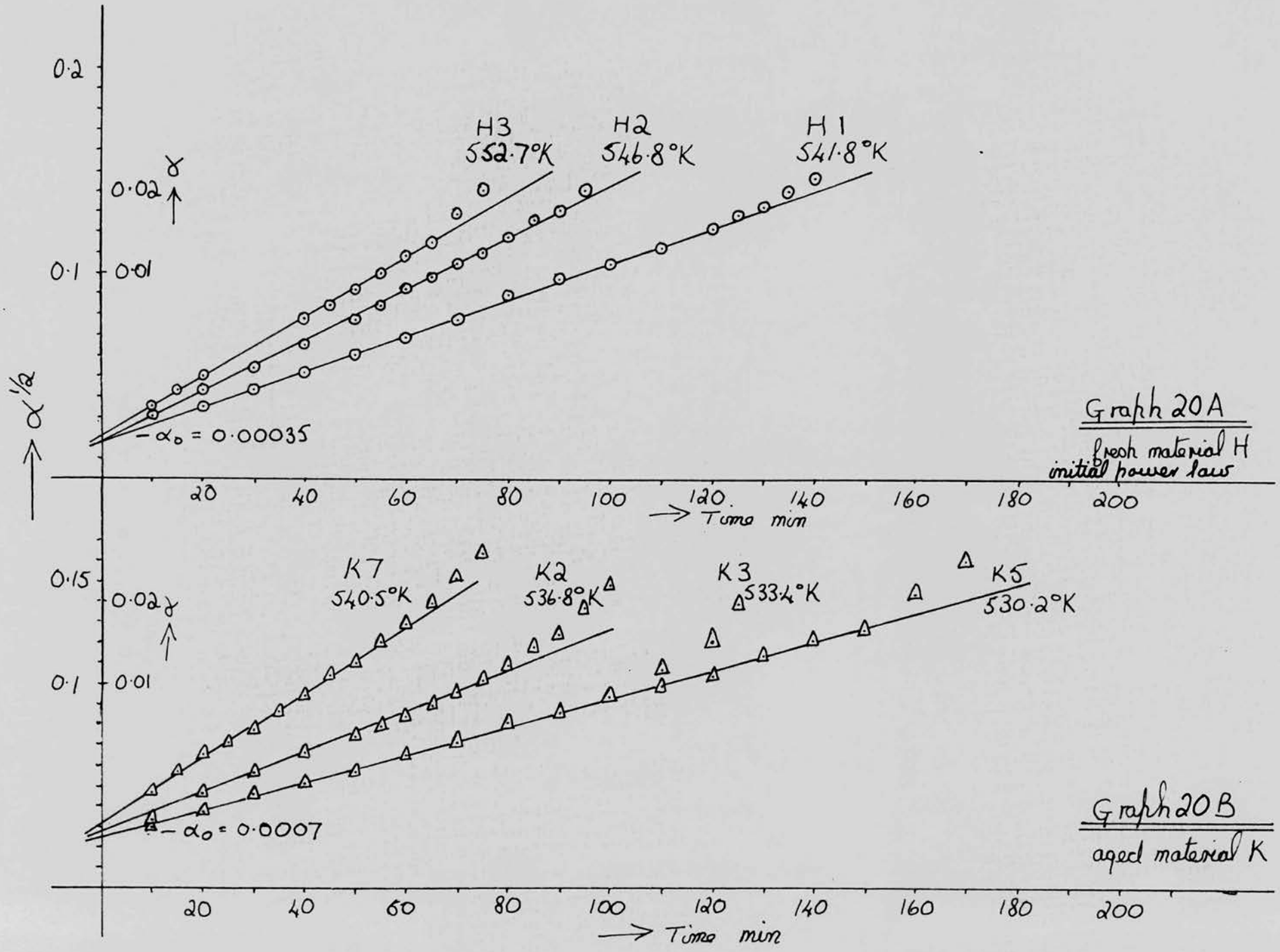
0·2
0·1
0·02 γ
0·01
H3
552·7°K
H2
546·8°K
H1
541·8°K
$\gamma^{1/2}$
$-\alpha_0 = 0.00035$
20
40
60
80
100
120
140
160
180
200
Time min
Graph 20A
fresh material H
initial power law
0·15
0·1
0·02 γ
0·01
K7
540·5°K
K2
536·8°K
K3
533·4°K
K5
530·2°K
$-\alpha_0 = 0.0007$
20
40
60
80
100
120
140
160
180
200
Time min
Graph 20B
aged material K

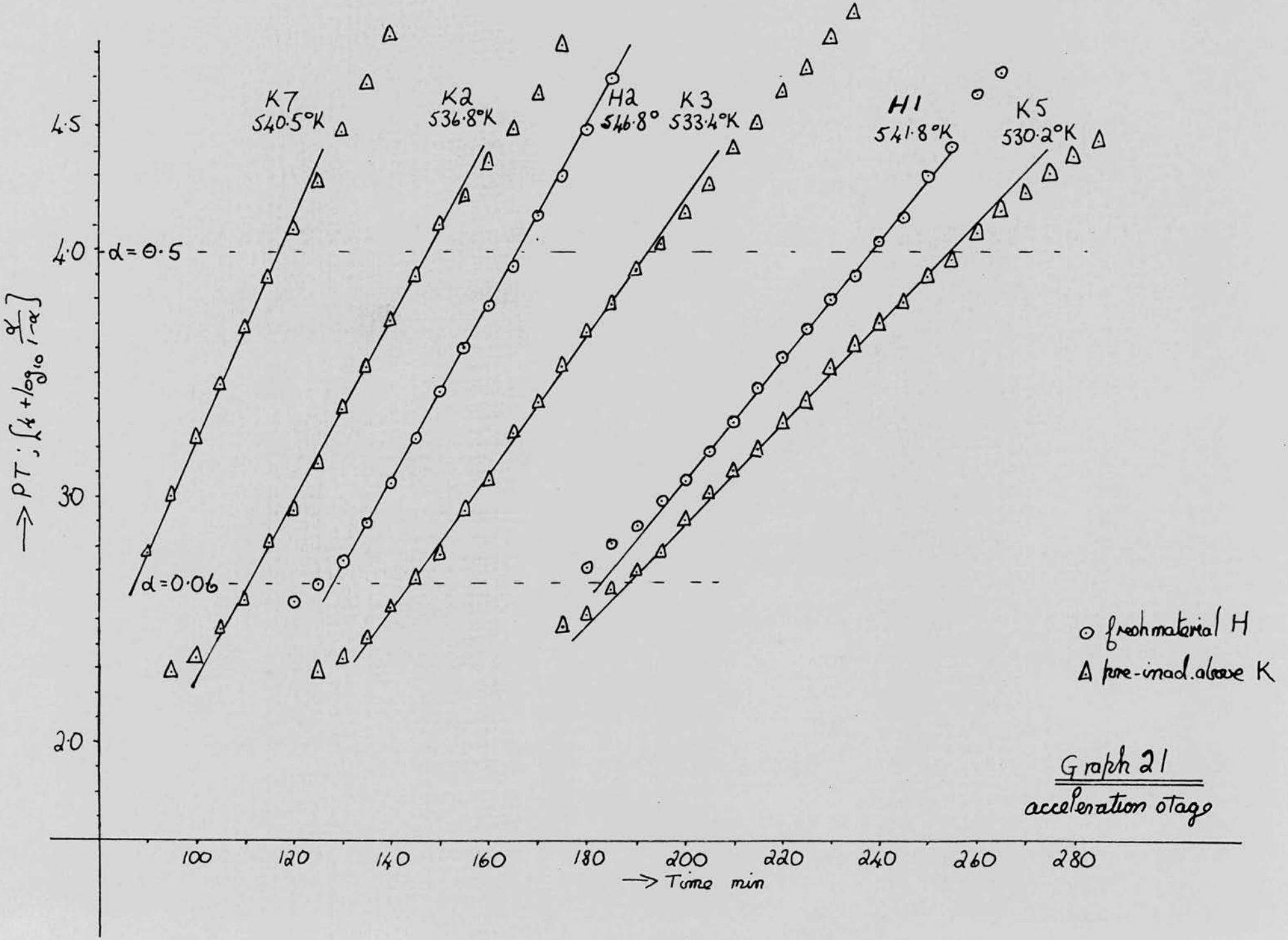

Graph 21
acceleration stage

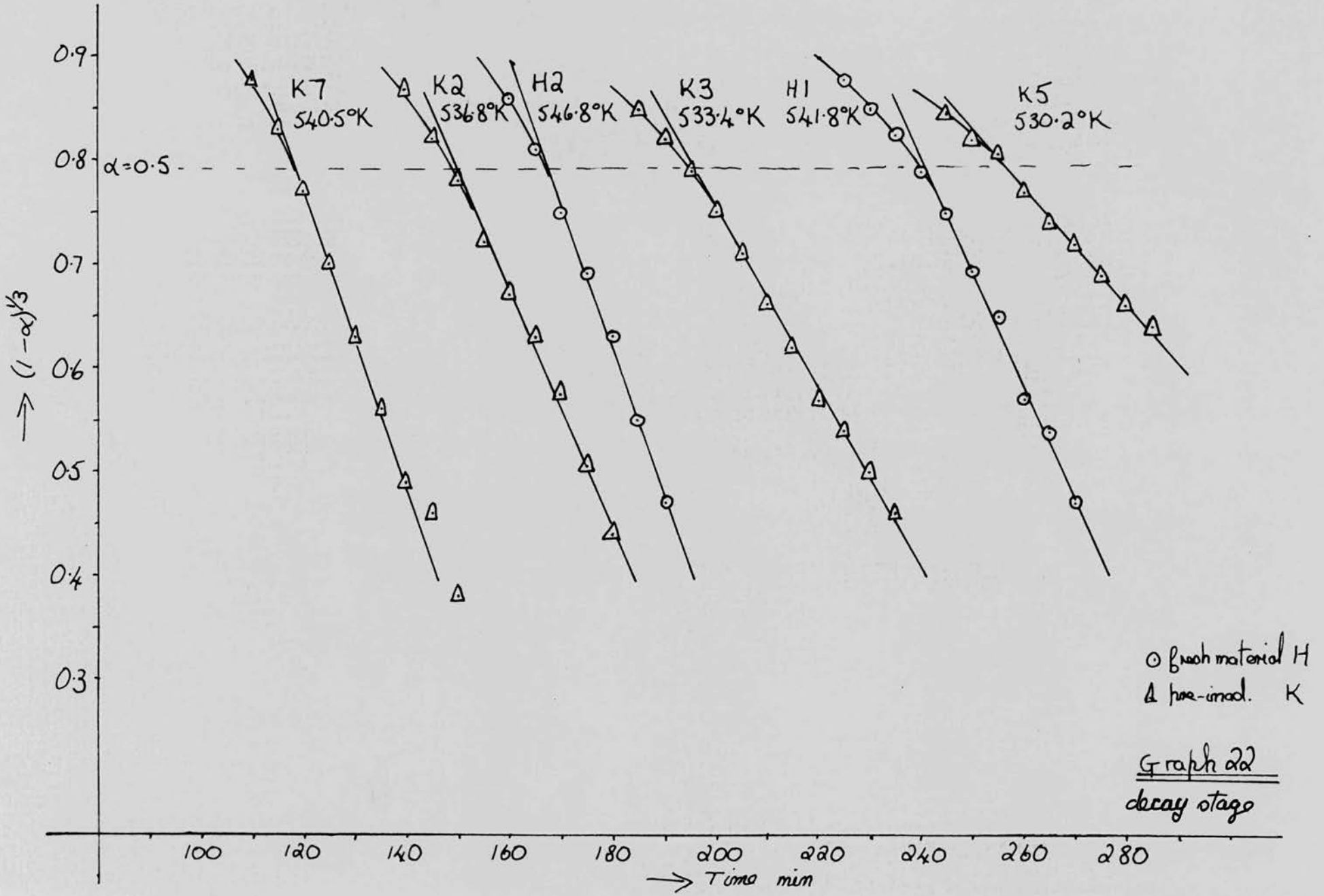

Graph 22

decay stage

2. 6. 6. Tables and graphs of rate constants

In tables 19 - 26 the rate constants for the various runs described in section 2.6.1 - 2.6.5 are tabulated, together with the respective temperatures.

R_I is the initial rate, $\frac{d\alpha}{dt}$, for section OA, (Graph I, following page 19). It was found by measuring the initial slope of the 'α' - 't' curves.

R_L is the constant rate for the linear stage AB in terms of $\frac{d\alpha}{dt}$ from the equation $\alpha = k_1 t + C$; thus R_L is equal to k_1.

$k_2^{\frac{1}{2}}$ and t_o are the constants from the equation $\alpha = k_2(t - t_o)^2$ representing the initial power law growth for the small crystals.

$k_4^{\frac{1}{4}}$ is the constant from the equation $(\alpha - \alpha_L) = k_4(t - t_o)^4$ representing the power law introduced by the pre-irradiation for the large crystals.

k is the Prout-Tompkins branching coefficient from the equation $2.3 \log_{10} \frac{\alpha}{1 - \alpha} = kt + C_1$.

R_M is the maximum rate of decomposition as measured from the 'α' - 't' curves.

k_3 is the constant from the contracting sphere equation $\alpha = 1 - \left[C - k_3(t - t_o)\right]^3$.

Table 19. Rate constants for material A, large fresh crystals.

Run	Temp $T^{\circ}K$	$\frac{1}{T} \times 10^3$	$R_I \times 10^5$	$R_L \times 10^5$	$R_M \times 10^3$	$k \times 10^2$	$k_3 \times 10^3$
A 8	560.6	1.784	27	19	38	15	27
2	555.2	1.801		11	30	12	20
12	551.2	1.814	18	8.2	20	7.9	17
13	551.2	1.814		9.0	19	8.2	16
21	545.5	1.833	18	5.0	12.0	5.5	8.8
22	545.5	1.833	10	6.1	12.3	5.3	8.8
26	540.9	1.849	6.1	3.3	8.8	3.8	5.6
29	540.9	1.849	5.5	2.9	8.2	3.7	6.1
34	535.7	1.867	3.6	2.0	5.9	2.9	3.7
42	530.4	1.885	3.2	1.3	-	-	-
46	530.4	1.885	3.4	1.3	-	-	-

Table 20. Rate constants for material B, material A aged.

B 5	545.5	1.833	7.0	24	23	11
1	542.5	1.843	5.5	20	21	9.1
6	539.6	1.853	4.0	16	16	7.8
3	538.0	1.859	2.6	14	13	6.7
2	537.4	1.861	2.5	14	14	6.6
4	531.3	1.882	2.1	8	6.2	4.3

Table 21. Rate constants for material C, large fresh crystals.

Run	Temp $T^{o}K$	$\frac{1}{T} \times 10^{3}$	$R_L \times 10^{5}$	$R_M \times 10^{3}$	$k \times 10^{2}$	$k_3 \times 10^{3}$	$k_4^{\frac{1}{4}} \times 10^{3}$
C 2	552.8	1.809	6.6	29	13.5	21	-
4	549.8	1.819	11	21	9.1	15.4	-
7	547.8	1.826	6.3	18	8.4	13	-
5	545.5	1.833	5.7	16	6.9	12	-
1	544.2	1.838	4.4	14	5.7	9.1	-
10	542.1	1.845	3.3	11	5.5	7.7	-
3	541.0	1.848	3.2	9.6	4.9	7.8	-
9	540.5	1.850	3.2	9.5	4.8	6.0	-

Table 22. Rate constants for material D, material C pre-irradiated.

D 1	541.8	1.846	10.2	26	13.4	14.0	5.5
3	538.5	1.857	8.0	20	10.8	10.1	4.3
7	537.6	1.860	7.6	19	12.3	10.0	4.0
2	532.6	1.866	6.1	17	8.3	8.8	3.3
5	531.0	1.877	4.5	13	7.3	6.6	2.7
4	529.0	1.890	3.6	10	4.7	5.5	1.9

Table 23. Rate constants for material F, small fresh crystals.

Run	Temp $T^{o}K$	$\frac{1}{T} \times 10^{3}$	$k_2^{\frac{1}{2}} \times 10^{4}$	t_o min	$R_M \times 10^{3}$	$k \times 10^{2}$	$k_3 \times 10^{3}$
F 9	560.6	1.784	-	-	62	-	-
3	555.2	1.801	27	8	40	18	30
14	551.2	1.814	21	10	27	11	19
20	545.5	1.833	15	15	18	8.4	13
23	545.5	1.833	14	17	19	9.2	14
27	540.9	1.849	-	-	11	5.5	9.0
28	540.9	1.849	10	23	12	6.2	8.6
35	535.7	1.867	7.5	42	8.0	3.7	6.2
43	530.4	1.885	5.0	51	-	-	-

Table 24. Rate constants for material G, material F aged.

G 1	539.6	1.853	9.0	35	17	9.6	11.5
3	535.0	1.869	7.0	32	12	6.0	7.1
2	529.2	1.890	5.0	50	8.0	3.7	4.5

Table 25. Rate constants for material H, fresh small crystals.

Run	Temp $T^{o}K$	$\frac{1}{T} \times 10^{3}$	$k_2^{\frac{1}{2}} \times 10^{4}$	t_o min	$R_M \times 10^{3}$	$k \times 10^{2}$	$k_3 \times 10^{3}$
H 3	552.7	1.809	17	13	36	13.8	20.0
2	546.8	1.829	12	14	20	8.2	14.0
1	541.8	1.847	8.5	20	14	5.6	10.0

Table 26. Rate constants for material K, material H pre-irradiated.

K 1	541.3	1.847	16	12	23	12.0	8
7	540.5	1.850	16	20	21.3	10.6	14
4	539.7	1.853	11.5	22	20.3	10.2	13
9	539.8	1.853	11.5	20	20.3	10.1	13
2	536.8	1.863	10.0	28	17	8.4	11
3	533.4	1.875	8.0	34	14	6.4	8.7
5	530.2	1.886	6.8	35	10.5	4.6	5.6
8	529.8	1.888	5.5	50	9.2	4.8	6.0

In the following graphs 23 to 27, the Arrhenius activation energy plots are shown for the various temperature dependent constants given in tables 19 to 26. The activation energies have been mainly estimated from materials A and F, as the experiments in these cases covered a wide temperature range. The activation energies obtained from materials B, C, D, G, H and K could not be distinguished experimentally from those of A and F.

These graphs clearly illustrate the effect of ageing and pre-

irradiation on the rate of decomposition. As previously noted, ageing of both large and small crystals only materially increases the rate of the acceleration stage, although there is a small increase in the rate for the pre-acceleration and decay stages. On the other hand pre-irradiation of large and small crystals, materially increases the rate of all the stages of the decomposition.

The differences between material A and C and between F and H is small, indicating reasonable reproduceability of different batches that were made under similar conditions.

The following activation energies apply to the different stages:

For the large crystals the value is

ca 45 kcal $mole^{-1}$ for the initial decomposition (stage OA, graph 1) as found from graph 23,

50 ± 5 kcal $mole^{-1}$ for the initial linear decomposition (stage AB) from the values of R_L as found from graph 23,

46 ± 4 kcal $mole^{-1}$ for the power law growth introduced by pre-irradiation (stage BB^1), as found from graph 24. This is obtained from values of $k_4^{\frac{1}{4}}$ and is thus the value for the linear progression of the interface, assuming the same activation energy for growth and activation.

For the small crystals the value is

41 ± 4 kcal $mole^{-1}$ for the initial power law growth as found from graph 24. This is obtained from values of $k_2^{\frac{1}{2}}$ and applies to the linear progression of the interface.

For both the large and small crystals the value is

46 ± 4 kcal $mole^{-1}$ from the maximum rate values, R_m, (graph 26) and from the Prout-Tompkins 'k' (graph 25) for the acceleration stage; also from the rate constant 'k_3' (graph 27) for the decay stage which is by means of the contracting sphere mechanism.

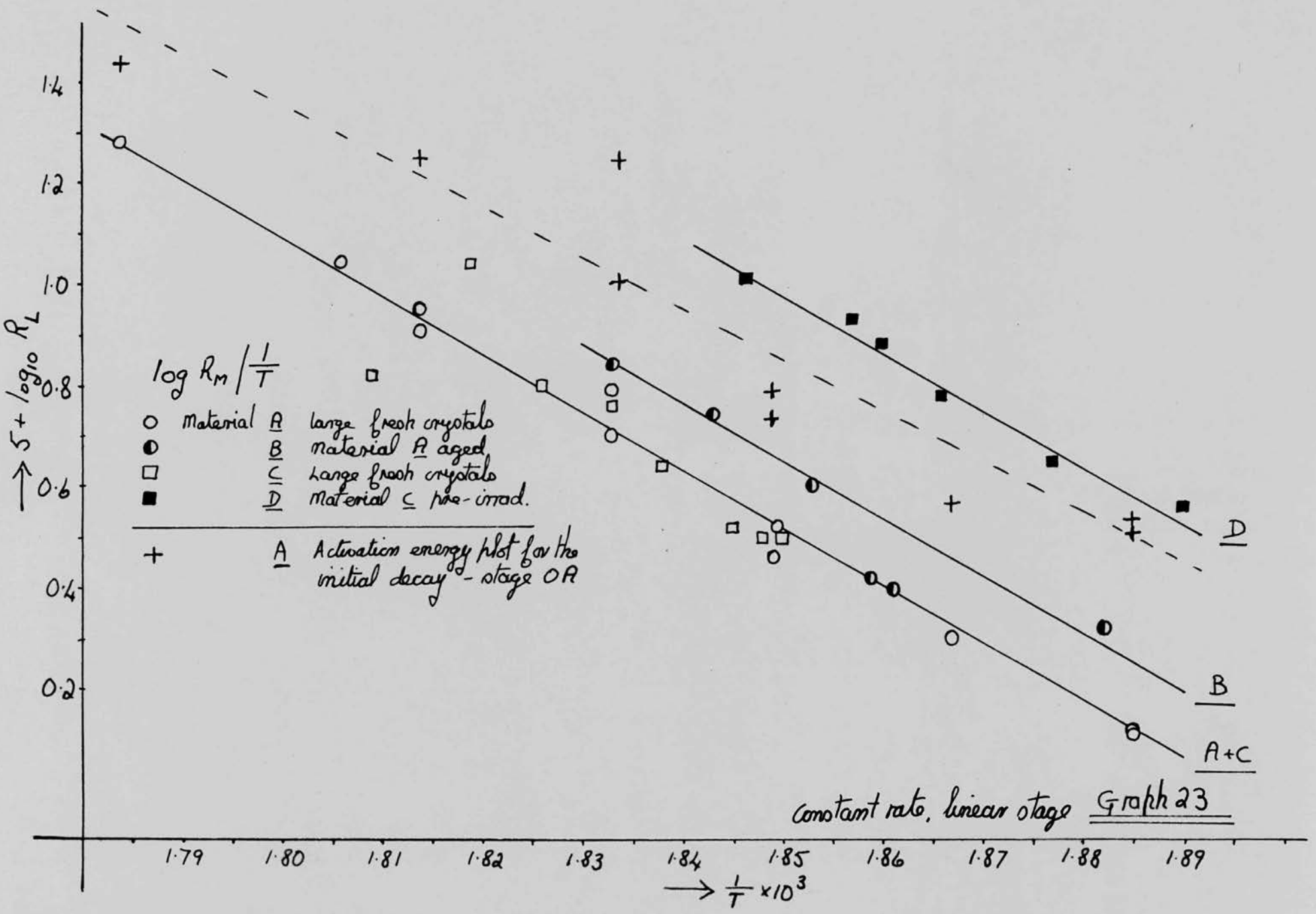
1·4
1·2
1·0
0·8
0·6
0·4
0·2
5+ log10 RL
log RM / 1/T
Material A large fresh crystals
B material A aged
C large fresh crystals
D material C pre-irrad.
A Activation energy plot for the initial decay - stage OA
D
B
A+C
constant rate, linear stage Graph 23
1·79
1·80
1·81
1·82
1·83
1·84
1·85
1·86
1·87
1·88
1·89
1/T ×10³

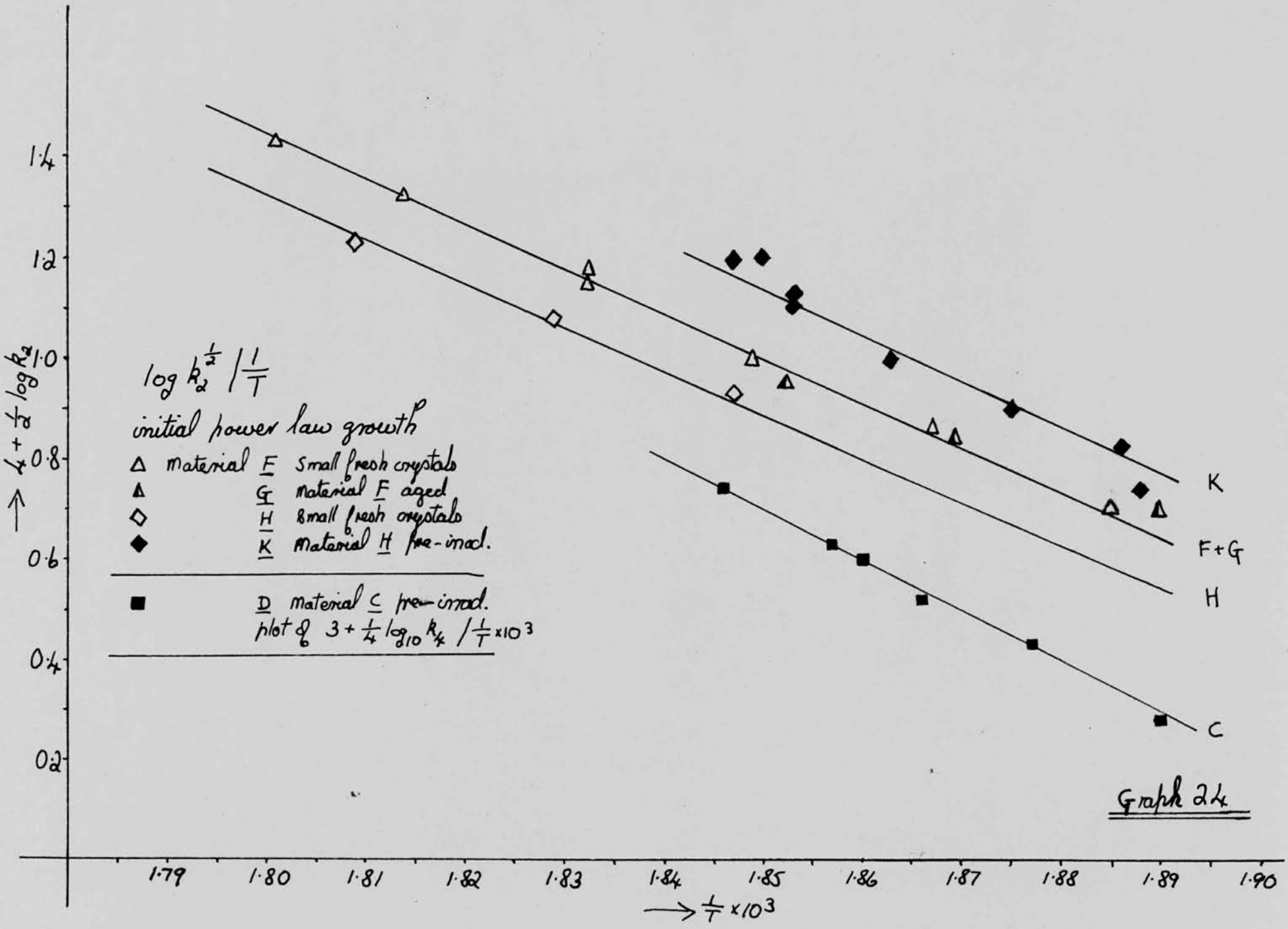
$\log k_2^{\frac{1}{2}} / \frac{1}{T}$
initial power law growth
△ material F Small fresh crystals
▲ G material F aged
◇ H Small fresh crystals
◆ K material H pre-irrad.
■ D material C pre-irrad.
plot of $3 + \frac{1}{4}\log_{10} k_4 / \frac{1}{T} \times 10^3$
$\rightarrow 4 + \frac{1}{2}\log k_2$
1·4
1·2
1·0
0·8
0·6
0·4
0·2
K
F+G
H
C
1·79
1·80
1·81
1·82
1·83
1·84
1·85
1·86
1·87
1·88
1·89
1·90
$\rightarrow \frac{1}{T} \times 10^3$

Graph 24

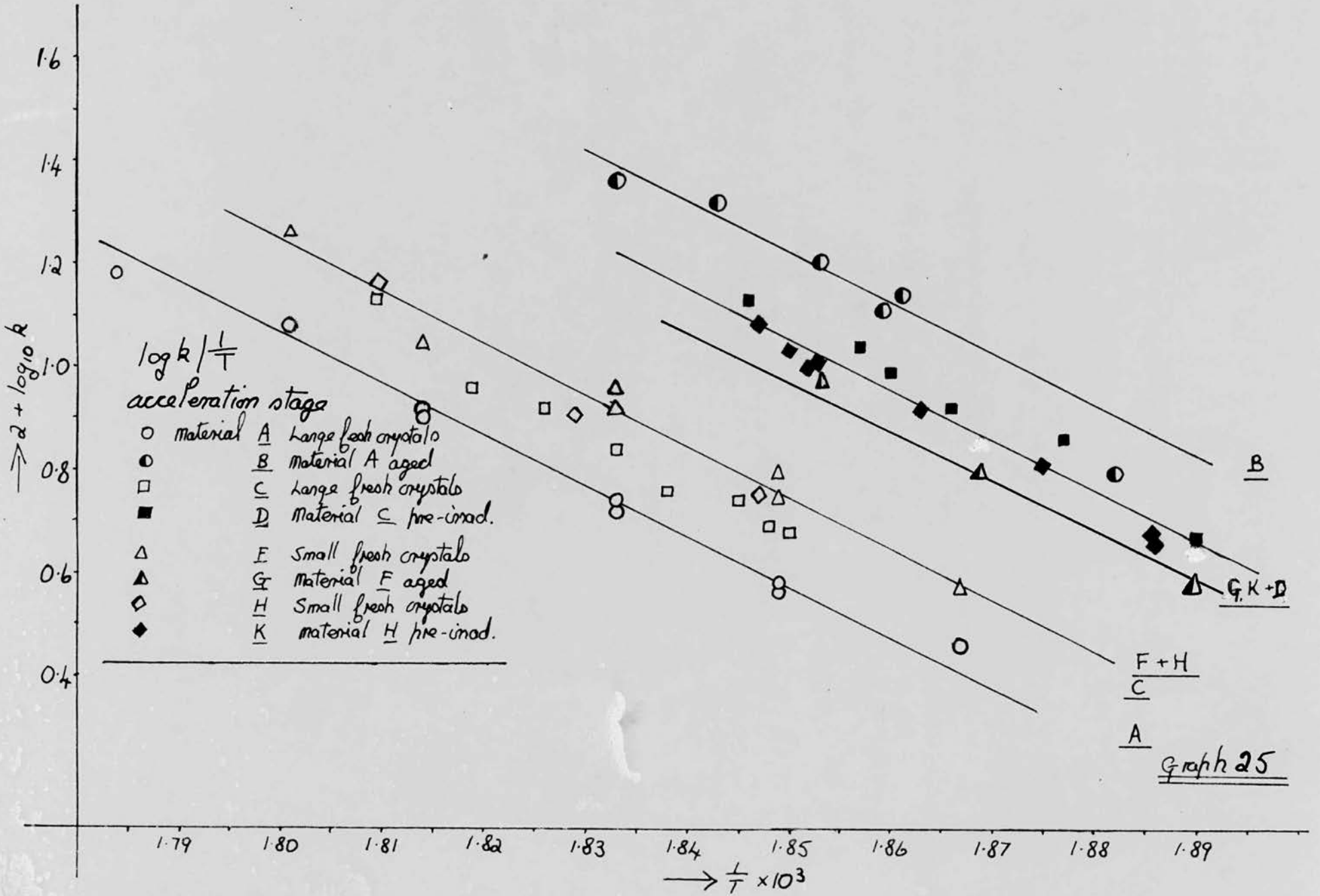
log k / 1/T
acceleration stage
material A Large fresh crystals
B Material A aged
C Large fresh crystals
D Material C pre-irrad.
E Small fresh crystals
G Material F aged
H Small fresh crystals
K material H pre-irrad.
B
G, K + D
F + H
C
A
Graph 25
2 + log10 k
1/T × 10³
1·6
1·4
1·2
1·0
0·8
0·6
0·4
1·79
1·80
1·81
1·82
1·83
1·84
1·85
1·86
1·87
1·88
1·89

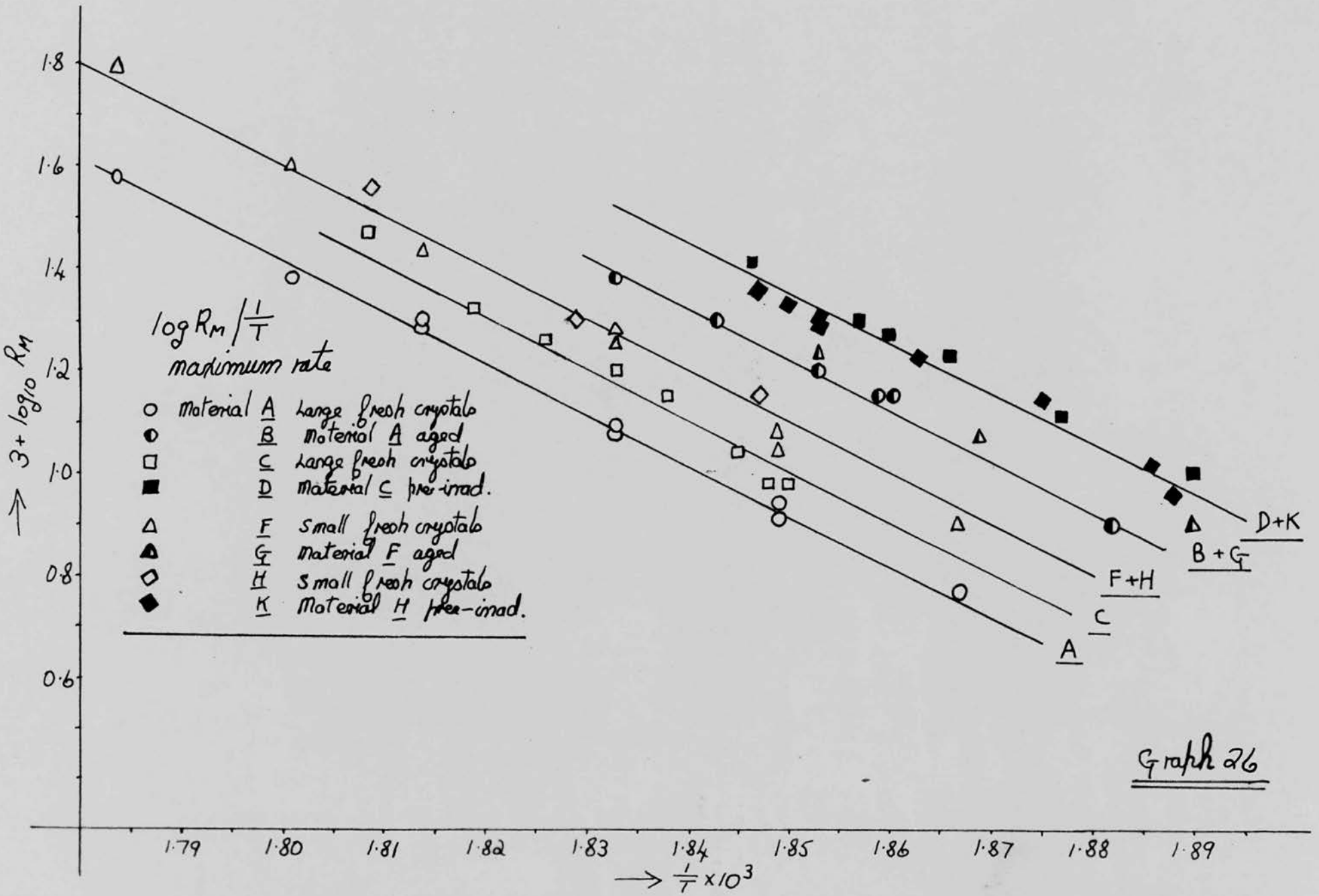
1·8
1·6
1·4
1·2
1·0
0·8
0·6
→ 3+ log10 RM
log RM / 1/T
maximum rate
material A Large fresh crystals
B Material A aged
C Large fresh crystals
D Material C pre-irrad.
F Small fresh crystals
G Material F aged
H Small fresh crystals
K Material H pre-irrad.
D+K
B+G
F+H
C
A
1·79
1·80
1·81
1·82
1·83
1·84
1·85
1·86
1·87
1·88
1·89
→ 1/T x10^3

Graph 26

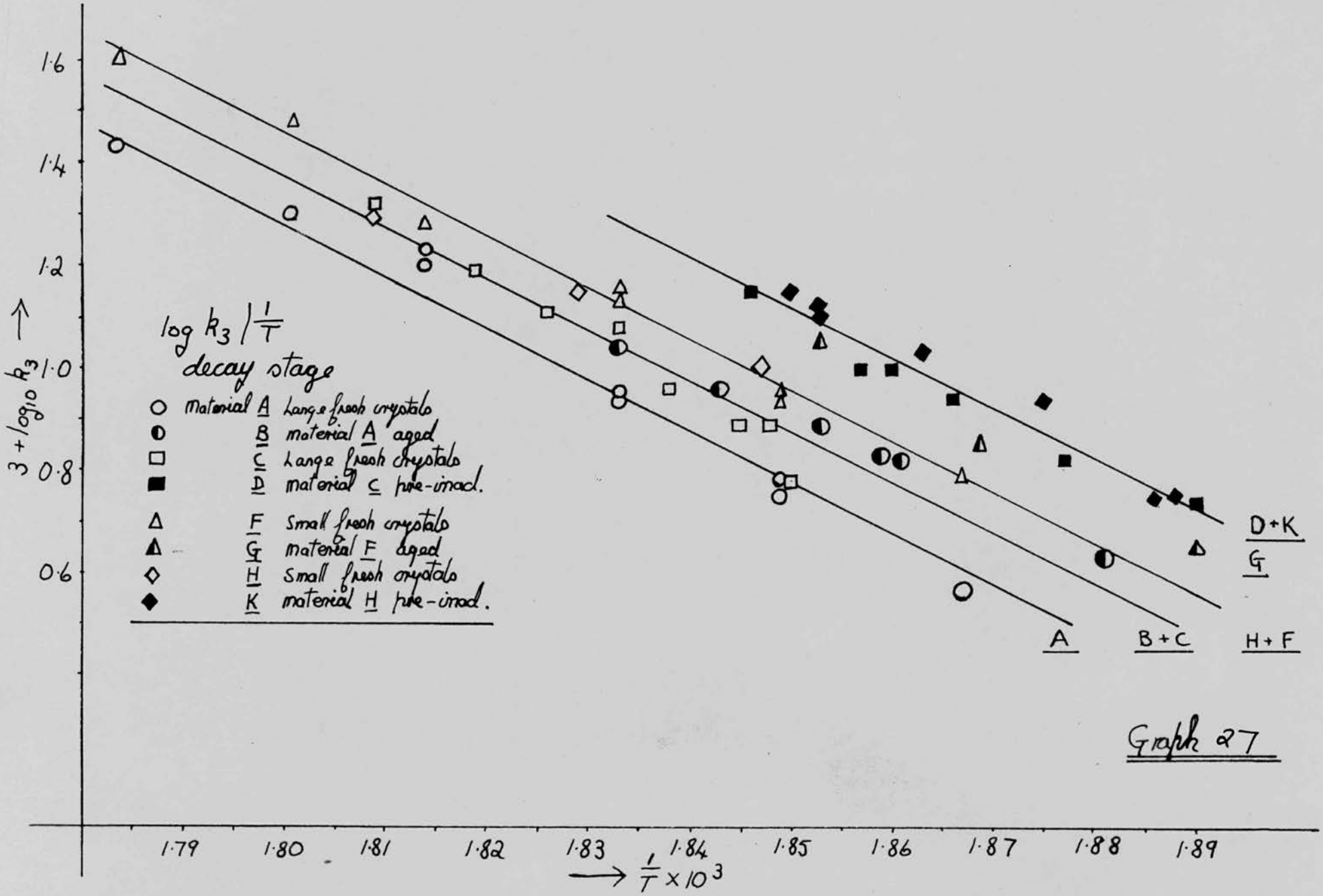
1·6
1·4
1·2
1·0
0·8
0·6
3 + log10 k3 ⟶
log k3 / 1/T
decay stage
material A Large fresh crystals
B material A aged
C Large fresh crystals
D material C pre-irrad.
F Small fresh crystals
G material F aged
H Small fresh crystals
K material H pre-irrad.
D+K
G
A
B+C
H+F
1·79
1·80
1·81
1·82
1·83
1·84
1·85
1·86
1·87
1·88
1·89
⟶ 1/T × 10^3

Graph 27

Finally in table 27 the rate constants are given for the runs performed on material E as described in section 2.6.3. These crystals had been stored for a year and then pre-irradiated for varying lengths of time. A graphical analysis of these results and their significance is given in the discussion.

Table 27. Rate constants for material E.

Temp 545.3°K

Run	Time of pre-irrad.	Time at α = 0.006 min	$R_M \times 10^3$	$k \times 10^2$	$k_3 \times 10^3$	α at end of accel.	$k_4^{\frac{1}{4}} \times 10^3$
8	0	87	17	21	8.1	0.25	-
16	0	90	20	21	11	0.25	-
9	2	75	29	22	15	0.35	-
10	3.25	65	37	22	16	0.40	-
12	7.25	60	39	23	19	0.40	-
14	14.9	40	40	24	26	0.45	6.2
15	18.5	29	45	24	27	0.45	7.5

2.7. Electrical conductivity measurements

For electrical conductivity measurements ground KIO_4 and KIO_3 were compressed at about 3 tons/sq. inch into strong hard cylindrical pellets 0.7 cm in diameter and 1 - 2 mm in height, in which spurious electrical effects due to poor contacts between individual particles[48] were probably minimised. A pellet was held between two 1 cm square platinum electrodes in a conductivity cell similar to that described by Jacobs[49], the electrodes being insulated from the cell by means of vitreous silica plates 3 mm thick, as in Fig. 2a.

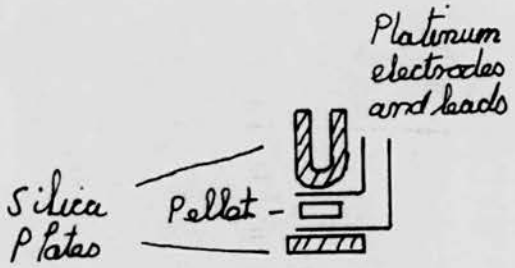

Fig 2a

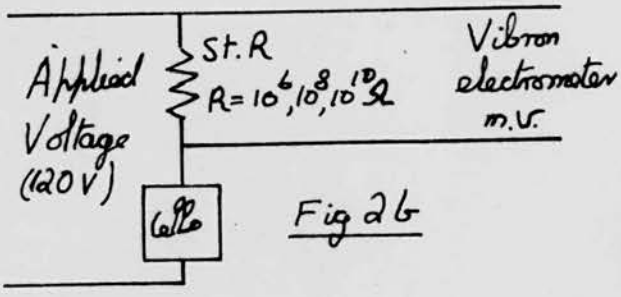

Fig 2b

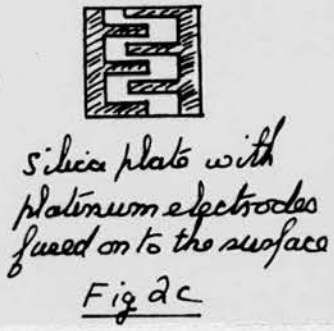

Fig 2c

The silica plates were pressed together by means of a brass screw device, thus ensuring good contact between the platinum electrodes and the pellet surface.

The cell was hung in a pyrex reaction vessel which could be continuously evacuated by means of a three stage oil diffusion pump, backed by a rotary oil pump. The platinum leads from the platinum electrodes were led out of the reaction vessel through seals in soda

glass quickfit B7 cones. The electrical circuit used is shown in Fig. 2b; the voltage drop across the precision resistors being measured by an E.I.L. Vibron Electrometer model. This circuit measured resistances from 10^8 - 10^{15} ohm.

From 400° - 490°K the specific conductivity of pellets of KIO_4 measured in vacuo after 24 h. preliminary evacuation at room temperature was given by $\sigma = 10^0 \exp(-30000/RT)$ ohm^{-1} cm^{-1}, with an error of ca ± 10%. A pellet made from material that had been irradiated for 50 h. as described in section 2.4. gave a similar result. For KIO_3 the conductivity was given by $\sigma = 10^{-1.8} \exp(-19000/RT)$ ohm^{-1} cm^{-1} within ± 10% in the temperature range 290° - 490°K. Measured resistances for pellets of KIO_4 and KIO_3 are given in the following table.

Temp T°K	Resistance (ohm) of KIO_4 pellet, 0.1 cm in height	Temp T°K	Resistance (ohm) of KIO_3 pellet, 0.15 cm in height
423	3.4×10^{14}	294	2.4×10^{15}
435	1.0×10^{14}	317	2.7×10^{14}
449	4.8×10^{13}	336	4.4×10^{13}
454	2.4×10^{13}	347	1.6×10^{13}
459	1.4×10^{13}	354	1.2×10^{13}
473	8.0×10^{12}	483	1.0×10^{10}
483	3.5×10^{12}		

As the specific conductivity of KIO_4 is similar to Sosman's results for vitreous silica[50], it was thought that the resistances measured might have been due to the silica insulators in the cell and not to the pellet. But calculations showed that the leak resistance of

the cell was $\frac{1}{100}^{th}$ of the resistance of the pellet. The specific conductivity of a plate of silica glass 1 mm thick gave results in agreement with Sosman's.

For KIO_4 and KIO_3 both the pre-exponential factors and activation energies are reasonably characteristic of structure sensitive condition[51], although the activation energy for KIO_4 is slightly higher than would be expected. The extremely low conductivity of KIO_4, (the same as for vitreous silica), indicates that the movement of ions probably plays little part in the isothermal decomposition. This is supported by the conductance (10^{-12} ohm^{-1} cm^{-1} at 540°K) being of a similar order of magnitude to that of barium azide[52] and silver oxalate[36] at their respective decomposition temperatures. In these cases it was concluded that a mechanism of ionic transport could not be applied.

An attempt to measure the photo-conductance of a 'film' of KIO_4 on a silica glass plate, with fused platinum electrodes (Fig. 2c), failed due to the resistance of the film being greater than that of the silica plate.

3. Discussion

Darwin[53] was one of the first to realise that a crystal is not a perfectly ordered array of lattice points, but is in fact a mozaic structure. These minute blocks of perfect crystal, of micron dimensions, are in imperfect alignment with each other. Darwin's 'mozaic model' was required to explain the observed intensity of the X-ray diffraction spots from a crystal.

The physical picture of real crystals is now reasonably well established[35], in terms of crystal dislocations and lattice defects. A comprehensive review of dislocation theory is given by Cottrell[54] although this mainly deals with metals. It is considered that crystals greater than ca 100 μ in linear dimensions are divided into grossly disorientated regions by subgrain boundaries that are about 10 μ apart. These boundaries are probably two dimension arrays of edges and screw dislocations, containing impurities absorbed during growth and are sites of mechanical weakness and high reactivity. The subgrains are traversed by a random network of single dislocations which delineate the crystal into irregular mozaic blocks of dimensions less than a micron.

These mozaic blocks contain further crystal imperfections - Frenkal and Schottly defects, which lead to other localized regions of disturbance.

The presence of defects is required to explain many chemical and physical phenomena in the solid state. The transport of matter depends on the existence of structural imperfections, and

many electrical and optical properties of ionic crystals are attributed directly to the presence of defects in an otherwise ordered arrangement. The dislocation theory has been confirmed in the work of Hedges and Mitchell[6]. They showed that the precipitation of photolytic silver in silver bromide, marked out line networks in the interior of the crystal having all the expected characteristics of a dislocation system.

It is within this framework that the kinetics of thermal decompositions have been explained, Tompkins and his co-workers setting the basis for the use of dislocation theory in their work on silver oxalate[36] and mercury fulminate[16].

The application of the above picture to potassium meta periodate indicates that the large crystals (300 μ) contain an extensive network of subgrain boundaries. The small crystals (40 μ) are approximately of subgrain size and probably have none, or very few, subgrain boundaries. The subgrains will be divided into mozaic blocks by a large array of single dislocations.

The chemistry of the reaction has been shown to be simple (2.1.). From a structural point of view tetragonal KIO_4[47] gives rise to monclinic (pseudocubic) KIO_3[46], although Goldschmidt[55] reported the cubic perovskite structure. The powder photographs obtained from analar KIO_3 and from the decomposition product were identical and showed marked splitting of the lines, which would not occur if the three lattice parameters were equal as in a cubic structure; thus supporting the mono-clinic (pseudo-cubic) lattice. This also allows for the existence of the iodate ion in the solid, which

could not be the case in a pure perovskite structure.

The decomposition is one of the few reported that gives a single unambiguous solid phase. Generally exothermic reactions of the type $A_s \rightharpoonup B_s + C_g$, result in the solid phase B being of uncertain composition, e.g. mercury fulminate, or having two or more components, e.g. potassium permanganate, while for the azides the solid phase is metallic. It is also worth noting that the cation K^+ remains unaltered during the decomposition.

With the apparent simplicity of the chemical and physical nature of the reaction it might be expected that the kinetics would follow a straightforward course; this has not proved to be the case.

Kinetics of the decomposition

From the Arrhenius activation energy plots, given in 2.6.6., table 28 is constructed showing the logarithm of the rate constants at 540°K for the different stages in the decomposition of materials A - K. The numbers in brackets represent the relative increase in the rate constants for the pairs of material.

Table 28

Material	Pre-acceleration $5 + \log_{10} R_L$		Pre-acceleration $4 + \frac{1}{2}\log_{10} k_2$		acceleration $2 + \log_{10} k$		acceleration 'α' at R_M		decay $3 + \log_{10} R_M$		decay $3 + \log_{10} k_3$	
A	0.5	(1.4)	-		0.6	(4.0)	0.5		0.9	(2.0)	0.8	(1.25)
B (aged)	0.65		-		1.2		0.2		1.2		0.9	
C	0.5	(3.2)	-		0.7	(2.5)	0.5		1.0	(2.2)	0.9	(1.6)
D (pre-irrad.)	1.0		-		1.1		0.4		1.33		1.1	
	α_o											
F	0.0005		1.0	(1.0)	0.75	(1.6)	0.5		1.1	(1.4)	0.95	(1.25)
G (aged)	0.0007		1.0		0.95		0.5		1.25		1.05	
H	0.00035		0.9	(1.8)	0.75	(2.2)	0.5		1.1	(1.8)	0.95	(1.4)
K (pre-irrad.)	0.0007		1.15		1.1		0.5		1.35		1.1	

Ageing and pre-irradiation with ultraviolet light figure prominently in the experimental work and thus a general discussion is now given of the effects.

Potassium metaperiodate does not undergo any chemical decomposition during storage, there being no visible difference between fresh and aged material for either the large or small crystals.

The different kinetics of the isothermal decomposition were the only measure of the physical changes that occurred with the passage of time.

Ageing in the case of mercury fulminate[16] was clearly chemical in nature, while for ammonium dichromate, Simpson, Taylor and Anderson[29] reported a change in the physical appearance of the crystals together with a possible loss of water, which resulted in the pre-acceleration period being reduced to zero.

For potassium metaperiodate the pre-acceleration periods are unaffected by ageing, which appears to principally affect the bulk of the decomposition (table 28), that is the acceleration and decay periods. As the water content of the crystals is less than 0.01%, it is not considered that this is responsible for the ageing effect. This was confirmed by storing aged crystals in the presence of water vapour for two weeks, after which no change was observed in the decomposition kinetics.

Ageing is probably a physical change, closely connected with imperfections, such as the system of dislocations, present in the bulk of the crystals. Tompkins and Young[35] have discussed the effect of physical ageing on the azides. The azides decompose by a mechanism that involves an aggregation of the cations to form a metallic nucleus, on the other hand at all stages in the decomposition of potassium metaperiodate an ionic lattice is present and the cation is unaffected by the decomposition. Their specific ideas are not applicable to potassium metaperiodate, but the concept of ageing and allied phenomena as involving lattice imperfections is of general use.

The effect of pre-irradiation with ultraviolet light on the subsequent thermal decomposition of solids is not uniform and a wide range of results have been reported. Pre-irradiation has no effect on the decomposition of potassium[38], casium[62] and rhubidium[76] permanganates and on ammonium dichromate[29]. For mercury fulminate[16], silver oxalate[36,37] and potassium azide[58] there is an appreciable photodecomposition during the pre-irradiation and the rate of the thermal decomposition is greatly increased. In the case of silver oxalate and potassium azide anionic vacancies are formed, which, at least in part, are responsible for the differences in the subsequent decomposition. This, of course, cannot occur in, what is by comparison, the insignificant photo-decomposition of potassium metaperiodate, as the metaperiodate ion is transformed into the iodate ion, an anionic vacancy is not created during the decomposition.

For potassium metaperiodate the effect is not limited to the pre-acceleration period as in lithium aluminium hydride[17], but extends to all stages of the decomposition. The rate constants for the pre-acceleration and acceleration periods are substantially increased and to a lesser degree those for the decay period. The effect on the acceleration period indicates that there are changes in the bulk of the crystal, perhaps of a similar nature to those occurring during ageing.

In solution the periodate ion shows maximum absorption at 220 mμ[56]; if this wavelength is responsible for the photolytic decomposition in the solid (2.4.), it is unlikely to penetrate a distance of more than a few lattice spacings[57]. The bulk

effect of the irradiation is probably due to longer wavelengths and may not then be the result of actual decomposition.

Effects associated with the yellow colouration observed after irradiation are not considered to have an effect on the subsequent decomposition[58] due to the rapid disappearance of the colour on heating.

It is essential to discuss the kinetics for the different materials as a unit, so that a physical picture can be developed that can accommodate both large and small crystals. As the exp. section has shown this has been achieved with the framework of the Prout-Tompkins equation for the acceleration period and the contracting sphere equation for the decay period of the reaction. These equations are considered to give the best representation of the experimental results, bearing in mind the wide diversity of materials examined.

The reaction has been divided for convenience into three stages (Graph 1), firstly the pre-acceleration period, secondly the acceleration or autocatalytic period and thirdly the decay period.

(1) The pre-acceleration period

For both large and small crystals the reaction before the main acceleration stage is considered to be due to the growth of the new phase, potassium iodate, at either internal or external surfaces of the crystals.

For the large crystals visual observations (2.5.) clearly

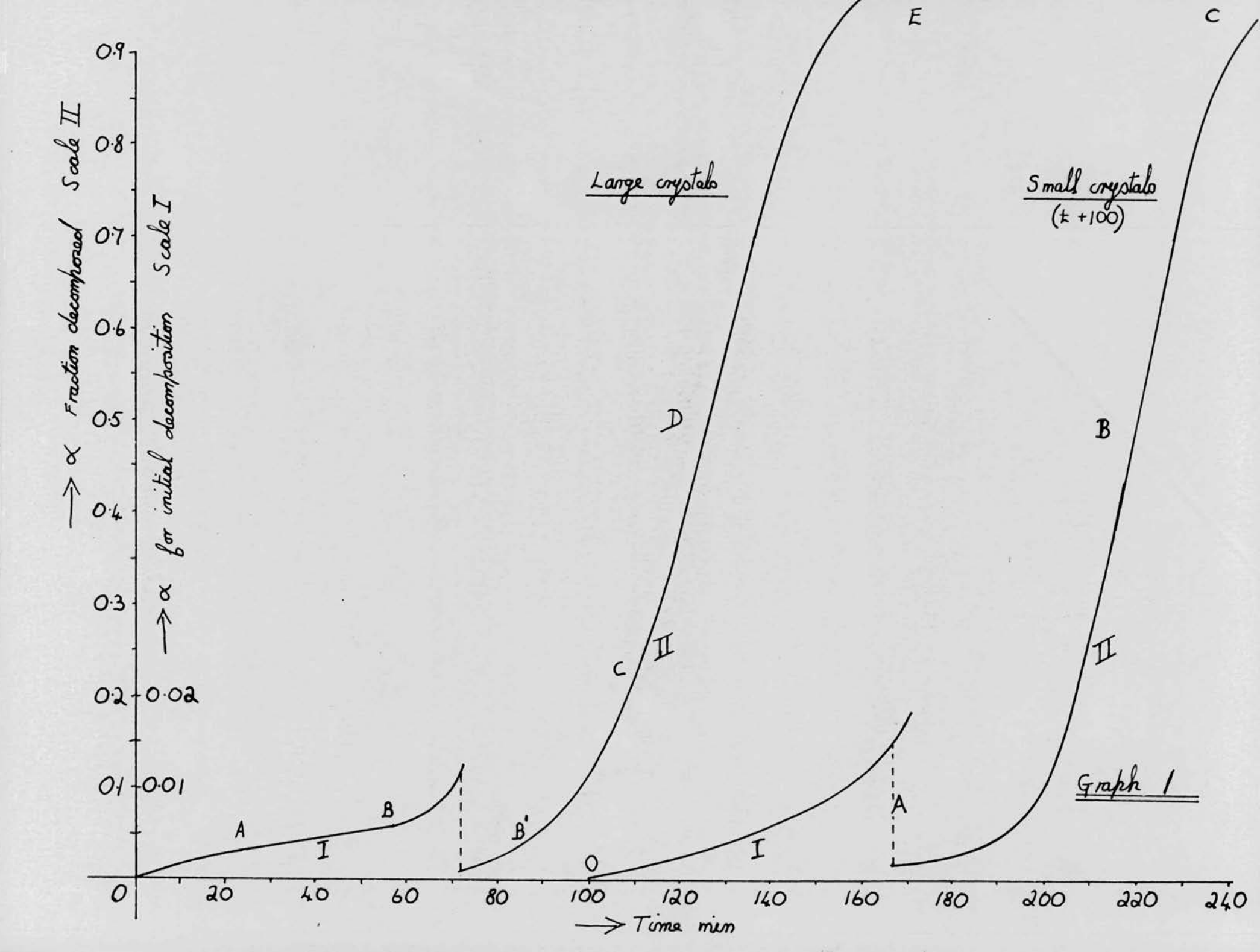
Large crystals
Small crystals
(± +100)
E
C
D
B
C
II
II
A
B
B'
O
A
I
I
Graph 1
→ α Fraction decomposed Scale II
→ α for initial decomposition Scale I
→ Time min
0·9
0·8
0·7
0·6
0·5
0·4
0·3
0·2
0·1
0·02
0·01
0
20
40
60
80
100
120
140
160
180
200
220
240

showed a distinct change in the mechanism at the end of the linear stage AB at α = ca 0.005, where vigorous decrepitation set in. Preceding AB there was an initial reaction, stage OA, which was completed at α = ca 0.003 and had an activation energy of approximately 45 kcal $mole^{-1}$ indicating a chemical reaction and not the desorption of gaseous products. This is considered to be decomposition at some of the subgrain boundaries (the internal surfaces) which creates a constant area interface that progresses into the subgrains giving rise to the linear stage AB. This process would correspond to the beginning of a contracting envelope mechanism. The extent of this reaction is reasonably independent of ageing and pre-irradiation, terminating at α = 0.005, but the magnitude of the rate constant R_L is substantially affected.

Materials A and C, the two similar batches of fresh crystals, have the same rate constant (see table 28) and thus a similar number of subgrain boundaries. This is not unreasonable as the crystals were prepared by the same procedure.

Ageing only slightly increases this rate and the wide scatter of points on graph 22 (2.6.6.) suggests that this is probably insignificant. Pre-irradiation more than doubled the rate and as it caused a small decomposition of the solid (2.4.) its effects seem to be, at least in part, one of nucleation at or near subgrain boundaries. The effect of irradiation in the constant rate reaction is similar to that found in thallous bromate[59].

Graph II (2.6.2.) shows a positive deviation from the

Prout-Tompkins equation, for the irradiated material below $\alpha = 0.06$, as compared with the unirradiated as seen in graph 10, where the Prout-Tompkins acceleration period starts directly after the linear period. This combined with the visual observation that the rapid break up of the crystals did not begin until $\alpha = 0.05$, indicates that pre-irradiation introduces a further mechanism prior to the acceleration.

A power law with n = 4, $(\alpha - \alpha_L) = k_4(t - t_o)^4$ graph 9 (2.5.2.), adequately fits the results from the end of the linear period to the start of the acceleration period. As 't_o' is approximately zero the mechanism starts from the beginning of the decomposition. This equation when interpreted within the concepts of Avrami[23] leads to three dimensional growth of nuclei, with a linear production of growth nuclei from germ nuclei. Thus irradiation produces germ nuclei which are converted at a constant rate to growth nuclei, by the limiting case of the exponential law[60] with a low probability of conversion.

Pre-irradiation of the large crystals produces two initial effects, firstly nucleation of subgrain boundaries leading to a higher rate for the linear stage due to an increased number of subgrain boundaries which decompose. This would be expected to lead to a higher value of α_L, but this reaction is swamped by the second effect, viz. the power law growth from the germ nuclei. The contribution to 'α' by this mechanism is small during the linear stage; for example in run D4 in the first 80 minutes the fractional decomposition due to the power law growth is 0.0002 about 10% of that from the constant rate reaction.

In turn growth from these nuclei is swamped by the Prout-Tompkins mechanism.

The surface area of the small crystals is a factor of 10 larger than that for the large crystals, for a given mass. This, combined with the probable absence of subgrain boundaries, brings into prominence the external surface.

Visual observations gave no indication as to the presence of a pre-acceleration stage. But from the appearance of the 'α' - 't' curves, for example graph 1, the first 2% of the reaction is completed in 50% of the total reaction time, a marked indication of an initial slow reaction. This is supported by the positive deviation from the Prout-Tompkins equation below $\alpha = 0.05$ in Graphs 17 (2.6.4.) and 21 (2.6.5.).

This initial decomposition up to $\alpha = 0.03$ was adequately fitted by a power law with n = 2, i.e. $\alpha = k_2(t - t_o)^2$. This process is consistent with the two dimensional growth on the surface of the crystal of a fixed number of growth nuclei present at the start of the decomposition. The large negative intercepts 't_o' on the time axis of the plot of $\alpha^{\frac{1}{n}}/t$ given in tables 23 - 26 is interpreted as due to a rapid initial growth of these nuclei as in silver oxide[21], anhydrous barium, styphnate trihydride[61] and cesium permanganate[62]. The value of 'α' at $t = 0$ is $\alpha_o = k_2 t_o^2$, and is a measure of the number of nuclei present.

From table 28 it is seen that the rate constant $k_2^{\frac{1}{n}}$ for the normal growth of these nuclei is the same before and after ageing, that is, for materials F and G respectively, and correspondingly

the values of α_o are approximately the same. Assuming the actual rate of growth of the interface is constant regardless of ageing (this is almost certain to be true) the equivalence of the experimental rate constants entails a similar number of nuclei initially present on the surface. It is therefore concluded that the surface of the crystal is unaffected by ageing.

The rate constant for the second batch of small crystals, material H, is 20% lower than that for the first batch, correspondingly the value of α_o is reduced from 0.0005 to 0.00035. Both these facts are indicative of a decrease in the number of surface nuclei in the second batch. This is not surprising as the surface of the crystals will be highly dependent on the conditions under which crystallisation took place, and although the same general procedure was used, the rate of rapid cooling was not strictly controlled.

Pre-irradiation of the fresh material increased the rate constant by about 80% and doubled the value of 'α_o', this being presumably entirely due to the nucleation of the surface during irradiation. This is neatly confirmed by noting that the estimated fractional decomposition due to the irradiation, 0.00035, is identical to the increase in the value of 'α_o'. Thus the surface effect of irradiation is to produce growth nuclei of potassium iodate.

The constant 't_o' represents the time of rapid growth and should be independent of the number of nuclei. To ascertain the truth of this statement the 'log t_o' for the various materials was plotted against the reciprocal of the temperature (graph 28)

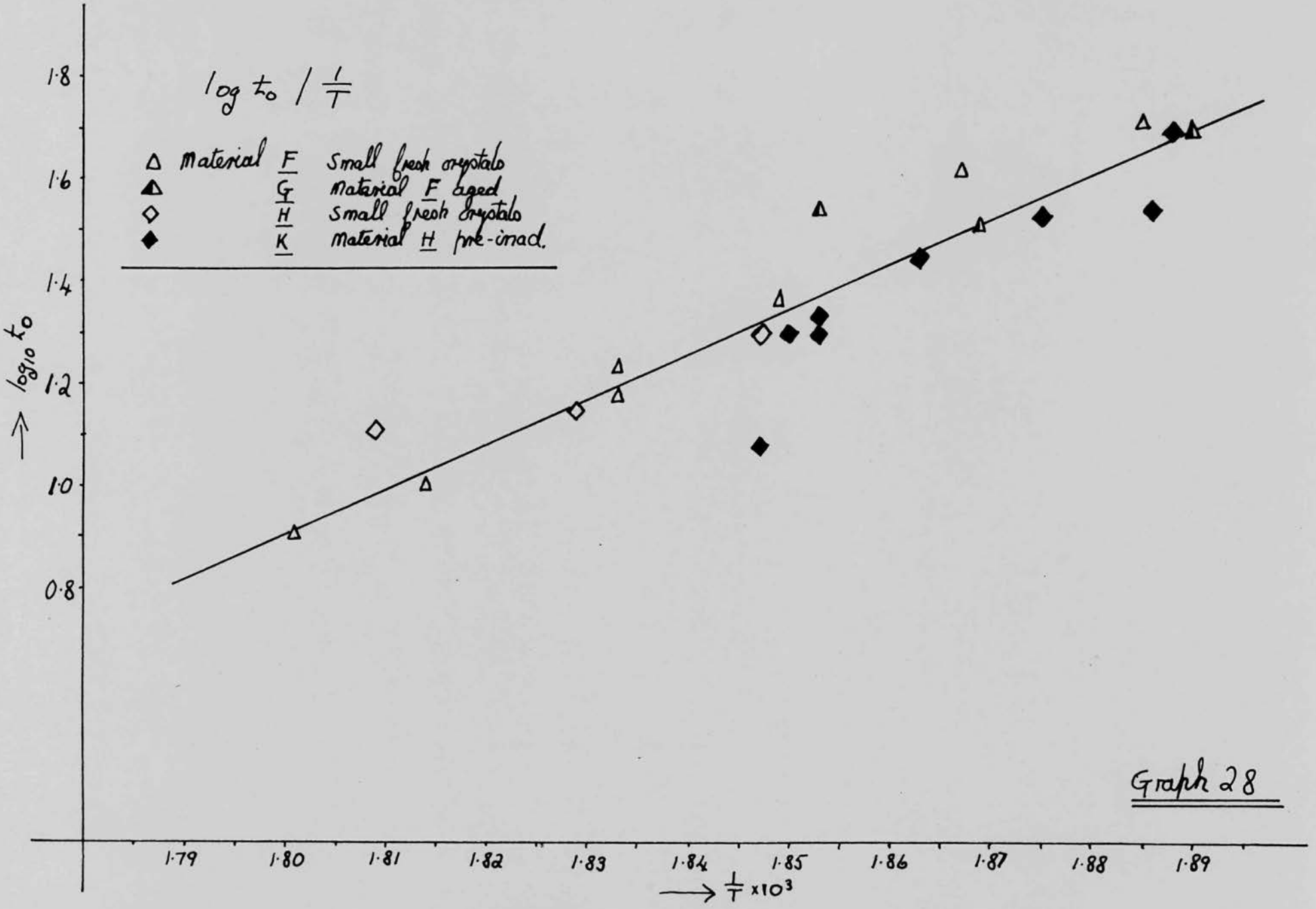
log t₀ / 1/T
△ Material F Small fresh crystals
◭ G Material F aged
◇ H Small fresh crystals
◆ K Material H pre-irrad.
→ log₁₀ t₀
1·8
1·6
1·4
1·2
1·0
0·8
1·79
1·80
1·81
1·82
1·83
1·84
1·85
1·86
1·87
1·88
1·89
→ 1/T x10³

Graph 28

from which it is seen that the points lie scattered about a single line. Thus 't_o' is independent of the number of nuclei as is expected. The activation energy deduced from the slope of this line is 41 ± 7 kcal mole^{-1} and is similar to that found for $k_2^{\frac{1}{2}}$, (41 ± 4 kcal mole^{-1}). This is demanded by the constancy of $k_2 t_o^2$, as the number of nuclei 'α_o' is not temperature dependent.

Thus ageing, pre-irradiation and mode of preparation have no effect on the rate of rapid growth, but pre-irradiation and mode of preparation do affect the number of nuclei.

The activation energy for the constant area interface reaction in the large crystals is 50 ± 5 kcal mole^{-1} which is higher than that for the bulk growth of 46 ± 4 kcal mole^{-1}. As both these values lie within the respective errors it is perhaps not a real difference. Generally the values reported in the literature for the activation energy of the pre-acceleration stage are lower than those for the acceleration stage, as is the case for the small crystals.

At the end of the pre-acceleration stage the large crystals are internally divided into subgrains by the decomposed material. On the other hand, the small crystals, which are about subgrain size, have their external surfaces covered by product. Thus the small and large crystals are in a similar physical state prior to the acceleration stage; although in the large crystals the main mass of the decomposed material is 'sandwiched' between unreacted material, while for the small crystals the product has only one

interface with the unreacted material.

(2) The acceleration period

The mechanism for the acceleration stage has to be consistent with both the pre-acceleration stage and decay stage. The decay stage for the different materials is in all cases best expressed by the contracting sphere mechanism. Thus at the end of the acceleration stage it is necessary to have small particles of periodate completely covered by reaction product.

The Prout-Tompkins equation reasonably represents the acceleration stage for large, small, fresh, aged and pre-irradiated material as seen from the respective graphs in the experimental sections 2.6.1. - 2.6.5. This equation can represent a mechanism by which the reaction spreads through the crystal by means of 'branching planes' of decomposed material as originally proposed by Prout and Tompkins[27] for potassium permanganate and restated by Herley and Prout[62] for the decomposition of cesium permanganate. The controlling factor in the rate of decomposition is the probability of branching 'k'.

Branching of the reaction interface occurs when the interface meets a dislocation in the crystal as was postulated for silver oxalate[36]. Equally, the stress set up at the reaction interface due partly to the different lattice dimensions of the reactant and product, cause cracking, probably at dislocations, these being points of weakness in the crystal lattice. The reaction then spreads down the cracks and the process is repeated. The branching of the interface does not continue unhindered for interference sets

in when a 'branching plane' meets a decomposed surface. The interference of the branching leads to the Prout-Tompkins equation, if there were not interference a pure exponential relationship would exist as originally put forward by Garner and Hailes[14].

The branching and thus the acceleration of the reaction cannot start until the necessary stresses have been created at the interface of the two phases. Prout and Herley[63] have reported that the Laue photographs of partially decomposed crystals of potassium and silver permanganate show asterism of the spots. This is interpreted as demonstrating the existence of strains in the crystals, which leads to the Prout-Tompkins mechanism. The disintegration of the large crystals of potassium metaperiodate follows the same pattern as that for potassium permanganate. The decrepitation which begins at the end of the linear stage (2.5.) is probably not a necessity of the mechanism but a result of it.

For potassium metaperiodate the stresses are produced by the decomposition of the internal and external surfaces which occurs in the pre-acceleration stages. For the decomposition of anhydrous barium styphnate trihydrate, Tompkins and Young[61] have proposed a similar mechanism of branching of the reaction interface due to stresses set up in the early stages of the decomposition.

Decomposition via dislocations will leave the crystal at the end of the acceleration stage divided into a large number of small particles, probably about the size of mozaic blocks. As the surfaces of the particles are covered by product the contracting sphere mechanism can now operate resulting in the start of the

decay stage.

The variation in the rate constant 'k_3' for the decay stage, is solely due to the number of particles present, and thus the degree of branching, at the end of the acceleration stage. This will now be developed from first principles.

The fraction of the particles decomposed, assuming spherical symmetry is,

$$\frac{\alpha - \alpha_i}{1 - \alpha_i} = \frac{\frac{4}{3}\pi a^3 - \frac{4}{3}\pi\left[a - m(t - t_o)\right]^3}{\frac{4}{3}\pi a^3}$$

where 'α' is the fraction of the <u>crystal</u> decomposed, as measured experimentally,

'α_i' is the fraction of the crystal decomposed at the start of the contracting sphere mechanism,

'a' is the radius of the spherical particles at 't_o' the time at the start of the contracting sphere mechanism,

'm' is the linear rate of growth of the interface into the centre of the crystal and

$\frac{\alpha - \alpha_i}{1 - \alpha_i}$, is the fraction of the <u>spherical particle</u> decomposed at time 't'.

Therefore rearranging,

$$\alpha = 1 - \left[(1 - \alpha_i)^{\frac{1}{3}} - \frac{m}{a}(1 - \alpha_i)^{\frac{1}{3}}(t - t_o)\right]^3 \qquad (1)$$

$$\text{Thus } 'k_3' = \frac{m}{a}(1 - \alpha_i)^{\frac{1}{3}} \qquad (2)$$

where 'k_3' was the experimentally found rate constant. If the total volume 'V_o' of the particles at 't_o' is $(1 - \alpha_i)\,V_o$ and

the number of particles is 'n', ['V' is volume of undecomposed crystals]

$$\frac{4}{3}\pi a^3 = \frac{V}{n_o} = \frac{(1-\alpha_i)V}{n}$$

$$\therefore \frac{(1-\alpha_i)^{\frac{1}{3}}}{a} = \left(\frac{4\pi}{3V}\right)^{\frac{1}{3}} n^{\frac{1}{3}} \qquad (3)$$

combining equations (2) and (3)

$$k_3 = \left(\frac{4\pi}{3V}\right)^{\frac{1}{3}} m\, n^{\frac{1}{3}} \qquad (4)$$

Thus assuming a constant rate of growth 'm' the value of 'k_3' depends solely on the number of particles.

Two factors characterize the acceleration period, firstly the rate constant 'k' (the branching coefficient), and secondly the extent of the acceleration period, as given by 'α' at the maximum rate.

For both large and small fresh crystals, A C F and H, the maximum rate occurs at $\alpha = 0.5$, but the value of 'k' (table 28) varies slightly. This variation in 'k' is paralleled by a similar change in the rate constant for the decay stage. This is consistent with the idea that the degree of branching governs the number of particles at the end of the acceleration stage. From the general similarities in the values of 'k' and 'k_3' for these materials, the conclusion can be drawn that the mozaic dislocation structures of the small crystals resembles that of the subgrains in the large crystals.

The effect of 18 months storage on the large crystals A is

very pronounced with a 300% increase in 'k' and the maximum rate brought forward from α = 0.5 to 0.2, but the rate constant for the decay stage is only increased by 25%. Ageing is considered to facilitate the branching process by reducing the stresses required to form a new interface at a dislocation. Thus the crystal is broken into small particles at an earlier stage in the decomposition, as a lower degree of decomposition of the interface is required to produce the branching.

The 25% increase in the rate constant for decay indicates an increase in the number of imperfections in the lattice at which branching occurs leading to a larger number of particles in the decay stage and thus a factor rate.

The constant 'k' for the aged small crystals G is only increased by 60% as compared with that for the fresh small crystals F and H, and the constant 'k_3' is increased by 25%, the maximum rate occurring at the same value of α = 0.5. The increased rate of decay indicates an increase in the number of particles as in the aged large crystals and thus a larger number of imperfections have participated in the acceleration, but as this continues to α = 0.5 the same stresses appear to be necessary to produce the branching unlike the case of the large crystals.

The pre-irradiated large crystals D show an increase in 'k' of 150% but a slight decrease in the extent of the acceleration period, the maximum rate occurring at α = 0.4. As the rate constant for decay has increased by 60%, irradiation has created branching points combined with a slight lowering of the stresses

required for branching leading to an earlier maximum rate. The value of 'k' after pre-irradiation is similar to that for aged crystals, suggesting that irradiation produces imperfections of a similar nature to those present in the crystal after ageing.

The rate constants for the acceleration and decay stages of the pre-irradiated small crystals K are identical to those of the pre-irradiated large crystals. This is to be expected as the small and large crystals had identical pre-treatment. The acceleration stage for the small crystals continues to $\alpha = 0.5$ and is not lowered as is the case for the large crystals. Thus the result of pre-irradiation of the small crystals is confined to the production of branch points, which is parallel to the limited effect of ageing in the small crystals.

The fact that the small crystals do not appear to show a shortening of the acceleration stage after ageing and pre-irradiation, as is observed for the large crystals, is perhaps due in some measure to the actual difference in size. The small crystals are $\frac{1}{400}^{th}$ the volume of the large.

Material E was crystals made in a similar manner to A and C but stored for one year and then pre-irradiated for varying lengths of time. Graph 29 illustrates the effects on the subsequent decomposition as a function of the length of pre-irradiation.

The most interesting feature is that the rate of acceleration, as measured by the branching coefficient 'k', is nearly constant regardless of the length of pre-irradiation. The effects of the irradiation is to extend the acceleration stage from $\alpha = 0.25$ to

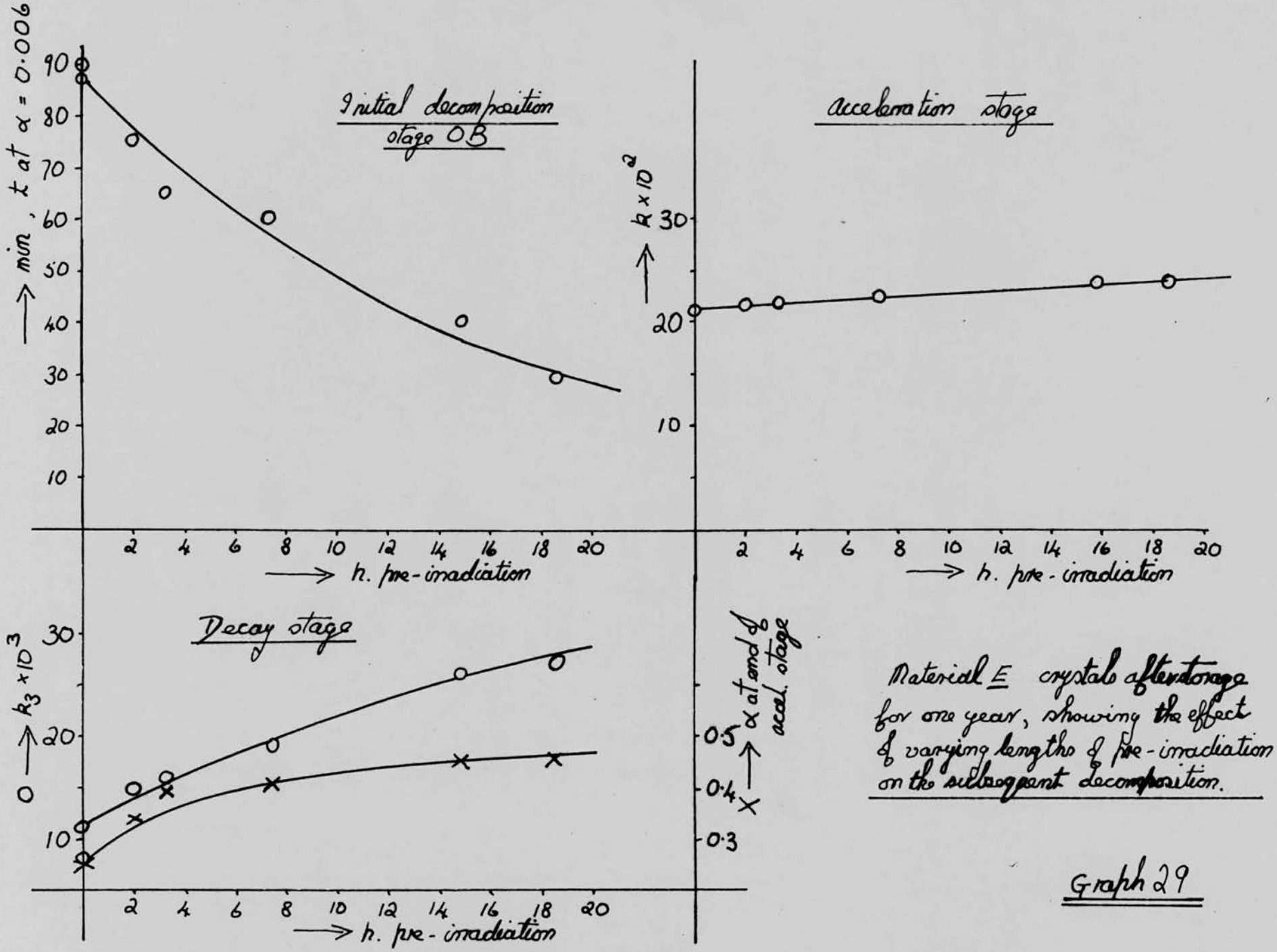

Material E crystals after storage for one year, showing the effect of varying lengths of pre-irradiation on the subsequent decomposition.

Graph 29

0.45 and increase the rate of decay. This fits into the previous picture that irradiation produces imperfections similar to those present in aged crystals; the resulting increase in the degree of branching leads to a larger number of particles and thus a faster rate of decay.

The time for the initial decomposition decreases with length of irradiation corresponding to the rate increases found for material D. Graph 14 (2.6.3.) illustrates that for run E 15 the power law growth has been introduced before the acceleration stage, confirming the results for material D.

(3) The decay stage

As is observed from graphs 6 (2.2.1.), 12 (2.2.2.), 18 (2.2.4.) and 22 (2.2.5.) the decay stage is well expressed in terms of the contracting sphere equation. Although for the aged small and large crystals there is a tendency for the equation to fail at $\alpha > 0.85$ probably due to collapse of the interface and unimolecular decay setting in.

The particles that are created by this mechanism are formed as a result of the branching planes of the acceleration stage dividing the crystal into roughly similar particles of probably $< 1\ \mu$ - mozaic block size - with their surfaces covered by product molecules. This reaction interface then contracts into the particle with an activation energy for the linear progression of the interface of 46 ± 4 kcal mole^{-1}, which is the same activation energy as that found for the acceleration stage. These 'mozaic blocks' contain a few or no dislocations so there

can be no increase in surface area by further branching. Thus the rate is entirely dependent on a fixed surface decreasing in area following the equation $\frac{d\alpha}{dt} = A(1 - \alpha)^{\frac{2}{3}}$ which when integrated gives equation (1).

From a comparison of the rate constants 'k_3' for the decay stage and the value of 'α' at the maximum rate, of any pair of materials, it is possible to deduce the change in the maximum rate. The rate of decomposition at the start of the decay stage is equal to the maximum rate, therefore $R_M = \gamma a^2 n$ where 'γ' is a constant. Combining this with equation (3)

$$R_M = \gamma (1 - \alpha_i)^{\frac{2}{3}} n^{\frac{1}{3}} \qquad (5)$$

Using the data in table 28 the maximum rates are compared for the different materials, as represented by the letters in brackets.

$$R_{M(A)}^{(B)} = \frac{1 - \alpha_i(B)^{\frac{2}{3}}}{1 - \alpha_{i(A)}} \times \frac{n(B)}{n(A)}^{\frac{1}{3}} \qquad (6)$$

$$= \frac{1 - 0.2^{\frac{2}{3}}}{1 - 0.5} \times 1.25$$

where $\frac{n(B)}{n(A)}^{\frac{1}{3}} = \frac{k_3(B)}{k_3(A)}$ from equation (4)

thus $R_{M(A)}^{(B)} = 1.73.$

Table 29 gives the calculated and experimental values of this ratio.

Table 29

Material	Ratio of R_M calculated from (6)	Ratio of R_M experimental
$\frac{B}{A}$	1.7	2.0
$\frac{D}{C}$	1.8	2.1
$\frac{G}{F}$	1.25	1.4
$\frac{K}{H}$	1.4	1.8

The agreement between the calculated and the experimental values is within 20%. This is considered reasonable bearing in mind the assumption that the particles are spheres all of equal size. The agreement is a general indication that the mechanism proposed is along the right lines although undoubtedly not as simple.

Further confirmation that the crystals break up into small particles was obtained from X-ray powder photographs. A 'powder photograph' of the uncrushed small crystals gave as expected a few spots, but a photograph of these crystals after decomposition resulted in lines as in a normal powder photograph. The decomposed crystals had the same external form as the undecomposed (2.5.). Thus decomposition internally divides the small crystals into disorientated parts, as would have been achieved by crushing.

The acceleration stage has been expressed in terms of the Prout-Tompkins equation, but the experimental results on this stage are not entirely conclusive. The kinetics for the large crystals A is better expressed by a power law with n = 3, corrected for the initial linear growth, although after ageing (B) the Prout-Tompkins equation is probably superior, generally fitting immediately after the linear stage. The Prout-Tompkins equation as derived is only strictly applicable when the maximum rate is at $\alpha = 0.5$, but it reduces to $\alpha = A \exp(kt)$ for values of 'α' up to 0.2. Thus for material B it would be truer to say that there was an exponential relationship, indicating non-interference of the branching. As it has been previously argued that there are nearly the same number of branch points (imperfections) in the crystals before and after ageing, but as there is interference in fresh material and not in aged, this supports the contention that the ease of branching at these imperfections is facilitated by ageing.

In graphs 30, 31 and 32, the relative merits of the Prout-Tompkins equation and the power law with n = 3, are compared for large and small crystals before and after pre-irradiation and for the large crystals when aged. Generally the Prout-Tompkins is superior and for fresh large crystals C, the power law is not applicable.

The fit for the power law equation can be improved if the fraction subtracted from 'α' is greater than that at the end of the pre-acceleration stage (α_L and α_p in this case), although there is little justification for this.

A power law with n = 3 necessitates the formation at the

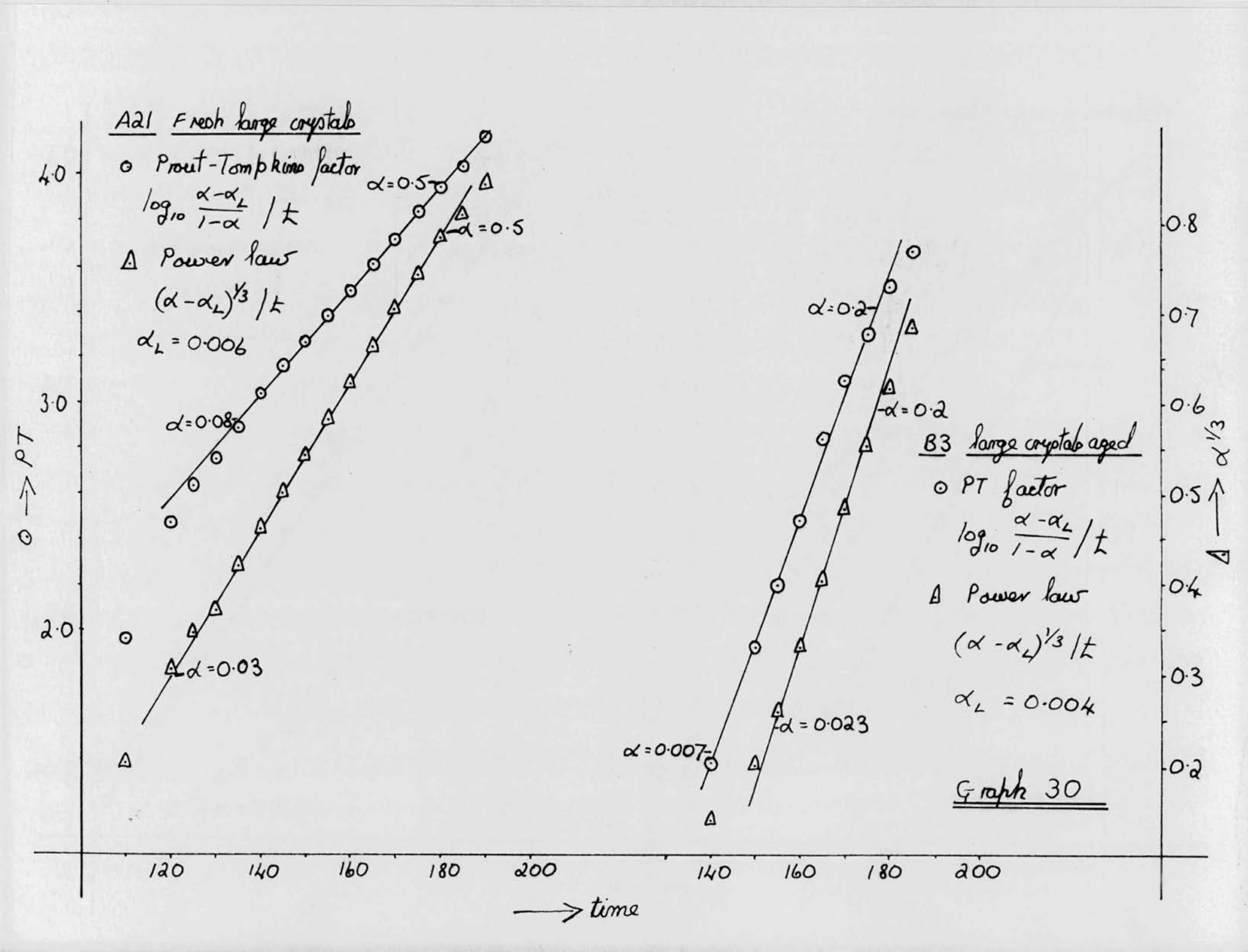
A21 Fresh large crystals
⊙ Prout-Tompkins factor
$\log_{10} \frac{\alpha-\alpha_L}{1-\alpha} / t$
Δ Power law
$(\alpha-\alpha_L)^{1/3} / t$
$\alpha_L = 0.006$
$\alpha = 0.5$
$\alpha = 0.08$
$\alpha = 0.03$
B3 large crystals aged
⊙ PT factor
$\log_{10} \frac{\alpha-\alpha_L}{1-\alpha} / t$
Δ Power law
$(\alpha-\alpha_L)^{1/3} / t$
$\alpha_L = 0.004$
$\alpha = 0.2$
$\alpha = 0.007$
$\alpha = 0.023$
Graph 30
⊙ → PT
Δ → $\alpha^{1/3}$
time
4·0
3·0
2·0
0·8
0·7
0·6
0·5
0·4
0·3
0·2
120
140
160
180
200
140
160
180
200

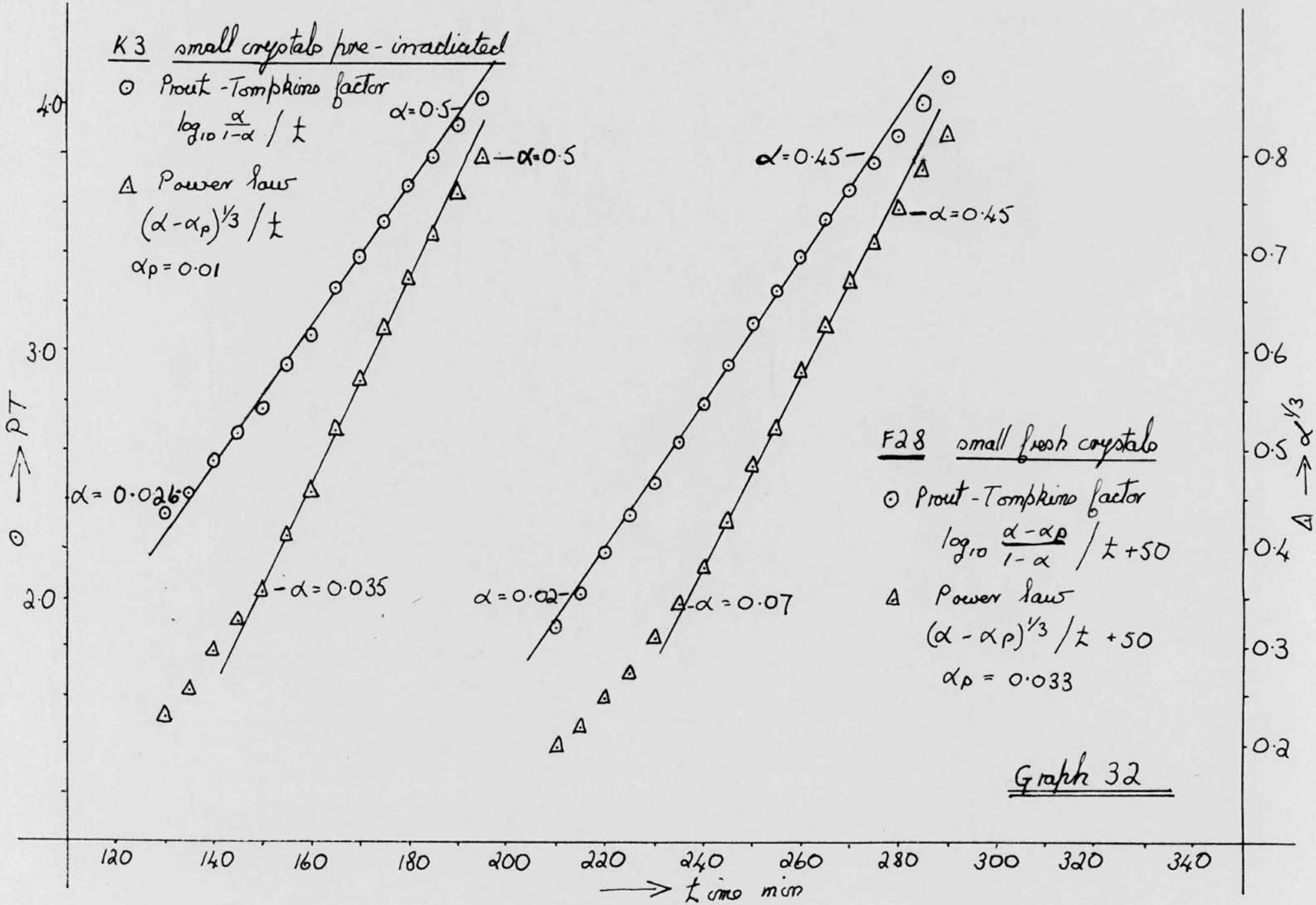
K3 small crystals pre-irradiated
○ Prout-Tompkins factor
$\log_{10} \frac{\alpha}{1-\alpha} / t$
△ Power laws
$(\alpha - \alpha_p)^{1/3} / t$
$\alpha_p = 0.01$
$\alpha = 0.5$
$\alpha = 0.035$
$\alpha = 0.026$
F28 small fresh crystals
○ Prout-Tompkins factor
$\log_{10} \frac{\alpha - \alpha_p}{1-\alpha} / t + 50$
△ Power laws
$(\alpha - \alpha_p)^{1/3} / t + 50$
$\alpha_p = 0.033$
$\alpha = 0.45$
$\alpha = 0.07$
$\alpha = 0.02$
Graph 32
○ → PT
△ → $\alpha^{1/3}$
→ t time min
4·0
3·0
2·0
0·8
0·7
0·6
0·5
0·4
0·3
0·2
120
140
160
180
200
220
240
260
280
300
320
340

end of the pre-acceleration stage, of growth nuclei, which then grow at specific sites in the crystal and coalesce at the respective maximum rates for the different materials. If the nuclei were uniformly distributed throughout the crystal the maximum rate would always occur at the same fractional decomposition, independent of the number of nuclei. As this is not the case for large aged and pre-irradiated material, the nuclei must grow as specific sites which are decreased in number after ageing. The plot of $\alpha^{\frac{1}{3}}/t$ gives intercepts on the time axis at $\alpha = 0$ that are large and positive and correspond to the time at the end of the pre-acceleration stage. Thus all the nuclei are formed at one instant at the end of the pre-acceleration stage which is hard to visualise, more so as this constitutes one half of the total reaction time.

The Prout-Tompkins mechanism is thus preferred both from the kinetic analysis of the 'α' - 't' curves and from the satisfactory manner in which the mechanism is in harmony with the overall picture of the decomposition.

In the course of the calculations the differential form of the Avrami equation $\frac{dt}{d\alpha}(1 - \alpha)\ln(1 - \alpha) = \frac{1}{n}t$, was considered to be a superior method of plotting the equation, compared with the normal form $\ln\left[-\ln(1 - \alpha)\right] = n \ln t + C$; as it eliminates the necessity of plotting the logarithm of the time, with all the uncertainties that this involves. In run C 5 (page 30), the Avrami equation was found not to apply; the value of 'n' varied from 30 to 4 as the decomposition progressed.

Chemical mechanism of the decomposition

The overall reaction is

$$KIO_4 \longrightarrow KIO_3 + \tfrac{1}{2}O_2 \qquad \Delta H = -9 \text{ kcal mole}^{-1}$$

when this is combined with

$$O_2 \longrightarrow 2O \qquad \Delta H = 117 \text{ kcal mole}^{-1}$$

it is found that

$$KIO_4 \longrightarrow KIO_3 + O \qquad \Delta H = 49.5 \text{ kcal mole}^{-1}.$$

Thus the thermal breakdown of the metaperiodate ion into an atom of oxygen, requires approximately 50 kcal $mole^{-1}$ for the rupture of the iodine-oxygen bond. This is comparable to the activation energies found experimentally, suggesting that they have a direct relationship with the primary chemical act.

The kinetics of the decomposition have been explained in terms of the decomposition of an interface which increases in area due to branching during the acceleration stage and decreases in area by means of the contracting sphere mechanism during the decay stage. Two factors control the rate of the reaction, the rate of linear progression of the interface and the area of the interface. The Polanyi-Wigner equation,

$$\frac{dn}{dt} = N \nu \exp(-E/RT),$$

is an expression for the rate of decomposition of the interface where

$\frac{dn}{dt}$ is the number of molecules decomposing per second,

N is the total number of molecules on the interface,

ν is the vibrational frequency responsible for the decomposition and is approximately equal to 10^{13} sec^{-1}, and E is the energy of

activation calculated from the temperature coefficient of the velocity of movement of the interface.

For the large crystals the area of the subgrain boundaries is the constant interface for the initial 'linear stage' constant rate reaction. A tentative estimate can be made of the area of the subgrain boundaries. If they are assumed to be 10 μ apart[16] and the crystal a cube of 300 μ in length, the area is ca 2×10^{7} μ^2. The area of a molecule is ca 2×10^{-7} μ^2 as calculated from the dimensions of the unit cell of 4 molecules with a = b = 5.75 A and C = 12.63 A[47]. Thus there are ca 10^{14} molecules on the surface of the subgrain boundaries. In run A 46 (page 25) the fraction of the crystal decomposed per second was ca 10^{-7} and as there are ca 10^{17} molecules in a crystal (calculated from the dimensions and weight), the rate of decomposition was ca 10^{10} molecules sec^{-1} at a temperature of 530°K. Using the Polanyi-Wigner equation with $N = 10^{14}$, $\nu = 10^{13}$, E = 50 kcal $mole^{-1}$ (page 50) and T = 530°K, the rate of the reaction is equal to

$$\frac{dn}{dt} = 10^{14} \times 10^{13} \times \exp(-50000/2 \times 530)$$
$$= 10^{7} \text{ molecules } sec^{-1}.$$

This is not an unreasonable agreement with the experimental value of 10^{10} molecules sec^{-1}, considering the approximations involved in estimating the interface area and the probable error in the activation energy. Thus the frequency factor 'ν' would have to be 10^{16} to bring the theoretical rate in line with the experimental.

The maximum rate is 300 times the constant rate for the

initial linear stage and assuming the same linear rate of progression of the interface there must have been a threehundred fold increase in the area of the interface. This is the expected increase in area if the subgrains are divided into particles 0.1 u in linear dimensions. This is in excellent agreement with the expressed view that the Prout-Tompkins mechanism divides the crystal into small particles the size of mozaic blocks. The application of the Polanyi-Wigner equation to the beginning of the contracting sphere stage leads to the same result as found for the initial linear stage, both the rate and interface area being increased by ca 300. But the value of E is 46 kcal $mole^{-1}$ (page 50) so the frequency factor is 10^{14-15}, which is in good agreement with the accepted value of 10^{13}.

Previous applications of the Polanyi-Wigner equation to chemical reactions, as distinct from polymorphic phase changes, have been limited to endothermic reactions primarily the dehydration of salt hydrates[64]. It was found that when the heat of reaction was similar to the activation energy[65], the frequency factor was ca 10^{13} sec^{-1}; but where the activation energy was considerably higher than the heat of the reaction the frequency factor was ca 10^{25} sec^{-1}. To explain these anomalous frequency factors the view has been put forward that a whole mozaic block undergoes instantaneous transformation on each act of excitation. This is called the Burgess and Mott trigger mechanism[66].

For potassium metaperiodate the heat of reaction for the probable primary chemical step is similar to the activation energy and the frequency factors are not anomalously high. Thus the simple interfacial character of the decomposition appears to be confirmed.

SECTION II

The isothermal decomposition of potassium permanganate-potassium perchlorate solid solutions

1. Introduction

Greenberg and Walden[69] have shown that potassium permanganate and potassium perchlorate form a continuous series of solid solutions, which obey Vegards additivity law.

In work on the kinetics of the isothermal decomposition of the solid solutions, Hinshelwood and Bowen[70, 71] in 1920-21 explained the acceleration stage of the decomposition in terms of a progressive disintegration of the crystal structure with a consequent increase in the effective surface area. Solution in potassium perchlorate caused a reduction in the rate of the reaction, due to the suggested increased stability of the permanganate ion in the perchlorate lattice. They found that only the permanganate ion decomposed.

No further work appears to have been published on the decomposition of the solid solutions and the following introduction will deal with the work performed on potassium permanganate alone.

The decomposition can be represented by[27]

$$2KMnO_4 \longrightarrow K_2MnO_4 + MnO_2 + O_2$$

although Simchen[72] has reported

$$4KMnO_4 \longrightarrow 2K_2O + 3MnO_2 + MnO_3 + 2\tfrac{1}{2}O_2$$

This can be interpreted as a further decomposition of potassium manganate into potassium oxide, manganese dioxide and oxygen.

When the decomposition is performed under isothermal conditions the addition of the products of the reaction to crystals of potassium permanganate appear to have little effect[27,72,69], but using a gradually rising temperature Roginsky and Schulz[73] and Hill[74,75] observed, for iron and other oxides, a catalytic effect. This has been explained in terms of the creation of nuclei, resulting from the diffusion of ions into the lattice. This process probably has a low activation energy[74] and is thus effective at low temperatures.

The kinetics of the decomposition have been interpreted in various ways. Prout and Tompkins[27] in a study on fresh crystals, in the temperature range 473 - 493°K, found that after a linear induction period[76] of 4 - 5% decomposition, the reaction time curve was well fitted by the Prout-Tompkins equation. Grinding of this material in an agate mortar removed the induction period.

Erofeev and Smirmova[77] found that their results fitted the Avrami[23] equation with n = 4 or 5. They interpreted this as three dimensional growth and one or two 'acts' required for the formation of the nuclei. For commercial or aged material the value of 'n' was 2, representing two dimensional growth of a fixed number of nuclei. The values of 'n' were obtained by plotting $\ln \left[\ln 1/1 - \alpha\right]$ against $\ln t$, where the slope of the line was 'n'. This is an insensitive analytical method and the kinetics deduced from their results are therefore open to doubt, but the differences between fresh and aged material remain.

Similarly Roginsky and Schulz[73] using commercial material

fitted their results to a power law with n = 3.

Hill and Welsh[78] found, that for the early stages of the acceleration period for fresh material, the increase of pressure with time could best be represented by the exponential relationship $\alpha = A \exp(kt + C)$. This confirms the results of Prout and Tompkins, as the Prout-Tompkins equation reduces to the exponential form initially. For aged material Hill obtained poor exponential relationships, which also agrees with the previous workers' results.

Komatsu[79] has shown that the rate of the decomposition is dependent on the crystal size, the rate increasing with decreasing size.

Thus for a comparative study of the kinetics of decomposition of solid solutions of different compositions, it is necessary to standardise the experimental conditions. In the following work all the crystals used had linear dimensions of 300 - 500 μ and each batch of crystals was made as required and used within two weeks. The crystals used can thus be considered as fresh material.

2. Experimental

2. 1. Growth of crystals

Analar potassium permanganate and Kahlbrawm's potassium perchlorate were used as starting materials. 500 ml of a saturated aqueous potassium permanganate solution at 60°C was allowed to cool to room temperature, in the dark, and then filtered through a sintered glass filter funnel. The filtrate was allowed to evaporate, in the dark, for approximately 12 hours. The supernatant liquid was decanted, the crystals rapidly dried and those of 300 - 500 μ in linear dimensions selected by sieving.

A second batch of crystals was made by the same procedure. Visual observations showed that the second batch was nearly free from external flaws, while the first batch had visible imperfections.

By use of the phase diagram for $KMnO_4$ - $KClO_4$ - H_2O, given by Greenberg and Walden[69], saturated solutions were prepared such that the solid phase deposited on evaporation would have the desired percentage of potassium perchlorate. The procedure as given for potassium permanganate was then followed with the following additions. 2.5 l. of solution were prepared and not more than 1 g. of solid was allowed to crystallise out so that the composition of the solid solutions remained virtually constant, thus ensuring reasonable homogeneity of the solid solutions produced. Due to the low solubility of potassium perchlorate as compared with permanganate, the rate of evaporation was increased by evaporating in a current of air.

It was found impossible to obtain by the above procedure

crystals of low percentage potassium permanganate, that were of the required crystal size. For this case a saturated solution of the required composition at 35°C was allowed to cool to room temperature. The resulting crystals were however markedly inferior to those produced by slow evaporation.

The solid solutions were analysed for potassium permanganate by addition of excess of standard ferrous ammonium sulphate solution and back titration with standard potassium permanganate solution. The presence of potassium perchlorate was shown not to affect the results.

In this way the following batches of crystals were prepared as required. The average dimensions were 300 - 500 μ.

By slow evaporation,

A 100 mole percent $KMnO_4$,

B 100 mole percent $KMnO_4$,

C large single crystal of $KMnO_4$,

D 89 mole percent $KMnO_4$,

E 70 mole percent $KMnO_4$,

F 52 mole percent $KMnO_4$.

By crystallisation from a saturated solution by cooling,

G 25 mole percent $KMnO_4$.

2. 2. Preliminary observations

Preliminary kinetic experiments on the solid solutions were carried out in an identical manner to those described in the first section. For pure potassium permanganate (material A)

the pressure-time curve corresponded to Prout and Tompkins results for large crystals, but the volume of oxygen produced was in agreement with the results of Simchen, indicating a possible decomposition of the manganate ion. The presence of low percentages of potassium perchlorate reduced the rate of the reaction but otherwise did not effect a change in kinetics from those observed for material A. For high percentages of potassium perchlorate (material G) the Prout-Tompkins equation did not apply and the volume of oxygen released was far in excess of the value predicted by Simchen.

Potassium perchlorate decomposes in vacuo at 800 - 820°K by a complicated mechanism[80]. This is 250° in excess of the temperature of decomposition of material G, but it was thought likely that the manganese dioxide produced in the decomposition catalysed the decomposition of the potassium perchlorate, thus explaining the large amount of oxygen produced. This was confirmed from the analysis of the product from G which showed the presence of chloride ions. However after only 10% decomposition of G no chloride ions were detected. A 50 - 50 mixture of $KClO_4$ and MnO_2 on heating at 570°K released oxygen, but not at 510°K.

It was therefore decided to study only the first 5 - 10% of the reaction and to limit the maximum temperature to 510°K. Under these conditions only the permanganate ion decomposes, agreeing with the conclusions drawn by Hinshelwood and Bowen.

2. 3. Experimental procedure

The apparatus and procedure used to record the variation of pressure with time is given in section I (2.2.). The pressure was measured by means of a Pirani gauge coupled to a recorder, giving a continuous record of the pressure-time curve. Full scale deflection of 10" on the recorder represented, on the average, 7% decomposition, and as the recorder chart was subdivided into 0.1" it was estimated that the % decomposition as read from the trace was accurate to 0.02% as this represented 0.03". Thus the course of reaction through a given 1% decomposition was accurately known. A theoretical final pressure was calculated on the basis of one molecule of oxygen from two molecules of permanganate. The measured pressures were converted to the fractional decomposition 'α' by dividing by the final pressure.

The rate of the reaction was determined by drawing tangents to the continuous pressure-time curve. With care this was found to be a fairly accurate procedure.

Hill and Welsh[78] have noted that a differential method of analysing the 'α' - 't' curves avoids the use of arbitrary parameters. A plot of $\frac{d\alpha}{dt}/t$ and $(\frac{d\alpha}{dt})^{\frac{3}{2}}/\alpha$ represent the power law equation with n = 2 and 3 respectively and $\frac{d\alpha}{dt}/\alpha$ represents the exponential equation. In the latter case the constant obtained from the plot is independent of the estimate of the fractional decomposition, and only depends on the relative change in the pressure reading. As it was intended to examine in

detail a small fraction of the total decomposition of the solid solutions this sensitive analytical procedure was used.

2. 4. Kinetics of the decomposition

The typical shape of the 'α' - 't' curves is shown in graph 1. For pure potassium permanganate there is an initial sigmoid section terminating at α = 0.007; this is followed by a linear stage which leads into the acceleration period. Runs D1 and F1 illustrate the effect of the potassium perchlorate; the initial decomposition as represented by the sigmoid is reduced and the linear stage is less pronounced. The overall rate of decomposition for the three examples is similar but the reaction temperature is increased as the potassium perchlorate content of the solid solutions rises. Graph 2 shows the rate-time curves for the above 'α' - 't' curves. The linear stage appears as a constant rate and sometimes following this there is a linear increase in rate with time. The true acceleration stage, following either the constant or linear rate period, commences at ca α = 0.02. Measurements on the decomposition did not extend past α = 0.07.

The curves have been analysed in terms of the following relationships between α, $\frac{d\alpha}{dt}$ and t, where 'α' is the ratio of the pressure at time 't' to the final pressure. Henceforth $\frac{d\alpha}{dt}$ will be represented by 'R'.

The initial sigmoid section of the curve has not been analysed in detail and the maximum rate, for this section, has been taken as a measure of the mechanism.

The linear relationship between 'α' and 't' is represented by $\alpha = k_L t + C$, thus $R = k_L = R_L$, with α_L the fraction

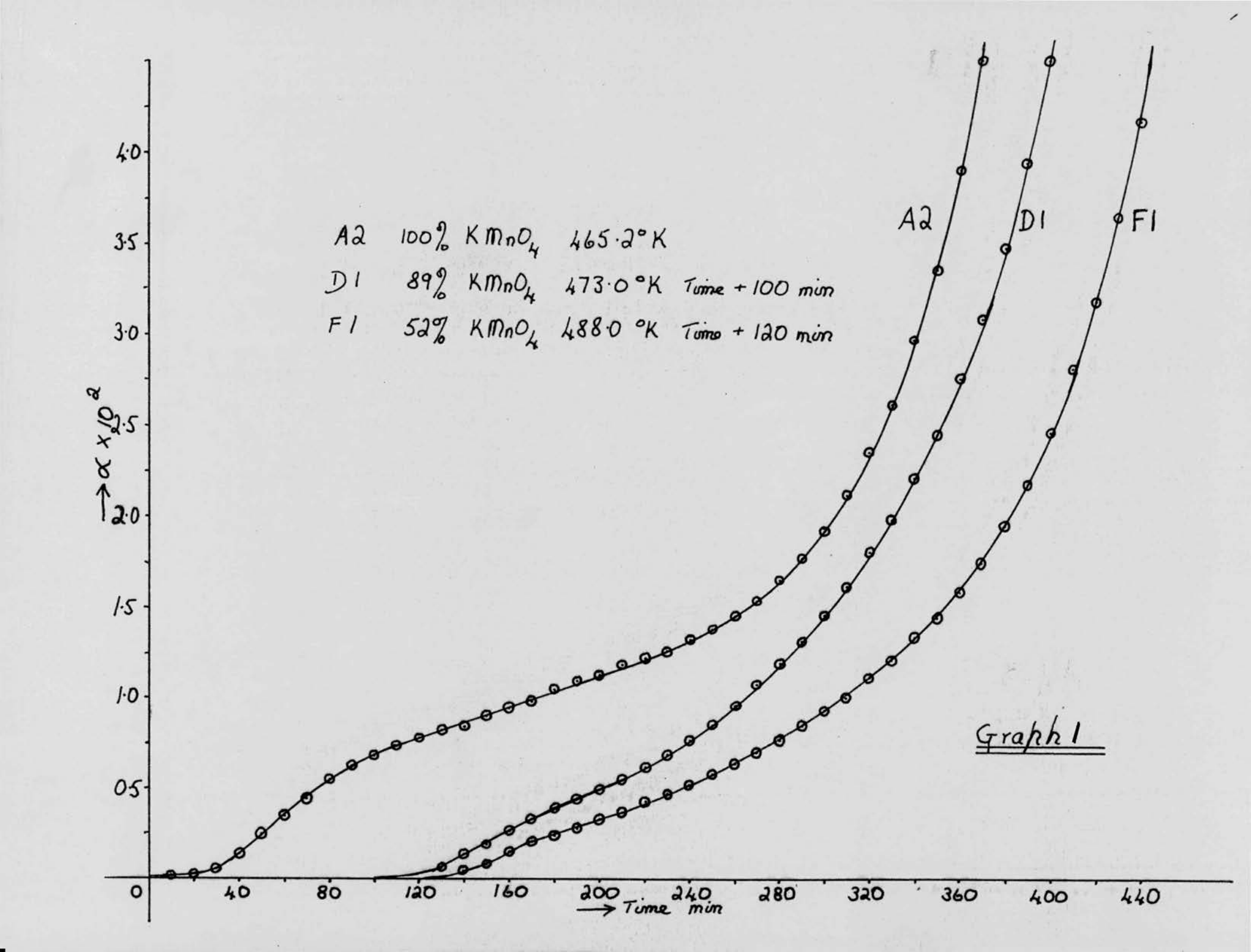
A2 100% $KMnO_4$ 465·2°K
D1 89% $KMnO_4$ 473·0°K Time + 100 min
F1 52% $KMnO_4$ 488·0°K Time + 120 min
A2
D1
F1
$\alpha \times 10^2$
4·0
3·5
3·0
2·5
2·0
1·5
1·0
0·5
0
40
80
120
160
200
240
280
320
360
400
440
Time min
Graph 1

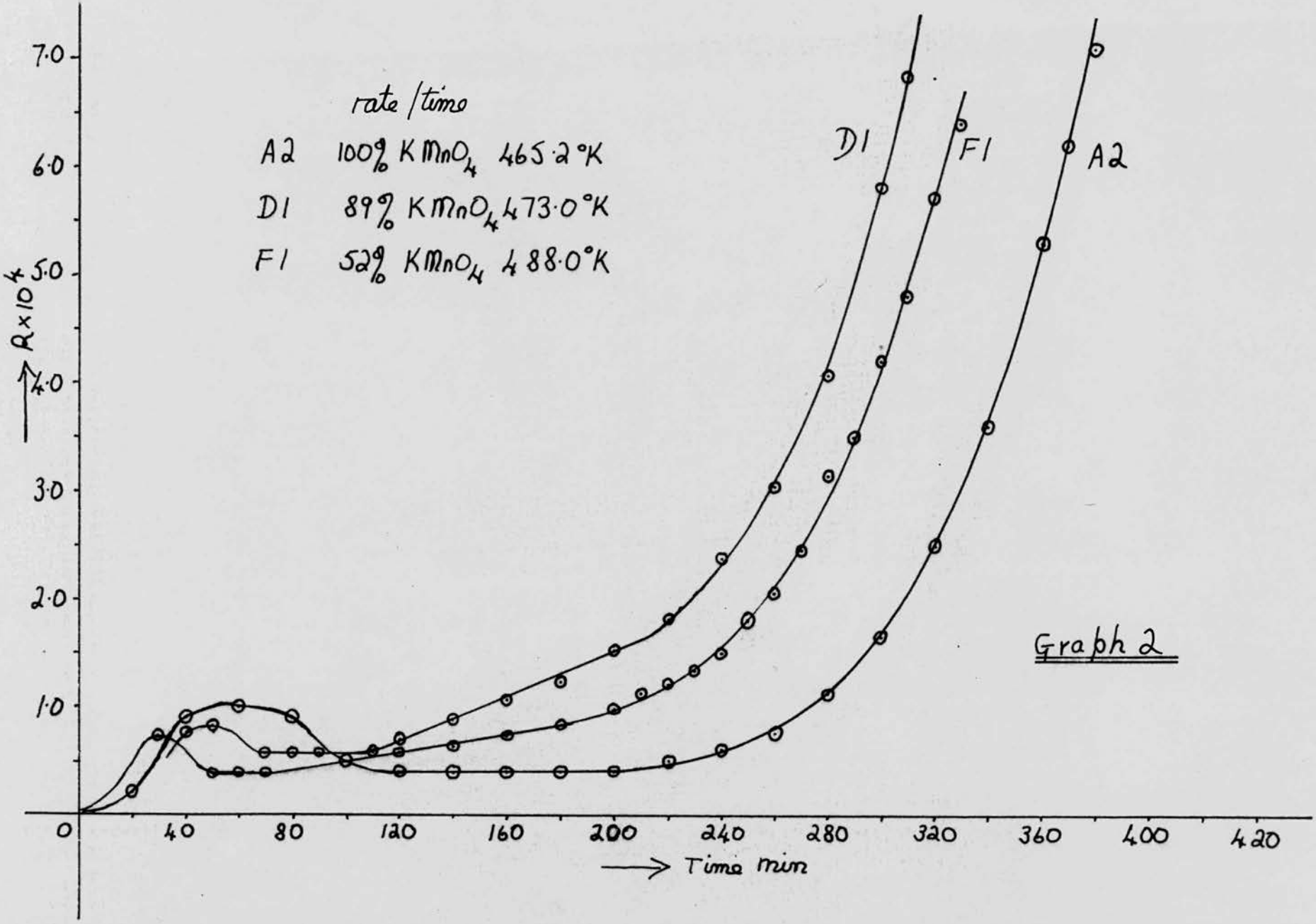
rate / time
A2 100% KMnO4 465·2°K
D1 89% KMnO4 473·0°K
F1 52% KMnO4 488·0°K
D1
F1
A2
R x 10^4
7·0
6·0
5·0
4·0
3·0
2·0
1·0
0
40
80
120
160
200
240
280
320
360
400
420
Time min
Graph 2

decomposed at the end of the linear stage. For the linear relationship between 'R' and 't', the equation $\alpha \propto k_2 t^2$ represents the relationship, and is called the 't^2-stage'.

The main acceleration period for the solid solutions A, B, D and E, that is those with greater than 70% potassium permanganate, followed the exponential relationship $\alpha = A \exp(kt)$ up to $\alpha = 0.07$ when the measurements were stopped. This agrees with the observations of Prout and Tompkins[27] and Hill[78]. The equation was plotted either in the form $\log_{10}(\alpha - \alpha_L)/t$ or R/α, and 'k' was readily found from the slope of the plots.

For the solid solution F, 52% potassium permanganate, the exponential equation for the acceleration stage was not satisfactory and a power law with n = 3 found to be superior. The power law equation $\alpha \propto k_3 t^3$ was plotted in the form $R^{\frac{3}{2}}/$. For solid solution G, 25% potassium permanganate, the acceleration stage of the reaction reduced to a power law with n = 2, as R was found to be constant.

The following tables and graphs show the majority of the runs performed at various temperatures in the range 460 - 520°K. The tables give the respective functions of 'α' as required by the above analysis and the graphs show the plots of the different functions.

In 2.4.4. the constants 'k_x' are tabulated for the various runs together with the respective Arrhenius activation energy plots.

2. 4. 1. Kinetics of the decomposition for pure potassium permanganate

In tables 1, 2, 3, 4 and 5 and graphs 3A, 4 and 5, the kinetics are illustrated for pure potassium permanganate. Two batches were made, material A appeared upon visual observations to contain more surface imperfections than the second batch B.

For both A and B the initial sigmoid reaction terminates at $\alpha = 0.006$; this is followed by the linear stage $\alpha = 0.006$ to 0.012. For material A the exponential equation fitted from the end of the linear stage, but for B there was a 't^2-stage' preceding the exponential relationship, which then applied from $\alpha = 0.025$.

The acceleration stage for A was analysed in terms of $\log_{10}(\alpha - \alpha_L)/t$, but for run A2, R/α was also plotted. The same value of 'k' was obtained from both equations and they both fitted from

Three further runs were performed on single large crystals of approximate dimensions 1 cm x 0.1 cm^2, run C3 is given as an example. The most notable features are the virtual absence of the initial sigmoid section, and the presence of a long linear stage from $\alpha = 0.006 - 0.036$.

Tables 1 and 2, analysis of A.

Tables 3 and 4, analysis of B.

Table 5, analysis of C.

Graph 3A, the 'α' - 't' curves for the initial decomposition

showing the sigmoid and linear stages. In graph 6B (2.4.2.) the R/t curves demonstrate the 't^2-stage' for B.

Graph 4, acceleration stage for A, a plot of $\log_{10}(\alpha - \alpha_L)/t$ illustrating the exponential relationship.

Graph 5, acceleration stage for B, a plot of R/α illustrating the exponential relationship.

Table 1. Material A 100% $KMnO_4$

Run	A2				A4		
Temp	465.2°K				458.3°K		
α_L	0.011				0.010		
Time min	$\alpha \times 10^2$	$\log(\alpha-\alpha_L)+4$	$R \times 10^3$	$(\frac{d\alpha}{dt})^{\frac{3}{2}} \times 10^6$	Time min	$\alpha \times 10^2$	$\log(\alpha-\alpha_L)+4$
10	0.01				40	0.03	
20	0.02		0.02		50	0.06	
30	0.05				60	0.12	
40	0.13		0.09		70	0.16	
50	0.25				80	0.22	
60	0.35		0.10		90	0.29	
70	0.44				100	0.35	
80	0.54		0.09		110	0.42	
90	0.62				120	0.45	
100	0.68		0.05		130	0.50	
110	0.73		0.04		linear increase of 'α' with time		
120	0.78						
130	0.82		0.04				
140	0.84						
150	0.90		0.04		310	1.02	
160	0.94		0.04		320	1.04	
170	0.98				330	1.07	
180	1.04		0.04		340	1.11	1.11
190	1.09				350	1.14	1.20
200	1.12		0.04		360	1.17	1.28
210	1.18				370	1.22	1.38
220	1.22		0.05		380	1.26	1.45
230	1.26				390	1.31	1.52
240	1.32	1.34	0.06	0.45	400	1.35	1.57
250	1.38				410	1.40	1.62
260	1.45	1.54	0.075	0.65	420	1.46	1.68
270	1.53				430	1.52	1.75
280	1.65	1.74	0.111	1.16	440	1.59	1.78
290	1.77				450	1.66	1.83
300	1.92	1.91	0.165	2.10	460	1.76	1.89
310	2.11				470	1.85	1.94
320	2.35	2.10	0.25	3.94	480	1.95	1.99
330	2.61				490	2.07	2.04
340	2.97	2.27	0.36	6.86	500	2.20	2.09
350	3.36				510	2.35	2.14
360	3.91	2.45	0.53	12.2	520	2.51	2.18
370	4.51	2.53	0.62	15.4	530	2.71	2.24
380	5.18	2.61	0.71	18.8	540	2.97	2.33

Table 2. Material A 100% $KMnO_4$

Run	A1		A3		A5		A6	
Temp	471.2°K		468.3°K		470.0°K		477.8°K	
α_L	0.012		0.012		0.012		0.011	
Time min	$\alpha \times 10^2$	$4 + \log(\alpha - \alpha_L)$	$\alpha \times 10^2$	$4 + \log(\alpha - \alpha_L)$	$\alpha \times 10^2$	$4 + \log(\alpha - \alpha_L)$	$\alpha \times 10^2$	$4 + \log(\alpha - \alpha_L)$
10	0.03				0.01		0.04	
20	0.10		0.03		0.03		0.12	
30	0.18		0.08		0.09		0.34	
40	0.36		0.20		0.25		0.61	
50	0.50		0.32		0.39		0.77	
60	0.62		0.46		0.56		0.95	
70	0.67		0.57		0.67		1.16	
80	0.75				0.74		1.41	1.48
90	0.80				0.82		1.67	1.75
100	0.87				0.92		2.00	1.95
110	0.93		linear increase		1.02		2.44	2.13
120	1.02		of 'α' with time		1.13		3.22	2.33
130	1.10				1.25		4.55	2.54
140	1.19				1.34		6.80	2.76
150	1.27				1.46	1.41		
160	1.37	1.23			1.63	1.63		
170	1.50	1.48			1.79	1.77		
180	1.70	1.70	1.17		2.01	1.91		
190	1.97	1.89	1.24		2.21	2.00		
200	2.35	2.06	1.33	1.11	2.54	2.13		
210	2.90	2.23	1.41	1.32	3.06	2.27		
220	3.67	2.39	1.54	1.53	3.65	2.39		
230	4.78	2.55	1.70	1.70	4.65	2.54		
240	6.26	2.70	1.89	1.84	5.72	2.65		
250	8.23	2.85	2.16	1.98	7.25	2.78		
260	10.6	2.98	2.50	2.11				
270	13.8	3.10	2.97	2.25				
280	19.2	3.25	3.56	2.37				
290	25.3	3.38	4.32	2.49				
300	33.0	3.50	5.20	2.60				
310			6.17	2.70				

Table 3. Material B 100% $KMnO_4$

Run	B1		B2		B5	
Temp	498.2°K		498.2°K		486.1°K	
Time min	$\alpha \times 10^2$	$R \times 10^3$	$\alpha \times 10^2$	$R \times 10^3$	$\alpha \times 10^2$	$R \times 10^3$
2						
4						
6	0.01					
8	0.03					
10	0.05		0.05			
12	0.18		0.17	0.88		
14	0.39	1.31	0.41			
16	0.665		0.70	0.64		
18	0.85	0.81		0.64		
20	1.0	0.81	0.96	0.69	0.27	0.62
22	1.18	0.81	1.11	0.79		
24	1.38	1.02	1.29	0.92		
25						
26	1.59		1.46			
28	1.85	1.36	1.70	1.16		
30	2.12		1.94			
32	2.48	1.81	2.24	1.64		
34	2.87		2.61	2.03		
35					0.88	0.38
36	3.36	2.47	3.12	2.72		
37			3.41	3.3		
38	3.96	3.40	3.76	4.1		
39			4.3	5.2		
40	4.78	4.70	4.85	6.4	1.11	0.38
42	5.95	6.70				
44					1.32	0.38
45						
50					1.57	0.52
55						0.61
60					2.19	0.72
65					2.56	0.83
70					3.04	0.96
74					3.51	1.20
78					4.02	1.40
82					4.70	1.87
86					5.55	2.36
90					6.65	3.12
92					7.28	3.6

Table 4. Material B 100% $KMnO_4$

Run		B4			B3
Temp		464.1°K			472.7°K
Time min	$\alpha \times 10^2$	$R \times 10^3$	$(R)^{\frac{3}{2}} \times 10^6$	$\alpha \times 10^2$	$R \times 10^3$
20				0.04	
30				0.10	
40	0.05			0.30	
50				0.52	0.26
60	0.17			0.73	0.108
70				0.84	0.108
80	0.38	0.134		0.94	0.108
90				1.08	
100	0.58			1.20	0.135
110				1.33	
120	0.73	0.049		1.49	0.172
130	0.78	0.049		1.64	
140	0.83	0.049		1.86	0.210
150	0.88	0.049		2.07	
160	0.93	0.049		2.29	0.248
170	0.99			2.55	0.28
180	1.06	0.064		2.86	0.32
190	1.10			3.18	0.39
200	1.19	0.070		3.63	0.45
210	1.26			4.14	0.56
220	1.33	0.076		4.77	0.69
230	1.41			5.54	0.85
240	1.49	0.087		6.59	1.13
250	1.58			7.80	1.36
260	1.68	0.095		9.40	1.67
270	1.76				
280	1.88	0.115	1.22		
290	2.01				
300	2.13	0.134	1.56		
310	2.27				
320	2.42	0.158	2.00		
330	2.59				
340	2.78	0.197	2.74		
360	3.22	0.243	3.8		
380	3.76	0.298	5.2		
400	4.41	0.352	6.6		
420	5.21	0.438	9.1		
440	6.21	0.545	12.6		
450	6.72	0.595	14.5		
460	7.40	0.634	16.0		

Table 5. Material C 100% $KMnO_4$

Run C3

Temp 464.4°K

Time min	$\alpha \times 10^2$	$R \times 10^4$
20	0.12	0.55
40	0.16	
60	0.27	0.63
80	0.41	0.79
100	0.60	0.84
120	0.79	1.10
160	1.21	1.10
200	1.67	1.15
240	2.13	1.18
280	2.63	1.18
300	2.91	1.18
320	3.13	1.18
340	3.53	1.18
360	3.62	1.22
380	3.87	1.30
400	4.15	1.36
420	4.44	1.58
440	4.80	2.03
450	5.01	2.38
460	5.30	2.93
470	5.60	3.2
480	5.95	3.9
490	6.42	4.7
500	6.96	5.6
510	7.59	6.5
520	8.4	7.6
530	9.3	8.7
540	10.4	10.1
550	11.5	11.2
560	12.8	13.3

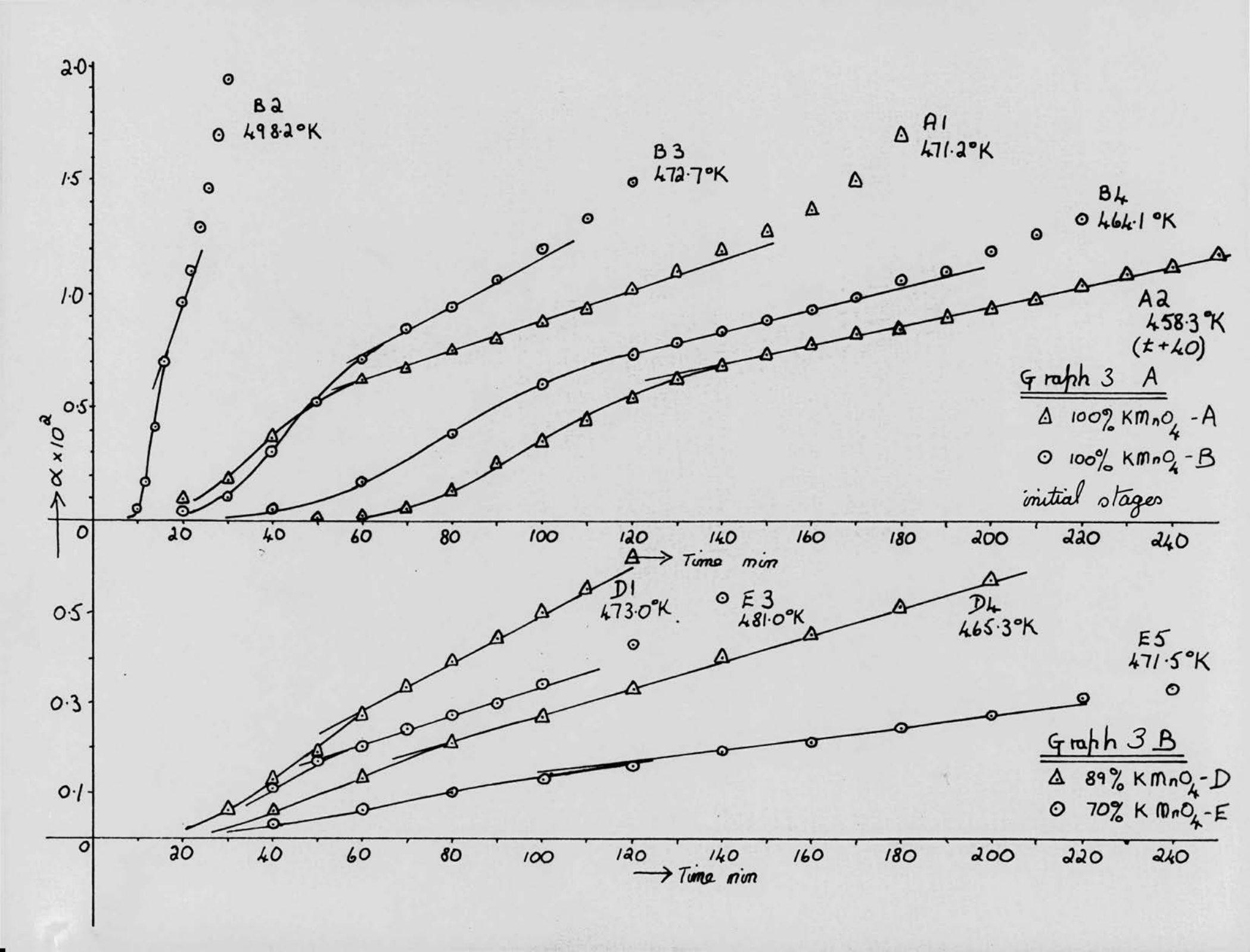
B2
498·2°K
B3
472·7°K
A1
471·2°K
B4
464·1°K
A2
458·3°K
(t+40)
Graph 3 A
△ 100% KMnO4 - A
⊙ 100% KMnO4 - B
initial stages
α x 10²
Time min
D1
473·0°K
E3
481·0°K
D4
465·3°K
E5
471·5°K
Graph 3 B
△ 89% KMnO4 - D
⊙ 70% KMnO4 - E
Time min

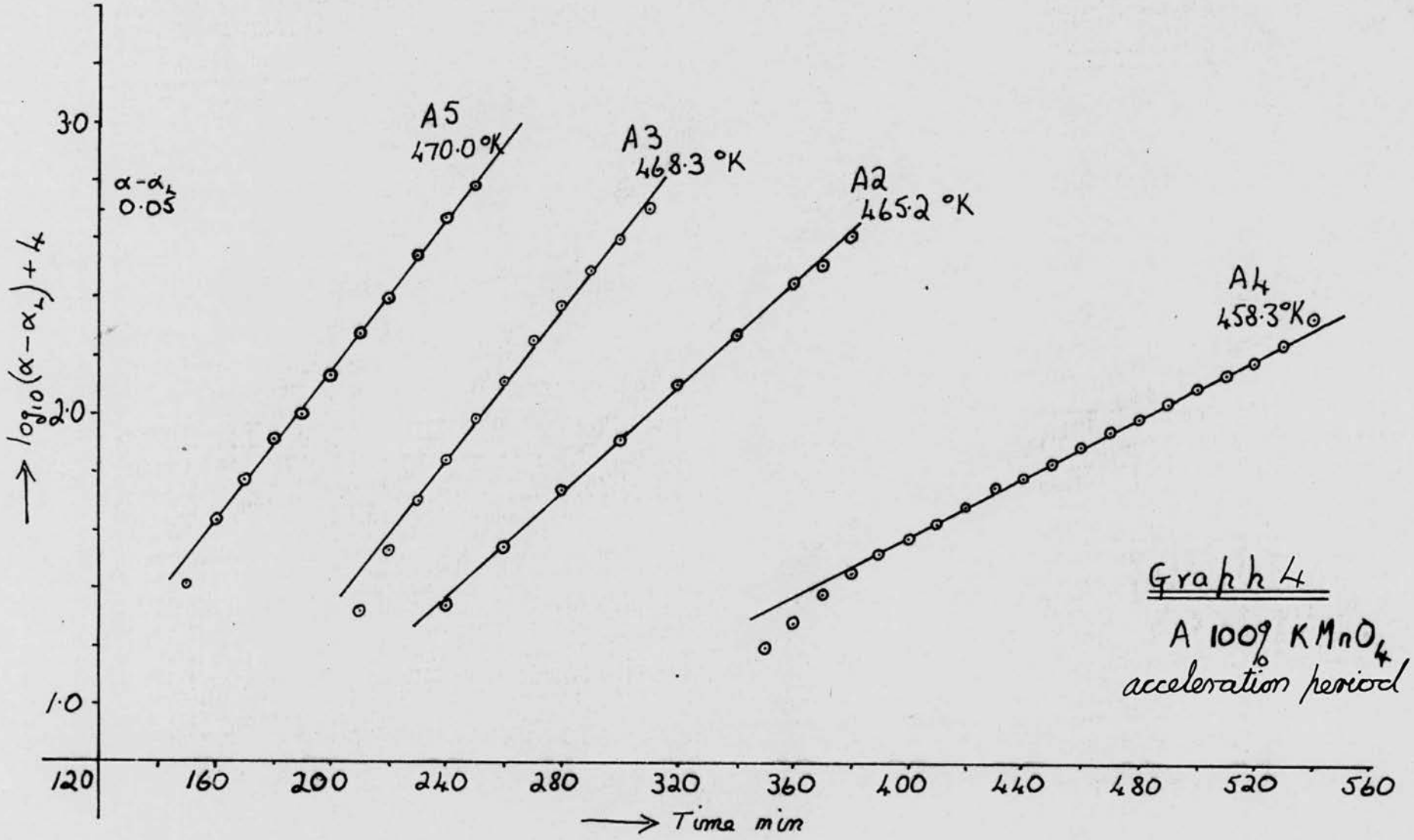

Graph 4

A 100% $KMnO_4$ acceleration period

Graph 5

100% $KMnO_4$: B
acceleration period

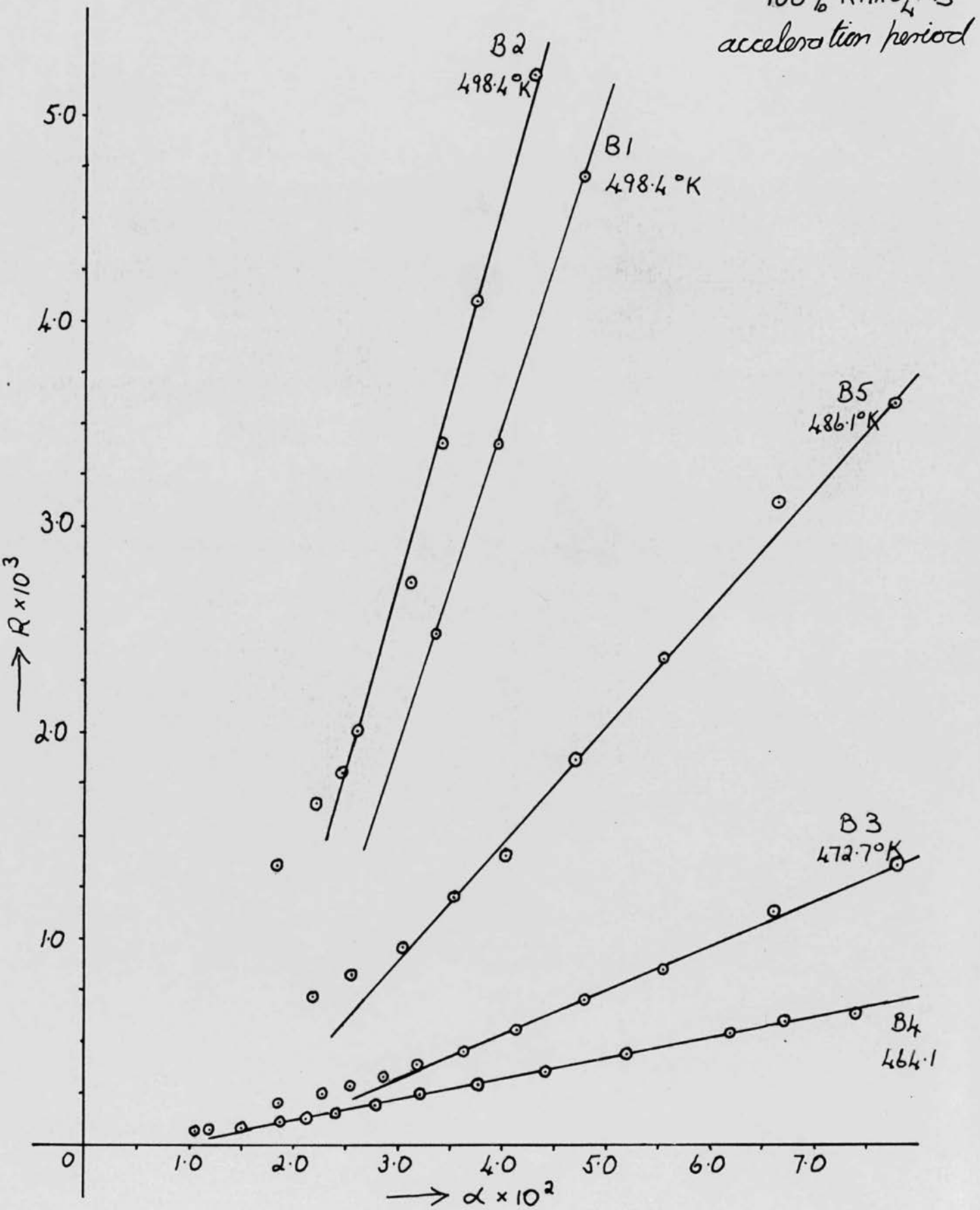

2. 4. 2. Kinetics of the decomposition for solid solutions D and E

In tables 6, 7, 8 and 9 and graphs 6 and 7 the kinetics are illustrated for the decomposition of solid solutions D and E containing 89 and 70% of potassium permanganate respectively. These solid solutions show the same general features as for pure permanganate B, but with a much decreased rate of decomposition. For D the initial sigmoid stage ceases at $\alpha = 0.003$ and the linear stage only extends from $\alpha = 0.003 - 0.005$, this being followed by the 't^2-stage' up to $\alpha = 0.015$. The acceleration stage is adequately fitted by the exponential equation from $\alpha = 0.02$.

For solid solution E the sigmoid stage is further reduced to $\alpha = 0.0015$ and the linear stage is probably present from $\alpha = 0.0015 - 0.0025$. The 't^2-stage' extends from $\alpha = 0.0025$ to 0.01 followed by the acceleration stage expressed by an exponential relationship but a power law with $n = 3$ is a feasible alternative.

Tables 6, 7 and 8, analysis of solid solutions D and E.

Graphs 6A and B, 't^2-stage', a plot of the R/t, showing the linear increase in rate with time.

Graph 7, acceleration stage, a plot of the R/α showing the exponential relationship. In graph 3B (2.4.1.) the 'α' - 't' curves are given for the initial decomposition, showing the sigmoid and linear stages.

Table 6. Material D 89% $KMnO_4$

Run	D1		D2		D3	
Temp	473.0°K		468.4°K		471.6°K	
Time min	$\alpha \times 10^2$	$R \times 10^3$	$\alpha \times 10^2$	$R \times 10^3$	$\alpha \times 10^2$	$R \times 10^3$
30	0.06				0.03	
40	0.13	0.077	0.03	0.031	0.07	
50	0.19	0.077	0.08			
60	0.27		0.13	0.051	0.20	0.062
70	0.33	0.056	0.20	0.047		
80	0.39	0.056	0.23	0.047	0.28	0.039
90	0.44	0.056	0.28		0.33	0.039
100	0.50		0.32	0.035	0.37	0.039
110	0.55	0.056	0.35		0.40	0.039
120	0.62	0.069	0.37	0.035	0.43	0.039
130	0.69		0.42		0.48	
140	0.77	0.087	0.45	0.035	0.54	0.050
150	0.85		0.50		0.59	
160	0.96	0.106	0.54	0.043	0.66	0.060
170	1.07		0.58		0.72	
180	1.19	0.126	0.64	0.052	0.78	0.069
190	1.31		0.69		0.86	
200	1.46	0.151	0.74	0.059	0.94	0.085
210	1.61		0.79		1.02	
220	1.80	0.180	0.86	0.066	1.12	0.098
230	1.99		0.93		1.22	
240	2.21	0.238	1.00	0.073	1.35	0.125
250	2.45		1.07		1.47	
260	2.76	0.303	1.17	0.088	1.63	0.148
270	3.09		1.27		1.78	
280	3.48	0.407	1.35	0.099	1.98	0.208
290	3.95		1.46		2.19	
300	4.51	0.580	1.56	0.112	2.45	0.278
305	4.86					
310	5.19	0.683	1.70		2.76	
315	5.55					
320	5.93	0.800	1.82	0.127	3.11	0.396
330			1.95		3.55	
340			2.11	0.147	4.07	0.545
360			2.47	0.199	5.36	0.74
370			2.68		6.15	
380			2.91	0.24		
390			3.18			
400			3.45	0.30		
410			3.80			
420			4.17	0.40		
440			5.06	0.48		

Table 7. Material E 70% $KMnO_4$

E1 485.5°K		E3 481.0°K			E4 489.1°K	
$\alpha \times 10^2$	$R \times 10^4$	$\alpha \times 10^2$	$R \times 10^4$	$(R)^{\frac{3}{2}} \times 10^6$	$\alpha \times 10^2$	$R \times 10^4$
0.11	0.90	0.05			0.18	0.51
0.17	0.24	0.11	0.60		0.22	0.51
0.19	0.24	0.17	0.33		0.26	0.51
0.20	0.24	0.20	0.33		0.32	0.70
0.25	0.38	0.24	0.33			
0.31	0.41	0.27	0.33		0.49	0.79
0.35	0.51	0.30	0.33			
0.41	0.61	0.34	0.40		0.69	1.05
0.47	0.69				0.77	1.08
0.55	0.79	0.43	0.48		0.92	1.33
0.63	0.85				1.06	1.60
0.72	0.95	0.53	0.54		1.23	1.94
0.81	1.04				1.43	2.51
0.92	1.15	0.64	0.62		1.73	3.34
1.04	1.4				2.13	4.80
1.21	1.7	0.77	0.70		2.78	7.64
1.39	2.0				3.72	11.3
1.61	2.4	0.92	0.80		5.15	17.1
1.90	3.2				7.14	
2.27	4.4	1.10	0.99			
2.82	5.6					
3.51	7.5	1.33	1.22	1.33		
4.47	9.8					
5.65	13.3	1.61	1.60	2.00		
		1.78				
		1.98	2.15	3.18		
		2.19				
		2.47	3.13	5.64		
		2.81	3.70	7.08		
		3.23	4.43	9.26		
		3.71	5.43	12.6		
		4.30	6.24	15.6		
		4.95	7.20	19.2		

2. 4. 3. Kinetics of the decomposition of solid solutions F and G

In tables 9, 10 and 11 and graphs 8 and 9 the kinetics are illustrated for the decomposition of solid solutions F and G, containing 52 and 25% of potassium permanganate respectively. The relative fractional decomposition of the different stages in the decomposition of F is similar to E, but the acceleration stage is best represented by a power law with n = 3.

For solid solution G the sigmoid decomposition was greatly increased extending to α = 0.01. This is almost certainly due to the method of preparation of the crystals, which resulted in extremely poor faces on the crystals and hence increasing the surface area. This will be discussed later. The 't^2-stage' was also increased and now extended from α = 0.01 - 0.025, this being followed by the acceleration stage expressed in terms of a power law with n = 2.

Tables 9, 10 and 11, analysis of solid solutions F and G.

Graph 8, acceleration stage for F, a plot of $R^{\frac{3}{2}}/\alpha$, showing the fit for a power law with n = 3.

Graph 9, 't^2-stage' and acceleration stage for G, a plot of R/t showing the fit for the power law with n = 2.

In graph 6A (2.4.2.) the 't^2-stage' is shown for solid solution F.

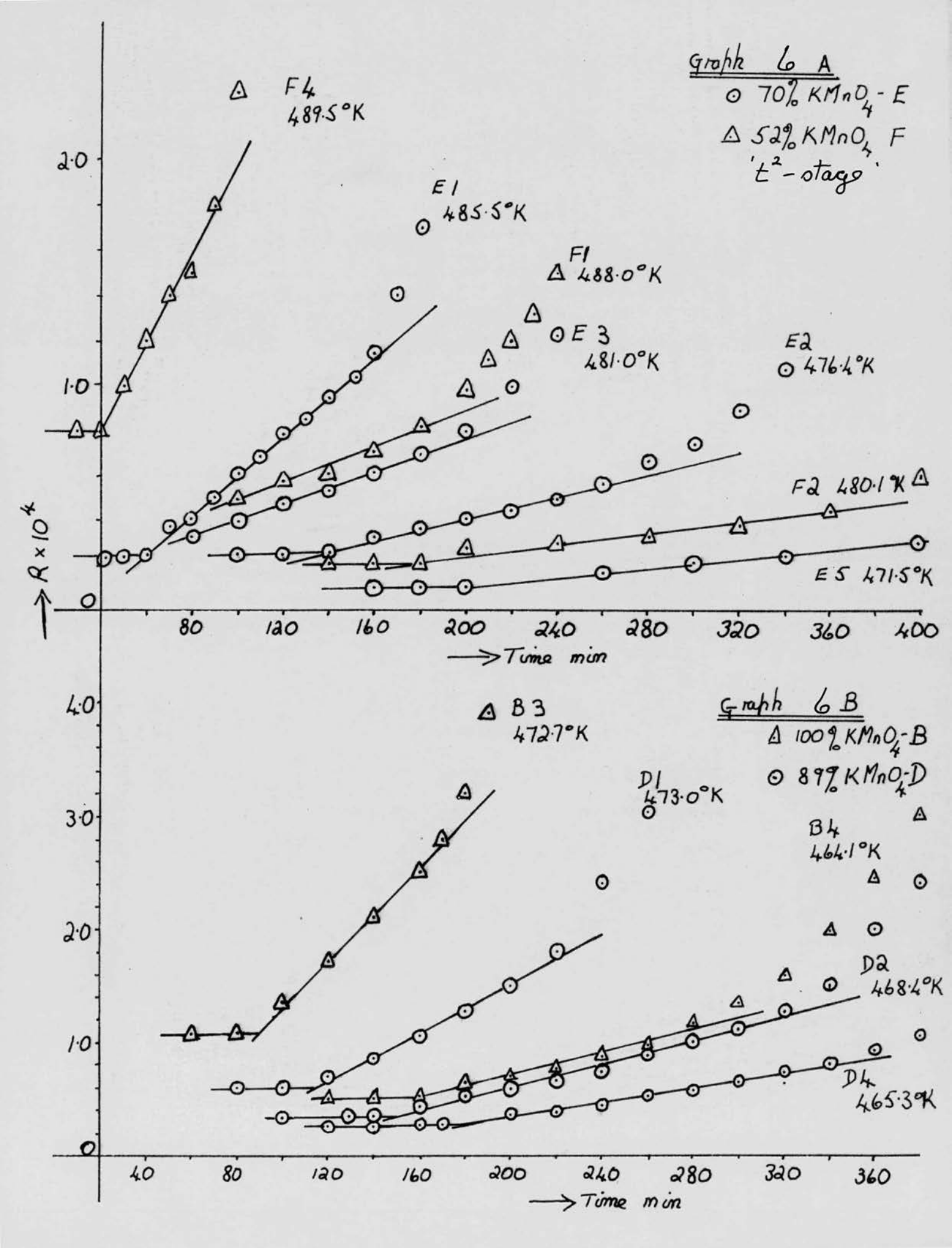
Graph 6 A
○ 70% KMnO4 - E
△ 52% KMnO4 F
't² - otago'
F4
489.5°K
E1
485.5°K
F1
488.0°K
E3
481.0°K
E2
476.4°K
F2 480.1°K
E5 471.5°K
R x 10⁴
Time min
Graph 6 B
△ 100% KMnO4 - B
○ 89% KMnO4 - D
B3
472.7°K
D1
473.0°K
B4
464.1°K
D2
468.4°K
D4
465.3°K
Time min

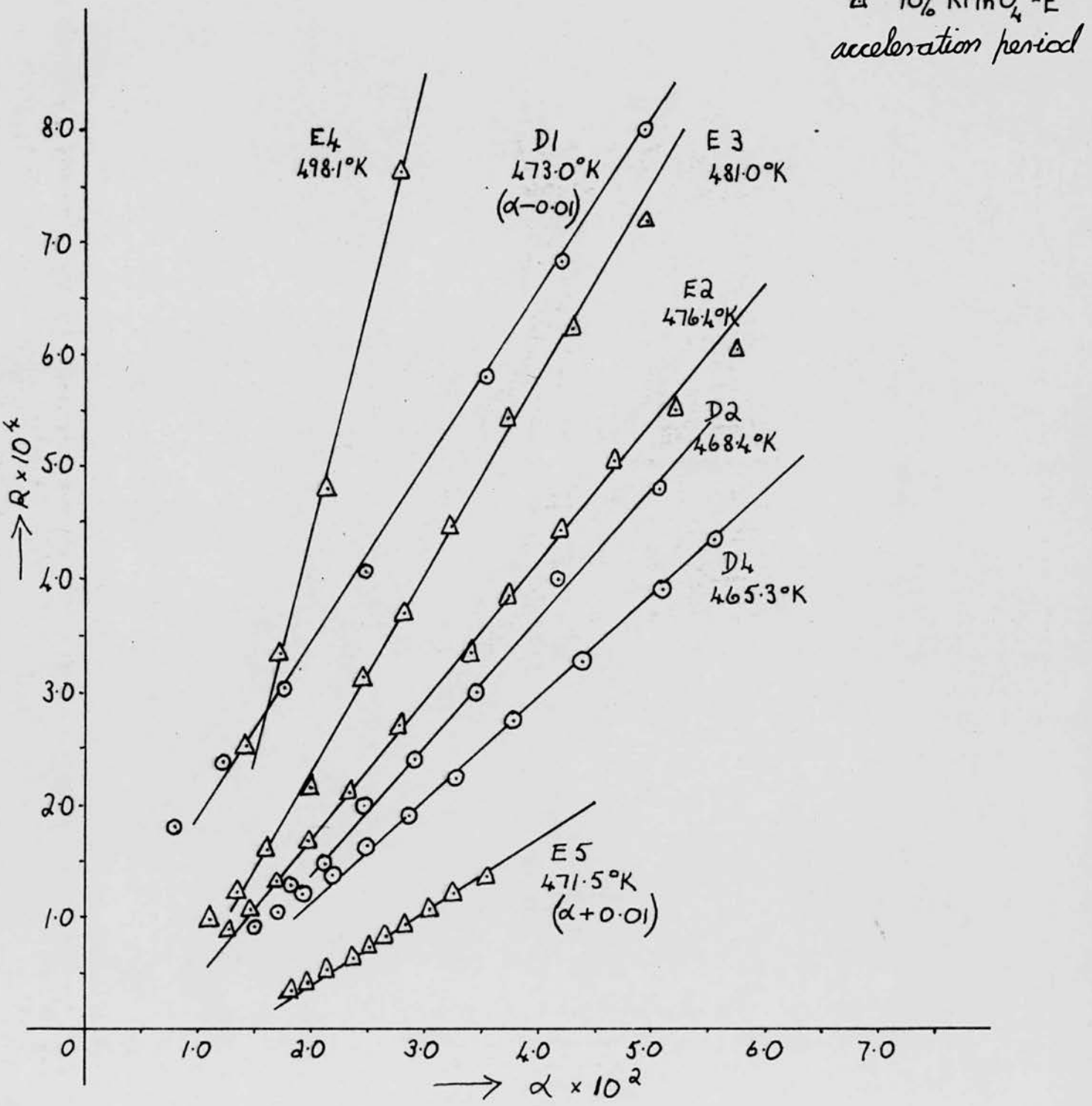
Graph 7
⊙ 89% KMnO4 - D
Δ 70% KMnO4 - E
acceleration period
E4
498·1°K
D1
473·0°K
(α−0·01)
E3
481·0°K
E2
476·4°K
D2
468·4°K
D4
465·3°K
E5
471·5°K
(α+0·01)
R × 10⁴
α × 10²
8·0
7·0
6·0
5·0
4·0
3·0
2·0
1·0
0
1·0
2·0
3·0
4·0
5·0
6·0
7·0

Table 10. Material F 52% $KMnO_4$

Run		F1			F4	
Temp		488.0°K			498.5°K	
Time min	$\alpha \times 10^2$	$R \times 10^4$	$R^{\frac{3}{2}} \times 10^6$	$\alpha \times 10^2$	$R \times 10^4$	$R^{\frac{3}{2}} \times 10^6$
20	0.04			0.16	2.1	
30	0.08	0.72		0.28	0.8	
40	0.16			0.39	0.8	
50	0.21	0.39		0.48	1.0	
60	0.24	0.39		0.60	1.2	
70	0.28	0.39		0.73	1.4	
80	0.33			0.87	1.5	
90	0.37			1.03	1.8	
100	0.43	0.50		1.22	2.3	
110	0.47			1.48	2.8	4.74
120	0.52	0.58	0.44	1.82	4.1	8.3
130	0.58			2.34	6.1	15.1
140	0.64	0.61	0.48	3.08	9.0	27.0
145				3.63	11.3	38.0
150	0.70			4.24	13.5	49.6
155				5.08	15.9	63.5
160	0.77	0.71	0.60	5.87	17.9	75.7
165				6.85	20.0	89.3
170	0.85			7.82	22.6	107
180	0.93	0.82	0.74			
190	1.00					
200	1.11	0.98	0.83			
210	1.21	1.12				
220	1.33	1.20	1.33			
230	1.44	1.32				
240	1.59	1.50	1.82			
250	1.75	1.80				
260	1.95	2.05	2.92			
270	2.17	2.46				
280	2.47	3.14	5.54			
290	2.81	3.5				
300	3.19	4.2	8.60			
310	3.65	4.8	10.5			
320	4.18	5.7	13.6			
330	4.77	6.4	16.1			
340	5.45	7.2	19.2			
350	6.22	8.0	22.7			

Table 11. Material G 25% $KMnO_4$

Run		G2			G3	
Temp		507.8°K			514.0°K	
Time min	$\alpha \times 10^2$	$R \times 10^3$	$R^{\frac{3}{2}} \times 10^6$	$\alpha \times 10^2$	$R \times 10^4$
20	0.50	0.76		0.50	12.7
30	0.76			1.00	
40	0.92	0.14		1.24	2.24
50	1.06	0.14		1.49	2.64
60	1.22			1.79	2.9
70	1.36			2.06	3.0
80	1.52	0.17		2.38	3.1
90	1.70			2.69	3.4
100	1.86	0.18		3.05	3.8
110	2.05			3.48	4.3
120	2.22	0.19		3.93	4.8
130	2.42			4.42	5.7
140	2.62	0.21		5.02	6.4
150	2.82			5.98	7.3
160	3.05	0.23	3.6	6.75	7.9
170	3.30			7.28	8.4
180	3.57	0.29	4.7		
190	3.88				
200	4.20	0.33	5.9		
210	4.51				
220	4.92	0.40	8.0		
230	5.37				
240	5.82	0.48	10.5		
250	6.63				
260	6.85	0.53	12.2		
270	7.40				
280	8.00	0.60	14.7		

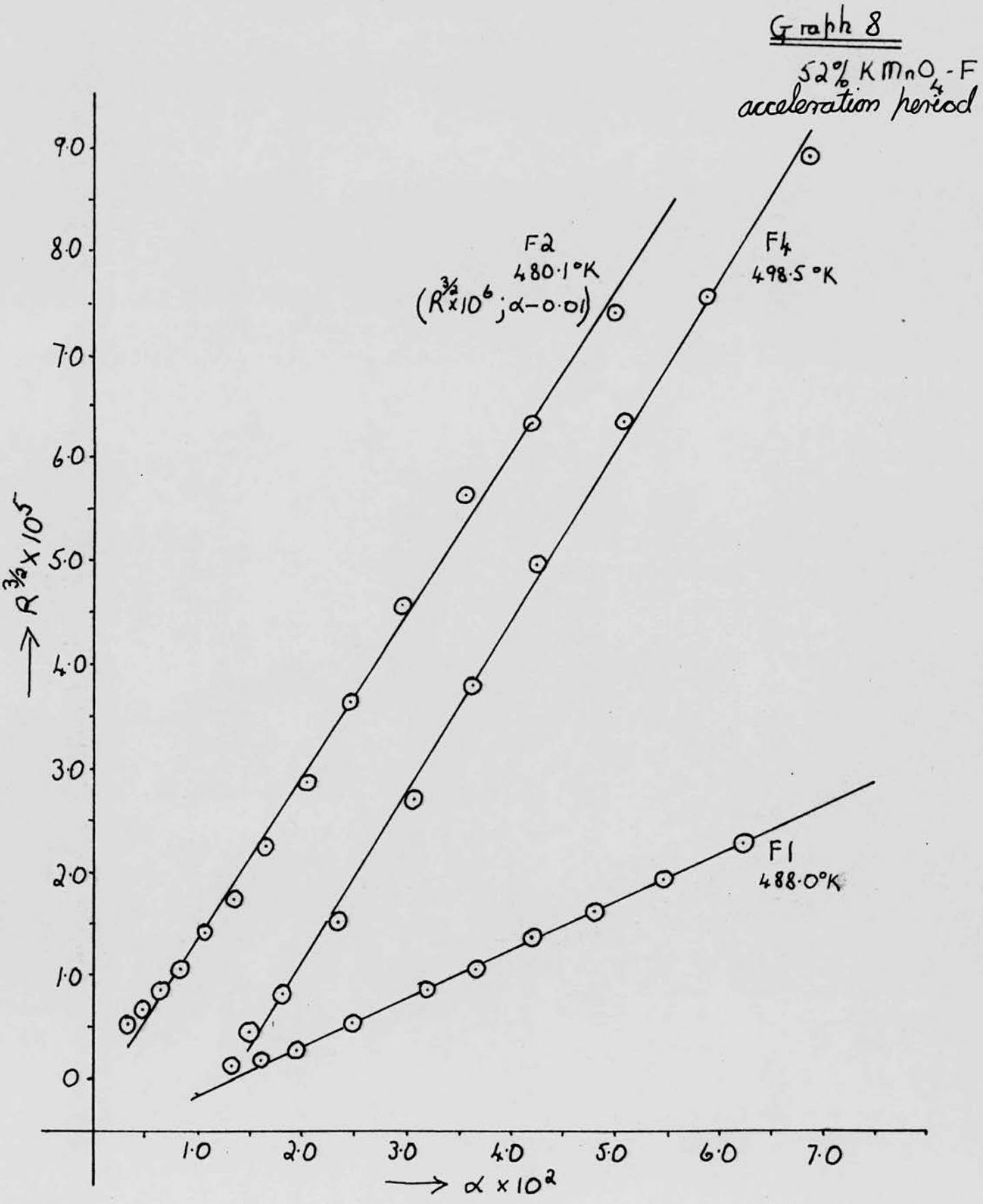
Graph 8
52% $KMnO_4$ - F
acceleration period
F2
480·1°K
$(R^{3/2} \times 10^6 ; \alpha - 0.01)$
F4
498·5°K
F1
488·0°K
$\longrightarrow R^{3/2} \times 10^5$
$\longrightarrow \alpha \times 10^2$
9·0
8·0
7·0
6·0
5·0
4·0
3·0
2·0
1·0
0
1·0
2·0
3·0
4·0
5·0
6·0
7·0

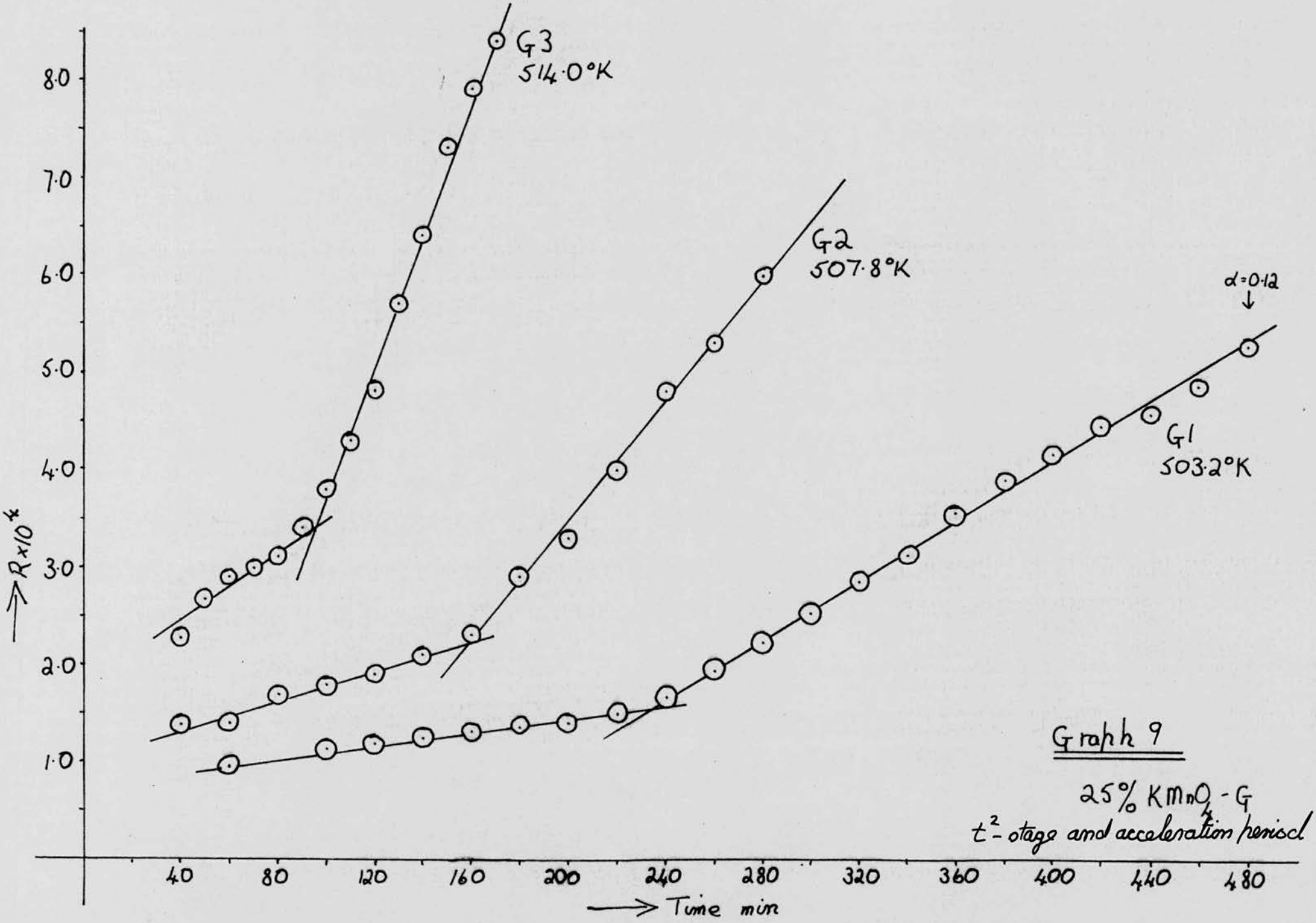
G3
514·0°K
G2
507·8°K
G1
503·2°K
α=0·12
8·0
7·0
6·0
5·0
4·0
3·0
2·0
1·0
R×10⁴
40
80
120
160
200
240
280
320
360
400
440
480
Time min
Graph 9
25% KMnO4 - G
t² - otage and acceleration period

2. 4. 4. Tables and graphs of rate constants

In tables 12 - 17 the rate constants for various runs described in section 2.4.1 - 2.4.3 are tabulated, together with the respective temperatures.

R_I is the maximum rate for the initial sigmoid decomposition.

R_L is the constant rate for the linear stage.

$k_2^{\frac{1}{2}}$ is the rate constant for the 't^2-stage' from the equation $\frac{d\alpha}{dt} = 2k_2t + C$ found from the R/t curves. Thus $\alpha \propto k_2t^2$ representing a power law with n = 2.

k is the rate constant for the acceleration stage from the equation $\alpha = A \exp(kt)$ found from the plot of $\frac{d\alpha}{dt}/\alpha$

$k_3^{\frac{1}{3}}$ is the rate constant for the acceleration stage in terms of the power law growth with n = 3, if $\alpha \propto k_3t^3$, $3^{\frac{3}{2}}k_3^{\frac{1}{2}}$ is found from plotting $(\frac{d\alpha}{dt})^{\frac{3}{2}}/\alpha$.

$k_{22}^{\frac{1}{2}}$ is the rate constant for the acceleration stage in terms of a power law with n = 2.

$2k_{22}$ is found from a plot of $\frac{d\alpha}{dt}/t$ in a similar manner to $k_2^{\frac{1}{2}}$.

As the kinetics have been expressed in terms of 'α', (the fraction of the potassium permanganate that has decomposed in a given time) the rate constants from the different solid solutions are comparable.

For material F and G the exponential equation does not apply, but R/α was plotted and the value of 'k' measured at $\alpha = 0.05$ so that the rate constants for the acceleration stage of the solid solutions could be compared on a relative basis.

Table 12. Rate constants for pure potassium permanganate A.

Run	Temp $T^{o}K$	$\frac{1}{T} \times 10^{3}$	$R_I \times 10^{5}$	$R_L \times 10^{5}$	$k_2^{\frac{1}{2}} \times 10^{4}$	$k \times 10^{2}$
A 6	477.8	2.092	30	17.4	-	4.83
1	471.2	2.122	17.5	7.0	-	3.75
5	470.0	2.130	18.0	9.2	-	3.0
3	468.3	2.135	13.6	5.5	-	2.9
2	465.2	2.150	10.5	4.3	-	1.9
4	458.3	2.182	6.4	2.7	-	1.2

Table 13. Rate constants for pure potassium permanganate B.

B 1	498.4	2.007	131	81	-	16
2	498.4	2.007	88	60	-	18
5	486.1	2.057	62	38	31	6.5
3	472.7	2.116	26	10.8	8.9	2.2
4	464.1	2.155	13.4	4.8	4.5	1.0

Table 14. Rate constants for solid solution D, 89% $KMnO_4$.

D 5	478.7	2.091	11	7.2	11	3.6
1	473.0	2.114	7.7	5.3	7.8	1.6
3	471.6	2.120	6.2	3.8	7.6	1.6
2	468.4	2.135	5.0	3.5	4.7	1.1
4	465.3	2.149	4.2	2.8	3.3	0.9

Table 15. Rate constants for solid solution E, 70% $KMnO_4$.

Run	Temp T^oK	$\frac{1}{T} \times 10^3$	$R_I \times 10^5$	$R_L \times 10^5$	$k_2^{\frac{1}{2}} \times 10^4$	$k_3^{\frac{1}{3}} \times 10^4$	$k \times 10^2$
E 4	489.2	2.045	13.6	5.1	7.1	-	4.1
1	485.5	2.060	9.0	4.2	6.6	-	2.7
3	481.0	2.079	6.0	3.3	4.1	-	1.7
2	476.4	2.099	3.6	2.6	3.5	-	1.2
5	471.5	2.123	2.2	1.1	2.2	-	0.65

Table 16. Rate constants for solid solution F, 52% $KMnO_4$

F 4	498.5	2.006	21	8.0	10	47	(3.2)
3	495.5	2.018	10	6.8	7.1	35	(2.6)
1	488.0	2.049	7.2	3.9	4.5	20	(1.5)
2	480.1	2.083	3.0	2.1	2.6	9.5	(0.7)

Table 17. Rate constants for solid solution G, 25% $KMnO_4$.

						$k_{22}^{\frac{1}{2}}$	
G 3	514	1.946	127	-	9.1	18.2	(1.1)
2	507.7	1.969	76	-	6.2	12.3	(0.8)
1	503	1.987	83	-	4.1	8.7	(0.6)

In graphs 10 and 11, the Arrhenius activation energy plots are shown for the various temperature dependent constants given in tables 12 - 17.

These graphs clearly illustrate the lowering of the rate constants with the increasing percentage of potassium perchlorate in the solid solutions. From graph 10 the activation energy of the rate constant 'k' for the acceleration is ca 39 kcal $mole^{-1}$, similar to the value found by Prout and Tompkins[27]. The solid solutions appear to have the same activation energy as for the pure potassium permanganate, although insufficient evidence is available to define clearly the activation energies.

Graph 10 also illustrates the activation energy plots for 'R_I', the maximum rate for the initial sigmoid decomposition. Pure permanganate (A and B) has an activation energy of 35 ± 5 kcal $mole^{-1}$ and there is an apparent increase for the solid solution rising to 46 ± 5 for F (52% $KMnO_4$).

In graph 11 the plots are shown for the linear and 't^2-stage', both of which have activation energies of 39 ± 6 kcal $mole^{-1}$, independent of perchlorate concentration. For the linear constant rate stage Prout[76] reported a value of 25.5 kcal $mole^{-1}$ which is definitely outside the maximum error for this work.

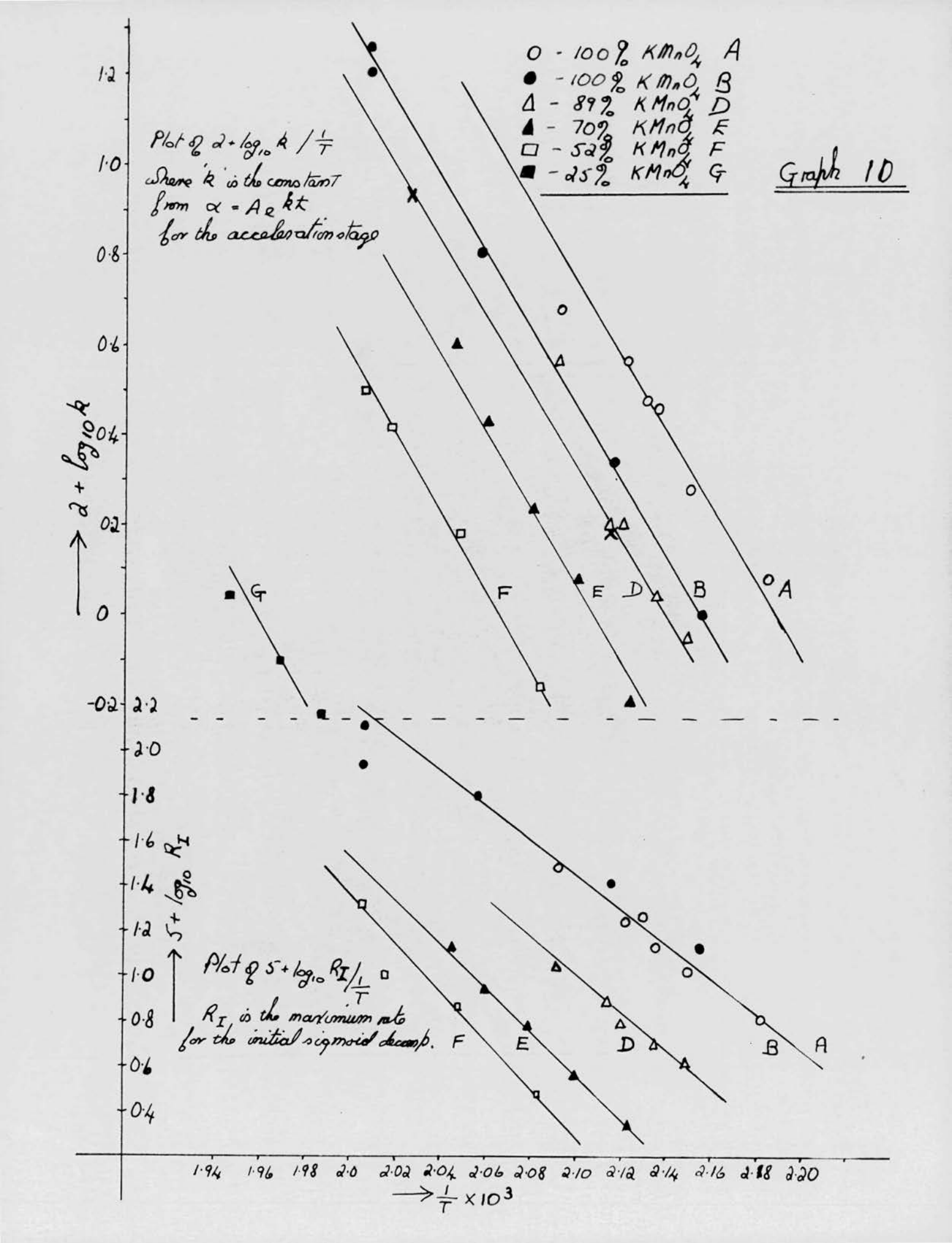
○ - 100% KMnO4 A
● - 100% KMnO4 B
Δ - 89% KMnO4 D
▲ - 70% KMnO4 E
□ - 52% KMnO4 F
■ - 25% KMnO4 G
Graph 10
Plot of 2 + log10 k / 1/T
where 'k' is the constant
from α = Ae^kt
for the acceleration stage
→ 2 + log10 k
1·2
1·0
0·8
0·6
0·4
0·2
0
-0·2
G
F
E
D
B
A
→ 5 + log10 RI
2·2
2·0
1·8
1·6
1·4
1·2
1·0
0·8
0·6
0·4
Plot of 5 + log10 RI / 1/T
RI is the maximum rate
for the initial sigmoid decomp.
F
E
D
B
A
1·94
1·96
1·98
2·0
2·02
2·04
2·06
2·08
2·10
2·12
2·14
2·16
2·18
2·20
→ 1/T × 10^3

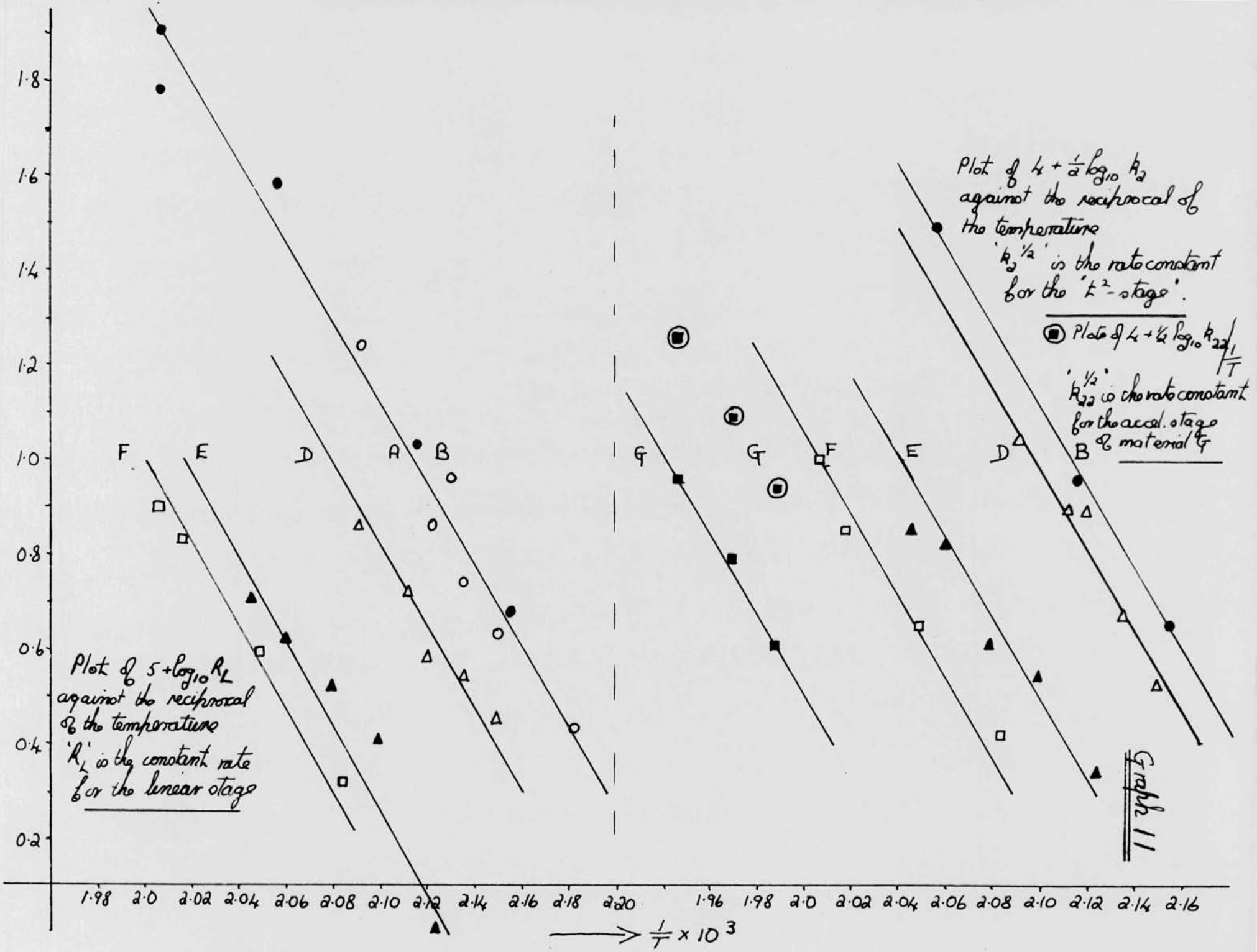
Plot of $5 + \log_{10} R_L$ against the reciprocal of the temperature
'R_L' is the constant rate for the linear stage
Plot of $4 + \frac{1}{2}\log_{10} k_2$ against the reciprocal of the temperature
'$k_2^{1/2}$' is the rate constant for the 't^2-stage'.
Plot of $4 + \frac{1}{2}\log_{10} k_{22}$ / $\frac{1}{T}$
'$k_{22}^{1/2}$' is the rate constant for the accel. stage of material G
Graph 11
F E D A B
G G F E D B
1·8 1·6 1·4 1·2 1·0 0·8 0·6 0·4 0·2
1·98 2·0 2·02 2·04 2·06 2·08 2·10 2·12 2·14 2·16 2·18 2·20
1·96 1·98 2·0 2·02 2·04 2·06 2·08 2·10 2·12 2·14 2·16
$\rightarrow \frac{1}{T} \times 10^3$

3. Discussion

Previous work on the isothermal decomposition of fresh large crystals of potassium permanganate has shown that the acceleration stage is best represented by an equation of the form $\alpha = A \exp(kt)$, at least up to $\alpha = 0.1$, and that this is preceded by a slow reaction[27,78]. The primary object of this work was to investigate the effects on the decomposition of the addition of potassium perchlorate to the potassium permanganate lattice. Hinshelwood and Bowen[70,71] noted that the rate of the decomposition fell, but they did not investigate any changes in the kinetics of the reaction.

Generally, all the materials showed an initial sigmoid decomposition, a linear stage and a 't^2-stage' where there was a linear increase in rate with time. These three stages will be considered as the pre-acceleration period. This is followed at ca $\alpha = 0.02$ by an acceleration stage which for the pure permanganate and the solid solutions with 89 and 72% permanganate is best expressed by the exponential relationship, but for solution F (52% $KMnO_4$) a power law with $n = 3$ is preferred.

The exponential and power law equations are compared in graph 12. For material G (25% $KMnO_4$) a power law with $n = 2$ is satisfactory as there is a linear increase in rate with time graph 9 (2.4.3.).

The various rate constants are compared in table 18, which is constructed from graphs 10 and 11. The logarithms of the rate constants at 490°K are tabulated, together with the ratio

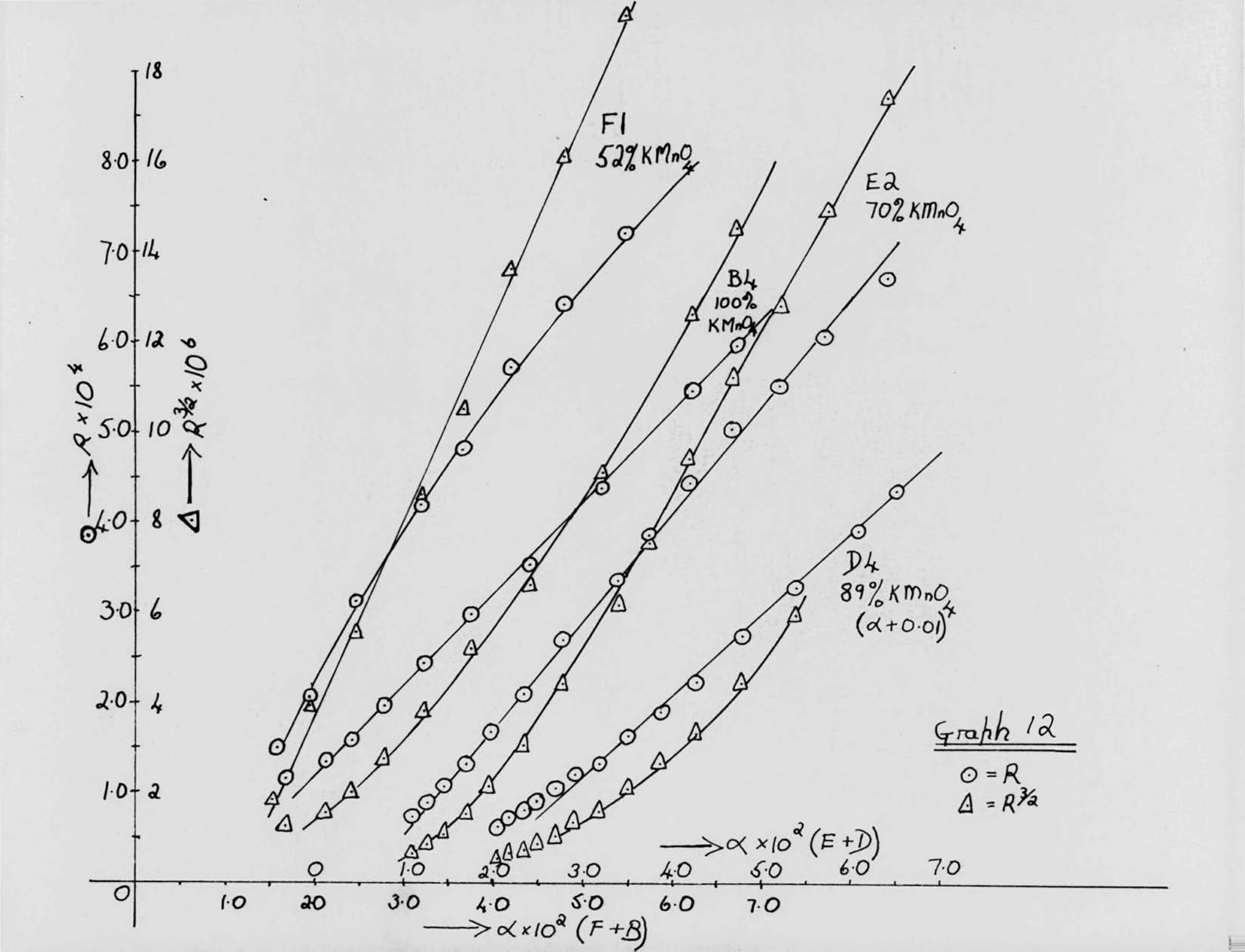
F1
52% KMnO4
B4
100%
KMnO4
E2
70% KMnO4
D4
89% KMnO4
(α+0·01)⁴
R x 10⁴
R^3/2 x 10⁶
α x 10² (F+B)
α x 10² (E+D)
Graph 12
○ = R
△ = R^3/2

of the rate constants for the solid solutions compared with those for pure permanganate B. This ratio represents the relative lowering of the rate constants due to the presence of the perchlorate. In graph 13 this ratio is plotted against the mole percent of potassium permanganate in the solid solutions.

Table 18

M	$\log_{10} R_I + 5$	$\frac{R_I}{R_I(B)}$	$\log_{10} R_L + 5$	$\frac{R_L}{R_L(B)}$	$\frac{1}{2}\log_{10} k_2 + 4$	$\frac{k_2}{k_2(B)}$	$\frac{1}{2}\log_{10} k + 2$	$\frac{k}{k(B)}$
A	1.9	1.0	1.62	1.0	-	-	1.25	1.9
B	1.9	1.0	1.62	1.0	1.62	1.0	0.95	1.0
D	1.5	0.39	1.33	0.51	1.49	0.74	0.83	0.76
E	1.1	0.16	0.80	0.15	1.0	0.24	0.58	0.54
F	0.9	0.10	0.65	0.10	0.7	0.12	0.22	0.23
G	-	-	-	-	0.15	0.03	-0.70	0.02

The relative decrease in the pre-acceleration rate constants (R_L, R_I, $k_2^{\frac{1}{2}}$) show the same pattern of a rapid lowering for the first 20 - 30% of perchlorate; this probably indicates that the three stages are involved with the same mechanism. For the acceleration period the effect of the perchlorate on the rate constant 'k' is less pronounced suggesting a different mechanism is involved. This is not unreasonable if the acceleration period involves the bulk of the crystal and the pre-acceleration the external and internal surfaces, as was the case for potassium metaperiodate.

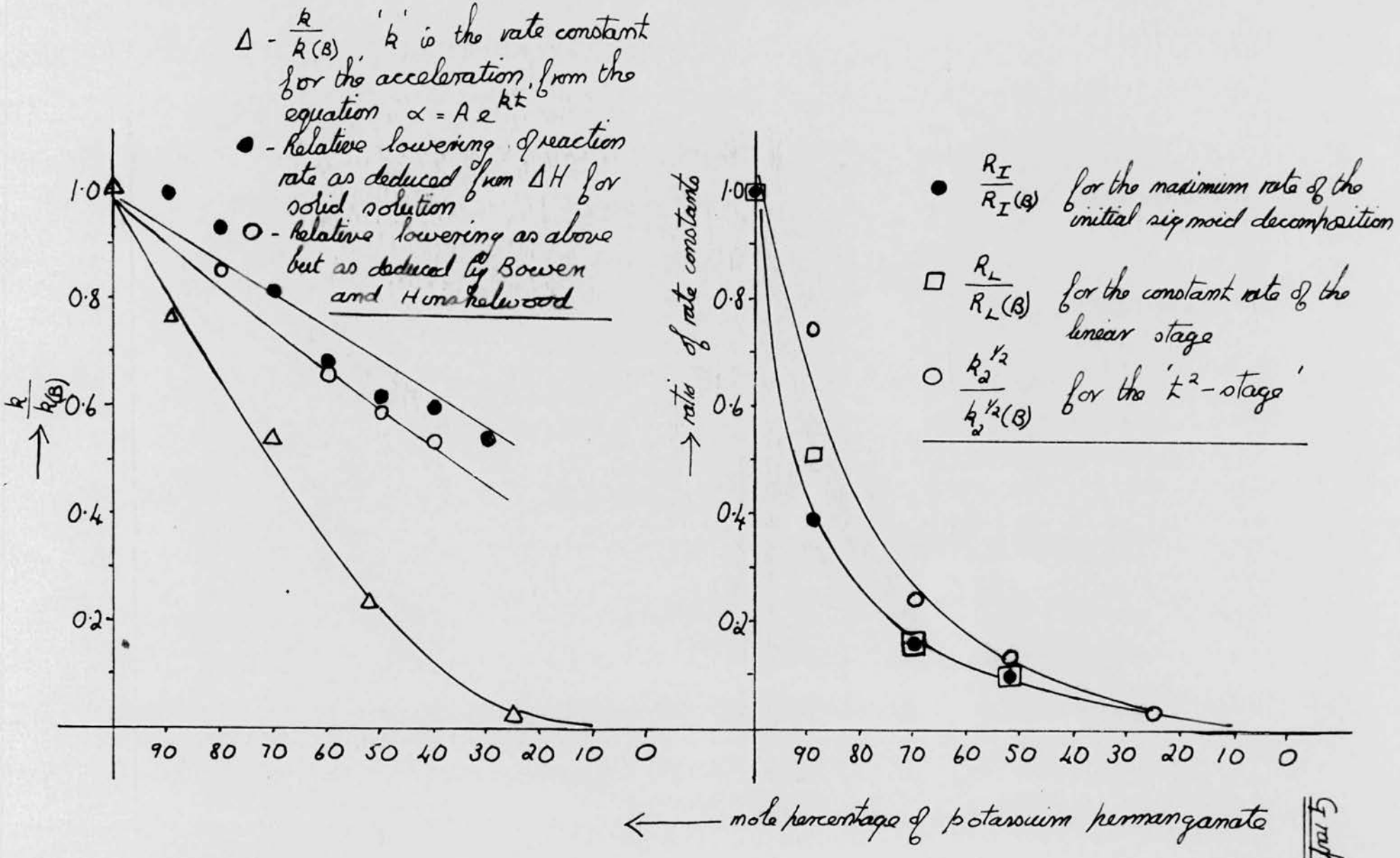
Δ - $\frac{k}{k_{(B)}}$ 'k' is the rate constant for the acceleration, from the equation $\alpha = A e^{kt}$
● - Relative lowering of reaction rate as deduced from ΔH for solid solution
○ - Relative lowering as above but as deduced by Bowen and Hinshelwood
$\frac{k}{k_{(B)}}$
1·0
0·8
0·6
0·4
0·2
90 80 70 60 50 40 30 20 10 0
● $\frac{R_I}{R_{I(B)}}$ for the maximum rate of the initial sigmoid decomposition
□ $\frac{R_L}{R_{L(B)}}$ for the constant rate of the linear stage
○ $\frac{k_2^{1/2}}{k_{2(B)}^{1/2}}$ for the 't²-stage'
rate of rate constant
1·0
0·8
0·6
0·4
0·2
90 80 70 60 50 40 30 20 10 0
mole percentage of potassium permanganate

Graph 13

The pre-acceleration period

The initial sigmoid decomposition that extended to α = 0.006 for the pure permanganate A and B was not present in the 'α' - 't' curve of a single large crystal (C 3, page 117), indicating a dependence on surface area. A similar initial sigmoid decomposition was found in ground barium permanganate but was not present for whole crystals[40]. This probably represents the decomposition of active spots on the surface and some of the subgrain boundaries, which creates a constant area interface that progresses into the subgrains giving rise to the linear stage. The value of 'α' at the end of the sigmoid stage decreases with increasing permanganate content (graph 3, 2.4.1.) due perhaps to a decrease in the number of active spots on the surface. Solid solution G (25% $KMnO_4$) is anomalous as the sigmoid extends to α = 0.01; this is probably due to the greatly increased surface area produced by the rapid crystallisation resulting in an increase in the number of active centres.

The linear stage is followed by a 't^2-stage' (graph 6) in all cases except pure permanganate A. The linear stage represents decomposition into the subgrains as was postulated for potassium metaperiodate, but if at the same time the decomposition spreads down undecomposed subgrain boundaries, the area of the interface will increase linearly with time giving rise to 't^2' kinetics. This is a similar mechanism to that proposed by Tompkins and Young[81] for the dehydration of barium styphnate monohydrate. The addition of perchlorate to the lattice lowers the initial sigmoid decomposition which probably entails a decrease in the number of

subgrain boundaries that have initially decomposed, and thus the boundaries decompose simultaneously with the linear growth into the subgrains which results in the 't^2-stage'. For solid solutions F and G (52 and 52% $KMnO_4$) the linear stage has virtually disappeared and thus the 't^2-stage' starts directly after the initial surface decomposition.

Acceleration period

If the acceleration period is interpreted in terms of the Prout-Tompkins mechanism the pre-acceleration period produces the strains along the internal surfaces that cause the branching[27,62,61]. The reduced values of 'k' (table 18) for the solid solutions may be due to (1) fewer imperfections at which branching occurs, (2) lower stresses at the interface of the reactant and products. As these are solid solutions the number of imperfections should be reasonably constant, so probably the second effect predominates.

For the solid solutions the product of the permanganate decomposition is embedded in potassium perchlorate, and as the perchlorate crystal lattice is identical to that of the solid solutions, the higher the percentage of perchlorate present the closer the structure of the product (including the perchlorate) will be to that of the solid solution. Thus the higher the percentage of perchlorate the lower the stress between the reactant and product. For $\frac{[Cl\ O_4^-]}{[Mn\ O_4^-]}$ of 0, $\frac{1}{9}$, $\frac{3}{7}$ (AB, D and E) there is a linear decrease in 'k' with respect to the $[Cl\ O_4^-]$, in agreement with the theory. The situation arises when the probability of

branching ceases to control the rate of the reaction and individual nuclei become of importance leading to three dimensional growth (F). When each permanganate ion is surrounded by a high proportion of perchlorate ions (3:1 in G) a coherent interface becomes impossible to maintain and two dimensional growth appears to apply with the reaction perhaps spreading in some sort of zig-zag fashion throughout the lattice. Thus the environment of the permanganate ion governs the kinetics of the decomposition.

The decomposition of pure permanganate A and B are identical for the initial sigmoid and linear stages, but the rate constant 'k' for A is 90% greater than that for B. This fact combined with the absence of a 't^2-stage' and the inferior external form of the crystals A indicates an increased density of dislocations leading to a higher rate of branching that can start directly after the linear stage. The value of 'k' found by Prout and Tompkins[27] for large single crystals corresponds to the value for D (89% $KMnO_4$). As the crystals used in the present experiments are about $\frac{1}{50}^{th}$ the size of those used by Prout and Tompkins a slower rate is to be expected according to Komatsu's general observations[78]. Boldyrev and Zakharov[82] have reported that the rate of decomposition of potassium permanganate varies for the different crystal faces, so both the size and shape affect the rate of decomposition.

Hill[32] has suggested, as an alternative explanation for the exponential acceleration of the decomposition, that nuclei are created by the diffusion of the product into the unreacted lattice. This is to some extent supported by the observations

of Hill and Wallace on the diffusion of molybdenum through the dislocation network of potassium permanganate[83]. The presence of perchlorate ions would not be expected to affect materially the diffusion of the product through the lattice as they are similar to permanganate ions. Thus the kinetics of the decomposition of the solid solutions should not be affected by the perchlorate content, which was not found to be the case.

Diffusion as a means of creating nuclei can be combined with the Prout-Tompkins mechanism by considering diffusion along the dislocations as included in the concept of branching. If the reaction interface branches when it meets a dislocation, the prior nucleation of the dislocation by diffusion, will perhaps assist the branching.

The lowering in the rate of the decomposition has been primarily explained in terms of a decrease in the rate of increase of the reaction interface, i.e. a change in the pre-exponential factor of the Arrhenius equation. Hinshelwood and Bowen[71] considered that the change in rate was due to an increase in activation energy as a result of the added stability of the permanganate ion in the perchlorate lattice. This was deduced from the heats of solution (water) of the solid solutions as given by Sommerfeld[84]. His results are shown in graph 14, the dotted line representing the additive heats of solution of potassium permanganate and potassium perchlorate, and the circles the heats of solution of the solid solutions. The heats of solution are slightly higher than the purely additive effect due

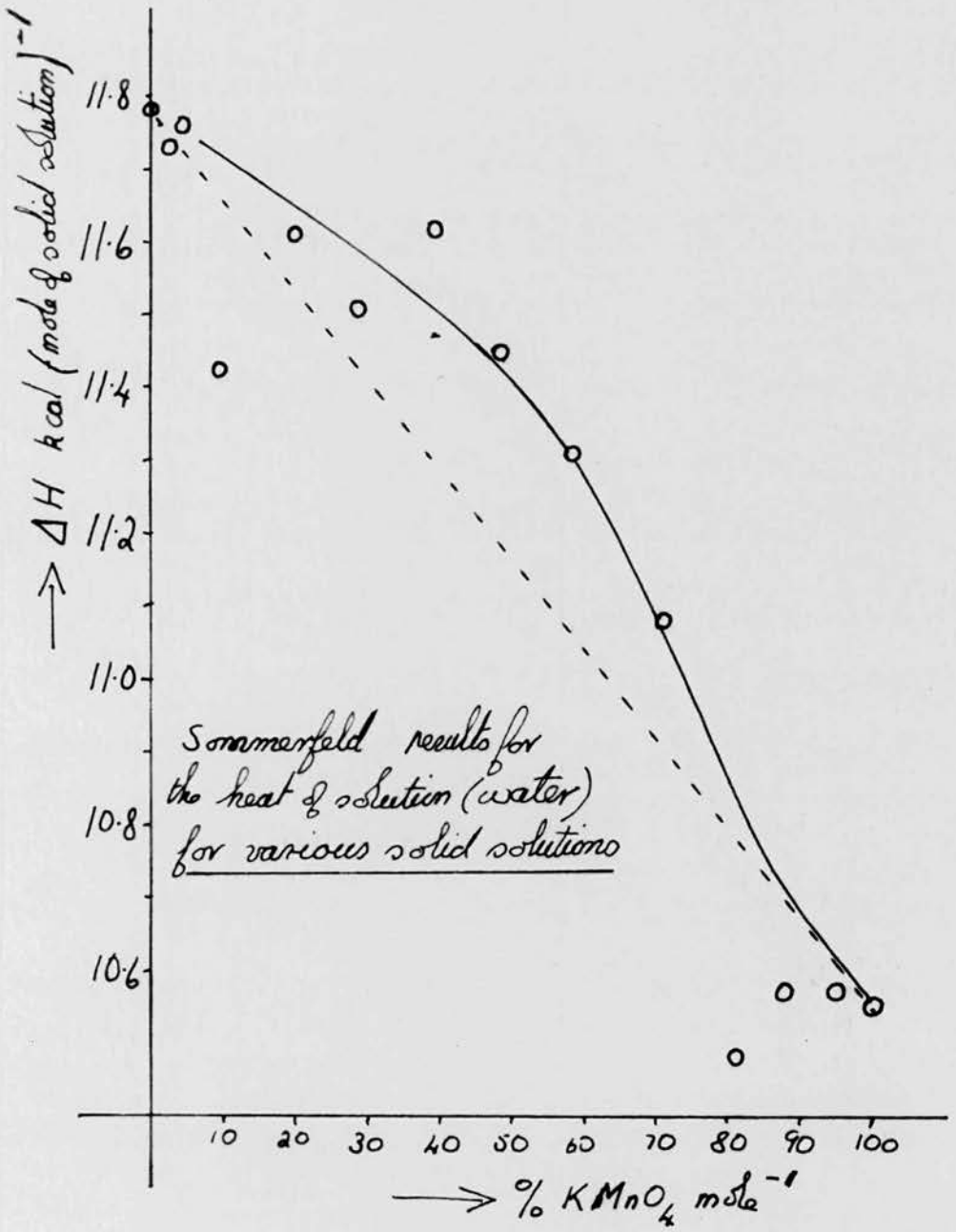
→ ΔH kcal (mole of solid solution)$^{-1}$
11·8
11·6
11·4
11·2
11·0
10·8
10·6
10 20 30 40 50 60 70 80 90 100
→ % $KMnO_4$ mole^{-1}
Sommerfeld results for the heat of solution (water) for various solid solutions

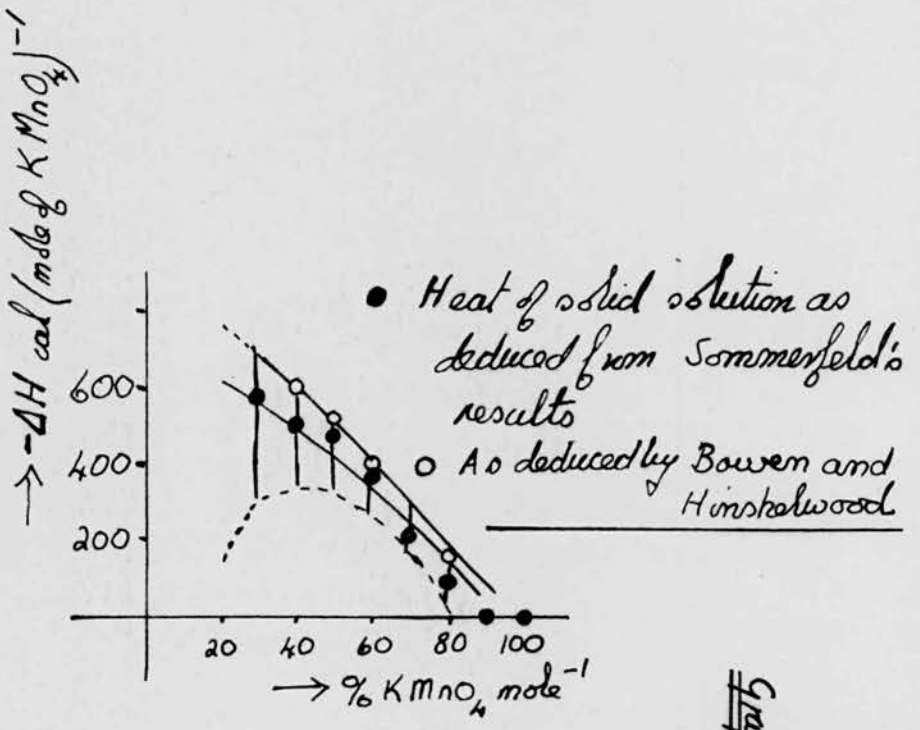
→ −ΔH cal (mole of $KMnO_4$)$^{-1}$
600
400
200
20 40 60 80 100
→ % $KMnO_4$ mole^{-1}
● Heat of solid solution as deduced from Sommerfeld's results
○ As deduced by Bowen and Hinshelwood

Graph 14

to the heat of solid solution. The values of the heat of solid solution per mole of potassium permanganate cannot be stated precisely due to the wide scatter of the points, and may lie anywhere within the dotted lines shown in graph 14.

Hinshelwood assumed that a change in the activation energy of the permanganate ion was caused by a difference in surroundings and was equal to the heat given out when passing from one surrounding to another. The relative rates of decomposition for different solid solutions can thus be calculated from the heats of permanganate/perchlorate. In graph 13 the relative decrease in rates are plotted, illustrating that the expected decrease in activation energies is insufficient to explain the decrease in rate.

The effect of the perchlorate ion on the acceleration period (the bulk effect) is mainly one of alteration in kinetics leading to a change in 'A factor', although the increase in activation energy will contribute to the decrease in rate. For the pre-acceleration period the rate constants are sharply decreased for only a small percentage of perchlorate and this may be due to a higher concentration of perchlorate at the surface and subgrain boundaries than in the bulk of the crystal. There would thus be less permanganate to decompose in the early stages. This necessitates a preferential adsorption of perchlorate at the main boundaries of the crystal during crystallisation.

The actual mechanism of the decomposition of the permanganate ion is probably complex and is not one of simple thermal breakdown as may be the case for the metaperiodate ion. Smirnova[85] has

suggested the following mechanism,

$$MnO_4^- \longrightarrow MnO_4 + e \qquad - (1)$$

$$MnO_4 \longrightarrow MnO_2 + O_2 \qquad - (2)$$

$$MnO_4^- + e \longrightarrow MnO_4^{=} \qquad - (3)$$

From his previous results[77] he has deduced, on somewhat dubious grounds, activation energies for the various steps and has shown that step one is the difficult stage. The first step is presumed to occur at the surface; the electron which is liberated moves in a conduction band until it is trapped by a permanganate ion. This mechanism allows for the production of manganate ions in the bulk of the crystal. The theory is plausible but the experimental grounds on which it is based are flimsy.

The conductivity of a single crystal of potassium permanganate was measured in the range 300 - 400°K by the same procedure as was used in section I (2.7.). The conductivity of the crystal could approximately be expressed by $\sigma = 10^{-2} \exp(-10000/RT)$ ohm^{-1} cm^{-1}, giving a conductivity of 10^{-7} ohm^{-1} cm^{-1} at 470°K. This is a high conductivity which perhaps supports the mechanism proposed by Smirnova. The photoconductance of potassium permanganate would perhaps throw further light on the mechanism of decomposition.

References

1. Burgess and Groen, Disc. Faraday Soc., 23 (1957) 183.
2. Hodkin and Taylor, J. Chem. Soc., (1955) 489.
3. Garner, Chemistry of the Solid State, ed. Garner, (Butterworths, London 1955), Chap. 8.
4. Langmuir, J. Amer. Chem. Soc., 38 (1916) 2263.
5. Cottrell, Progress in Metal Physics, Vol. I, (Butterworths, London 1949), Chap. 2.
6. Hedges and Mitchell, Phil. Mag., 44 (1953) 223, 357.
7. Cottrell and Bibby, Proc. Phys. Soc. Lond. A, 62 (1949) 49.
8. Wischin, Proc. Roy. Soc. A172 (1939) 314.
9. Bright and Garner, J. Chem. Soc., (1934) 1872.
10. Cooper and Garner, Trans. Faraday Soc., 32 (1936) 1739.
11. Jacobs and Tompkins, Chemistry of the Solid State, ed. Garner, (Butterworths, London 1955), Chap. 7.
12. Garner, Ibid., Chap. 9.
13. Farmer, J. Chem. Soc., (1922) 174.
14. Garner and Hailes, Proc. Roy. Soc., A139 (1933) 576.
15. Vaughan and Phillips, J. Chem. Soc., (1949) 2736, 2741.
16. Bartlett, Tompkins and Young, J. Chem. Soc., (1956) 3323.
17. Garner and Haycock, Proc. Roy. Soc., A211 (1952) 335.
18. Garner and Gomm, J. Chem. Soc., (1931) 2123.
19. Thomas and Tompkins, Proc. Roy. Soc., A209 (1951) 550; A210 (1951) 111.
20. Garner and Reeves, Trans. Faraday Soc., 51 (1955) 694.
21. Garner and Reeves, Trans. Faraday Soc., 50 (1954) 254.
22. Herly and Prout, J. Amer. Chem. Soc., 82 (1960) 1540.

23. Avrami, J. Chem. Phys., 7 (1939) 1103; 8 (1940) 212; 9 (1941) 177.

24. Erofeyev, C.R. Acad. Sci. U.R.S.S., 52 (1946) 511.

25. Mampel, Z. Phys. Chem., A187 (1940) 43, 235.

27. Prout and Tompkins, Trans. Faraday Soc., 40 (1944) 488.

28. Bircumshaw and Harris, J. Chem. Soc., (1939) 1637; (1948) 1898.

29. Simpson, Taylor and Anderson, J. Chem. Soc., (1958) 2378.

30. Glasner and Steinberg, J. Inorg. Nuclear Chem., 16 (1961) 279.

31. Garner, Trans. Faraday Soc., 34 (1938) 979.

32. Hill, Trans. Faraday Soc., 54 (1958) 685.

33. Prout and Tompkins, Trans. Faraday Soc., 43 (1947) 148.

34. Haynes and Young, Disc. Faraday Soc., 31 (1961) in press.

35. Tompkins and Young, Disc. Faraday Soc., 23 (1957) 202.

36. Finch, Jacobs and Tompkins, J. Chem. Soc., (1954) 2053.

37. Boldyrev, Zakharov, Eroshkin and Sokolova, Doklady Acad. Nauk., 129 (1959) 365.

38. Prout, J. Inorg. Nucl. Chem., 7 (1958) 368.

39. Herley and Prout, J. Inorg. Nucl. Chem., 16 (1960) 16.

40. Herley and Prout, J. Phys. Chem., 65 (1961) 208.

41. Mellor, Treatise on Inorganic Chemistry, Vol. II, 406.

42. Selected Values of Chemical Thermodynamic Properties, (National Bureau of Standards, circular 500).

43. Crouthamel, Meek, Martin and Banks, J. Amer. Chem. Soc., 73 (1951) 82.

44. Millar and Wilkins, Anal. Chem., 24 (1952) 1253.

45. Sawkill, Proc. Roy. Soc., A229 (1955) 135.

46. Smith, Nature, 115 (1925) 334.

47. Hylleraas, Z. Physik., 39 (1936) 308.

48. Wagner and Hantlemann, J. Chem. Phys., 18 (1950) 72.

49. Jacobs, J. Sci. Instr., 30 (1953) 204.

50. Sosman, International Critical Tables, Vol. 4, 341.

51. Jacobs and Tompkins, Quart. Reviews, 6 (1952) 238.

52. Thomas and Tompkins, J. Chem. Phys., 20 (1952) 662.

53. Darwin, Phil. Mag., (6) 27 (1914) 315, 675; 43 (1922) 800.

54. Cottrell, Dislocations and Plastic Flow in Crystals, (Oxford 1953).

55. Goldschmidt, Strukturbericht, (1913-26) 311.

56. Crouthamel, Meek, Martin and Banks, J. Amer. Chem. Soc., 71 (1949) 3031.

57. Mott and Gurney, Electronic Processes in Ionic Solids, (Oxford 1948), page 95.

58. Jacob and Tompkins, Proc. Roy. Soc., A215 (1952) 265.

59. Simpson and Taylor, J. Chem. Soc., (1958) 3323.

60. Ref. 11, page 188.

61. Tompkins and Young, J. Chem. Soc., (1957) 4281.

62. Herley and Prout, J. Chem. Soc., (1959) 3300.

63. Herley and Prout, Nature, 188 (1960) 717.

64. Garner, Ref. 11, Chap. 8.

65. Britton, Gregg and Winsor, Trans. Faraday Soc., 48 (1952) 63.

66. Boer, Disc. Faraday Soc., 23 (1957) 171.

69. Greenberg and Walden, J. Chem. Phys., 8 (1940) 645.

70. Hinshelwood and Bowen, Phil. Mag., (6) 40 (1920) 569.

71. Hinshelwood and Bowen, Proc. Roy. Soc., A99 (1921) 203.

72. Simchen, Bull. soc. chim. France, (1954) 638.

73. Roginsky and Schulz, Z. phys. Chem., A138 (1928) 21.

74. Hill, Proc. Roy. Soc., A226 (1954) 455.

75. Hill, Trans. Faraday Soc., 53 (1957) 1136.

76. Herley and Prout, J. Phys. Chem., 64 (1960) 675.

77. Erofeev and Smirnova, J. Physic. Chem. U.S.S.R., 25 (1951) 1098; 26 (1952) 1233.

78. Hill and Welsh, Trans. Faraday Soc., 56 (1960) 1059.

79. Komatsu, J. Chem. Soc. Japan, 78 (1957) 1452.

80. Harvey et al., J. Amer. Chem. Soc., 76 (1954) 3270.

81. Tompkins and Young, Trans. Faraday Soc., 52 (1956) 1245.

82. Boldyrev and Zakharov, Russian J. Phys. Chem., 34 (1960) 208.

83. Hill and Wallace, Nature, 178 (1956) 692.

84. Sommerfeld, 'Neues Jahrbuch fur Minerologie,' Brilage Band XIII (1900) 443.

85. Smirnova, J. Physic. Chem. U.S.S.R., 29 (1955) 135; 30 (1955) 2649.